UNIVERSITEIT VAN PRETORIA
UNIVERSITY OF PRETORIA
YUNIBESITHI YA PRETORIA

TRANSPORT MECHANISMS OF URANIUM AND THORIUM IN FRACTURED ROCK AQUIFERS

By

Yazeed Van Wyk

Submitted in fulfillment of the requirements for the degree
M.Sc: Engineering and Environmental Geology

in the

FACULTY OF NATURAL AND AGRICULTURAL SCIENCES
(Department of Geology)

at the

UNIVERSITY OF PRETORIA

Supervisor
Prof. KT Witthueser

Co-Supervisors
Prof. JL van Rooy
Mr. M Dippenaar

Date of submission
June, 2010

DECLARATION

I, Yazeed Van Wyk, hereby declare that the work presented in this dissertation is my own unless referenced otherwise. I also declare that this work has not been submitted at any other institute for any degree, examination or other purpose.

---------- ----------

Signed Date

ABSTRACT

Transport mechanisms of uranium and thorium in fractured rock aquifers

Y. Van Wyk
MSc Thesis
Department of Geology

Key words:

Beaufort West, hydrogeology, fractured rock aquifer, radioactivity, transport mechanisms, tracer test, pumping test, flow conceptualisation.

The Karoo has been receiving considerable attention since the early 1970's when uranium mining was at its peak, with numerous research studies being instigated to look at all aspects of uranium mining. It has recently been observed that there seems to be resurgence in uranium exploration in and around the town of Beaufort West. A study on the transport mechanisms of uranium and thorium in fractured-rock aquifers, initiated in the hope of understanding the actual processes controlling radionuclide mobilisation, is reported here.

Hydrochemical investigations of the various boreholes were sampled for water quality in June, 2009. The hydrochemical description is typical of shallow fresh groundwater, changing composition to a more sulphate hydrochemical facies along the flow path. While the geochemistry of groundwater in the study area seems to have minimal effects on uranium concentrations, the low levels of uranium in boreholes sampled suggest the importance of hydrological and lithological variability on the measured concentrations. Nevertheless, the uranium concentration is within the recommended levels as specified in the US-EPA, WHO and SA water quality guidelines and thus poses no immediate threat to the general public. Analysis of pumping and tracer tests, reveals that the fractured-rock aquifer can be highly transmissive and that transport can take place via multiple flow paths having different hydraulic properties. Tracer diffusing into stagnant water zones within fracture asperities and the rock matrix are seen as an important

retardation mechanism, that has implications for remediation should the aquifer be contaminated by radionuclides. In terms of conceptualising flow at a local scale, aperture sizes ranging from (563-828µm) along with high flow velocities (1.90E-03m/s), points to the importance of bedding-plane fractures as conduits of groundwater flow. The groundwater flow has been influenced by dolerite dykes creating compartments isolated from each other, suggesting a highly complex aquifer system. Based on the conceptual model, it is shown that these structures can create unique, site specific flow conditions.

The integration of all available data into the conceptual model provides an effective research tool that can be built upon as a basis for further research.

ACKNOWLEDGEMENTS

It is a pleasure to thank the many people who made this thesis possible.

First, I would like to acknowledge the Council for Geoscience, Water Research Commission and the Institute for Groundwater Studies for providing the funding necessary to carry out this study. I must also express my sincere gratitude to the many farmers who welcomed me into their homes and allowing me to sample their water, without their participation, this study would not have been possible.

It is difficult to overstate my gratitude to my M.Sc, supervisor, Prof. Kai Witthueser. With his enthusiasm, his inspiration, and his great efforts to explain things clearly and simply, helped make Hydrogeology fun for me. Throughout my thesis writing period, he provided encouragement, sound advice, good teaching, good company, and lots of great ideas. *"Danke, dass ihr Vertrauen in mich".*

I would also like to thank Mr. Leslie Strachan., Dr. Shafick Adams., Mr. Humberto Saeze., and Mr. Martin Holland for always being there with advice and guidance.

Far and away the biggest thanks go to my parents, Sarifa and Ebrahim Van Wyk. By showing me the beauty in the natural world, valuing education so highly, and most importantly instilling me with good morals and values. They have molded me into the person I am today.

Finally, I owe the greatest thanks of all to my older and wiser sisters, Shamila and Tasneem. The support, advice, compassion, and love each of you has provided me over the past three years, and for as long as I can remember, have provided me with the foundation for everything I have ever accomplished. Each of you has, in one way or another been a role model for me, and I love you all more than I can ever hope to express in writing.

Pretoria, 2010

TABLE OF CONTENTS

LIST OF FIGURES

LIST OF TABLES

LIST OF APPENDICES

SYMBOLS AND ABBREVIATIONS

A(r)	-	cross – sectional area of flow (L^2),
B	-	leakage factor (L),
B	-	aperture (L)
b’	-	aquitard thickness (L),
c	-	concentration in the mobile (fracture) zone [ML-3]
Dh	-	hydrodynamic dispersion coefficient [L_2T-1
f	-	friction factor
f	-	<1 for smooth walls
f	-	>1 for rough walls.
h (r,t)	-	change in hydraulic head from h(r,0) = 0 (L),
K’	-	hydraulic conductivity of the aquitard (L/t).
K	-	hydraulic conductivity (L/T),
N	-	flow dimension,
Δp	-	pressure gradient
Q	-	pumping rate (L^3/t),
r	-	radial distance to the pumping well (L),
Re	-	Reynolds number
R_f	-	retardation coefficient of fracture surface [-]
r_o	-	distance where straight line intercepts the zero drawdown axis (L)
S	-	storativity (dimensionless),
Ss	-	specific storage (1/L).
Δs	-	drawdown per log cycle of time (L),
T	-	transmissivity (L^2/t),
t	-	time (in days or minutes)
t_o	-	time, where the straight line intersects zero – drawdown axis (T, d).
v	-	average solute velocity in the fracture [LT-1]
W (u, r/B)	-	leaky artesian well function,
Γ	-	gamma function.
Ψ	-	friction factor
ε	-	fracture roughness
Γ	-	dynamic viscosity.

Amu	-	Atomic mass unit
BTC	-	Breakthrough Curve
Deff	-	Effective diffusion coefficient
DWA	-	Department of Water Affairs
EC	-	Electrical conductivity (µS/cm)
ESSO	-	New Jersey Standard Oil
GRF	-	Generalized radial flow
MAPE	-	Mean annual potential evaporation
MCM	-	Multi-Channel Model
MCL	-	Maximum Contaminant level
MPa	-	Mega Pascal
MDA	-	Minimum detectable activity
mSv/a	-	Millisieverts per annum
$Mlbs^2$	-	Million pounds
Mbgs	-	Meters below ground surface
NRMP	-	National Radioactive Monitoring Programme
NGA	-	National Groundwater Archives
ppb	-	Parts per billion
Pe	-	Peclet number
RDL	-	Reference dose level
SFDM	-	Single Fissure Dispersion Model
TBR	-	Tweeling Brandwag Renosterkop
US-EPA	-	United States Environmental Protection Agency
WRC	-	Water Research Commission
WHO	-	World Health Organization
UO_2^{2+}	-	Uranyl dioxo ion

CHAPTER 1 - INTRODUCTION

1.1 BACKGROUND AND CONTEXT OF THE STUDY

The huge demand for groundwater in South Africa has increased dramatically over the years, especially in certain rural areas of the country. Groundwater is generally considered as a safe and viable option compared to surface water. However, this is not always the case as groundwater can be contaminated by hazardous trace, and more importantly radioactive constituents. The geogenic and anthropogenic contamination of groundwater by heavy metals and radionuclides poses a direct threat to water supplies, while the contamination of surface soils poses an unrealised but equally important threat to groundwater resources. The Water Research Commission (WRC) granted a project to a consortium of researches to develop a sampling and monitoring protocol for radioactive elements in fractured rock environments. The research outcomes are intended to support the implementation of the National Radioactive Monitoring Programme (NRMP) of the Department of Water Affairs (DWA).

The focus of this thesis within the framework is to look at the various transport mechanisms responsible for the mobilisation of radioactive elements in fractured rock aquifer systems. Beaufort West, which is situated at the main Karoo basin, was chosen as a study area because of its anticipated growth within the next few years where there are a seemingly resurgence in uranium exploration and possibly mining south of the town. It is therefore expected that the towns demand will soon exceed the current water supply. Based on the Karoo basin having undergone extensive research in the past, especially as a result of uranium mining, there was a high possibility of potential contamination impact on groundwater in the region.

1.2 RESEARCH OBJECTIVES

The rate of uranium release in oxidised environments is governed by the speciation of uranium in the solid phase. Uranium in particular is very mobile and soluble under oxidising conditions, whereas thorium as a daughter on the other hand is rather immobile and insoluble under similar conditions. As a result, uranium can be a major contaminant in the subsurface, where it can be distributed amongst (1) the dissolved species in pore water, (2) the sorbed species on mineral surfaces, and (3) the discrete uranium – containing mineral phases (Figure 1.1).

The main objectives of this study are thus:

- To address the present knowledge gap with respect to uranium and thorium speciation in groundwater of fractured rock aquifers;
- To identify the main transport mechanisms responsible for their mobilisation in the subsurface environment;
- To apply recent advances to characterise flow regimes in fractured rock aquifer systems, with special reference to tracing the distribution of contaminants in fractured media and
- To conceptualise possible flow dynamics on a local scale.

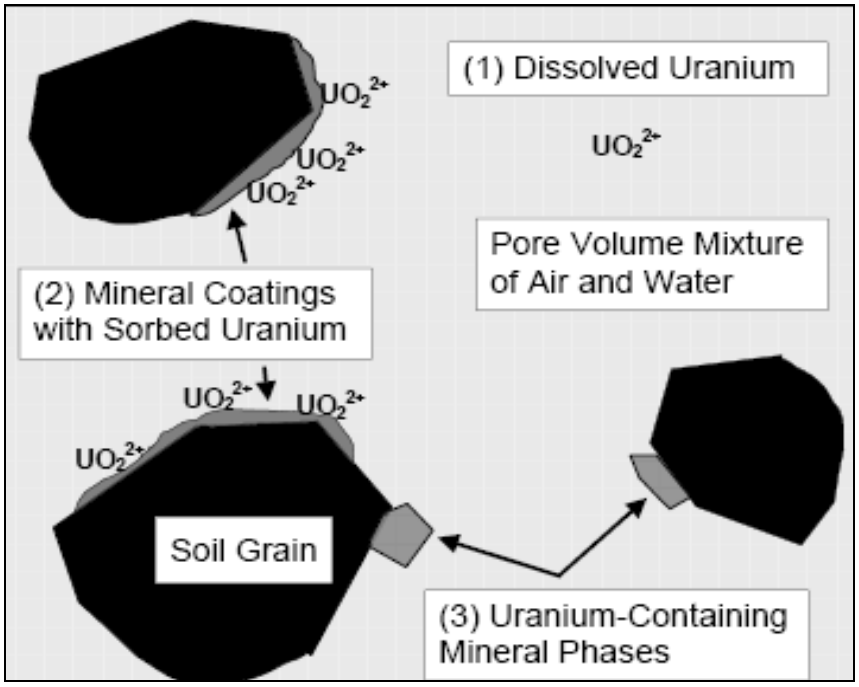

Figure 1.1 Conceptualisation of the distribution of uranium in the porous media (Giammar, 2001).

1.3 PREVIOUS STUDIES

Most research studies relating to uranium in the Karoo basin dealt with using selected trace elements and major ions in subterranean waters as potential indicators for uranium mineralisation (Brunke, 1977; Van der Merwe and de Beer, 2006). Whilst, other studies looked at the importance of geological lineaments and fractures as targets for drilling and abstracting groundwater from fractured rock aquifers (Rose and Conrad, 2007). Vogel et al., (1980) conducted a study in Beaufort West using isotopes of uranium, and other environmental tracers in groundwater as an adjunct to major development of groundwater resources in the area. The emphasis of the above mentioned studies focused primarily on the development and quantification of the water resource and its effective management. However, no studies relating to the actual processes controlling radionuclide mobilisation has been done in the past.

1.4 THESIS STRUCTURE

The following is a brief outline of the structure and content of the thesis. The first chapter contextualises the study by discussing the research objectives upon which, the study is based. Following the introduction a review chapter of local and international literature related to the various components of the study is given. A description of the study area follows where the climate, physiography, geology, and hydrogeology are discussed. The methodology adapted for the study is fieldwork orientated. The importance of which, is to understand the aquifer system in order to conceptualise local flow dynamics. Chapter 4 deals with the results along with the discussions. In the final chapter conclusions are drawn along with some recommendations for future research.

CHAPTER 2 - LITERATURE REVIEW

2.1 INTRODUCTION

The fundamental characteristics of fractured rock aquifers lie in their extreme spatial variability of hydraulic conductivity, transmissivity, storativity and hence groundwater flow rate. Thus the need to characterise these aquifers cannot be overemphasised as it will help in solving key issues related to the importance of fractures on groundwater flow and transport, to investigate at what scale fractures become important and, finally, how fractures determine transport, flow velocity and flow direction (National Research Council, 1996). These issues are of great concern as they form the basis of our understanding of how fractured rock aquifers behave. The parallel plate model of groundwater flow has been widely used to understand flow in a single planar fracture (National Research Council, 1996). However, the parallel plate flow represents an idealised case typically studied at a laboratory scale. Fracture flow in nature on the other hand is rather channeled within fractures due to the rough nature of apertures, and the tortuous nature and convolutions of aperture patterns. This chapter will mainly be dealing with the various transport mechanisms such as advection, dispersion, matrix diffusion, decay and sorption with the aim of identifying which processes are more dominant, and under what circumstances. Finally a look at the radionuclides of uranium and thorium and their behavior in fractured rock aquifers is given.

2.1.1 Characterising Fractured Rock Aquifers

According to (Cook, 2003), aquifers can be considered to fall in a continuum between porous media and conduit systems. This is illustrated in Figure 2.1, whereby a classification of fractured rock aquifers is given. Models in general are based on certain assumptions and groundwater models are no exception to this rule. Fractured rock models often assume that fractures are planar and parallel, though seldom the case in reality, but which provide us with a good foundation in understanding groundwater behavior in fractured rocks. It is this very concept of the fracture as planar network of interconnected voids that lead to the analogy with porous media (National Research

Council, 1996). The characterisation of fractured rock aquifers requires information on both the fractures and their surrounding matrix, with the rock matrix generally being described by its pore size distribution expressed in terms of effective porosity (η) and hydraulic conductivity (K).

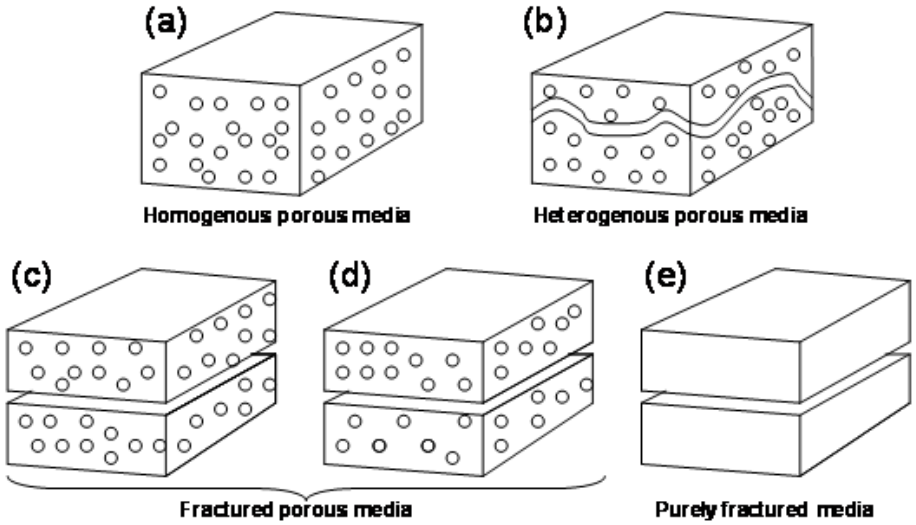

Figure 2.1 Classifications of fractured rock aquifers (Cook, 2003).

As has already been pointed out, fractures are not uniformly distributed in formations, and with the complex connectivity of fractures and their wide range of hydraulic properties, convoluted flow paths are bound to exist in fractured rock aquifers. It is thus important when characterising fractured rocks that the orientation, spacing, length, aperture, connectivity and surface roughness measurements be noted (Cook, 2003). Of equal importance is the characteristic of the rock matrix, whereby the measurements of matrix porosity and permeability helps to determine the extent to which fractures are likely to dominate flow. In the case where fractures are open, fracture permeability is likely to exceed matrix permeability and therefore allow groundwater flow to be dominated by fractures. Measurements of matrix diffusion coefficients largely determine the extent to which solutes will be retarded relative to water movement (National Research Council, 1996).Caution needs to be applied when measurements of rock matrix properties are carried out on surface samples as results may be affected by weathering and decompression processes.

2.1.2 Pumping tests in fractured rock aquifers

In groundwater investigations, hydraulic tests are used to obtain estimates of hydraulic conductivity and storativity of the aquifer medium. These properties are useful in determining the advective transport of contaminant plumes and in designing effective groundwater remediation systems. Pumping tests, including constant – rate and step – drawdown tests, are amongst the most common hydraulic test procedures applied in fractured rock aquifers. According to Kruseman and de Ridder, (1991), the principle of a pumping test is to pump water from a borehole and measure discharge and drawdown in observation boreholes at known distances from the pumping borehole. These measurements can then be substituted into appropriate well – flow equations in order to calculate the hydraulic characteristics of the aquifer.

There are other cost effective methods, such as slug and bail tests, permeameter tests, and grain – size analysis, that offer economical ways of obtaining data to estimate aquifer parameters when a pumping test is not feasible. However, scale effects need to be accounted for when using these methods. In the following section some of the methods including (Theis, 1935; Cooper and Jacob, 1946; Hantush and Jacob, 1955; Barker, 1988) for evaluating pumping tests in general and not limited to fractured rock aquifers (assuming equivalent porous media) are given.

2.1.2.1 Theis method (unsteady-state flow)

The first mathematical treatment of unsteady – state domain of Darcian groundwater flow to a borehole in a confined aquifer is credited to Charles Vernon Theis, who published the analytical solution in 1935. Some of the simplifying assumptions that are required for mathematical convenience are listed below (Fetter, 1999):

1. Aquifer is homogenous, isotropic, uniformly thick, and of infinite extent.
2. The potentiometric surface is horizontal initially.
3. Borehole fully penetrates the confined aquifer resulting in horizontal flow to the borehole and flow is laminar (Darcy's law dictates).
4. Storage within borehole can be neglected.
5. Water is removed from storage and responds instantaneously with declining head.

The solution for predicting drawdown in a borehole at a radial distance from the pumped borehole is known as the Theis equation:

$$s = \frac{Q}{4\pi T} W(u) \qquad \text{Equation 1}$$

Where,

Q = pumping rate (L^3/t),

T = transmissivity (L^2/t),

s = drawdown (L)

W(u) in the above equation is termed the well function and is the infinite series part of the analytical solution to the unsteady, radial groundwater flow equation that is approximated by:

$$W(u)\left[-05772 - \ln u + u - \frac{u^2}{2 \cdot 2!} + \frac{u^3}{3 \cdot 3!}\frac{u^4}{4 \cdot 4!} + - \ldots\right] \qquad \text{Equation 2}$$

This particular well function is a function of u, where:

$$u = \frac{r^2 s}{4Tt} \qquad \text{Equation 3}$$

Where,

r = radial distance to the pumping well (L),

S = storativity (dimensionless),

T = transmissivity (L^2/t),

t = time (in days or minutes)

2.1.2.2 Cooper – Jacob (Straight-line method)

The Cooper – Jacob method (Cooper and Jacob, 1946), commonly referred to as the straight line method is a simplification of the (Theis, 1935) solution for flow to fully penetrating boreholes in confined aquifers. Cooper – Jacob, (1946) noted that after the pumping borehole has been running for some time, the well function (u) becomes sufficiently small (< 0.05) and the higher power terms (beyond ln u) of the infinite series of (equation.2) becomes negligible. The same assumptions apply to the Cooper – Jacob analytical solution as the Theis solution, with the addition of there being “no recharge”. Because recharge affects the slope of the log (time) vs. drawdown curve to flatten as the recharge in the zone of influence of the borehole matches the discharge. For the Cooper – Jacob straight line method, drawdown is plotted with an arithmetic scale on the y – axis versus time plotted with a logarithmic scale on the x – axis. The value of transmissivity and storativity may be calculated by the following equations:

$$T = \frac{2.3Q}{4\pi\Delta S} \qquad \text{Equation 4}$$

and

$$S = \frac{2.25Tto}{r^2} \qquad \text{Equation 5}$$

Where,

T = transmissivity (L^2/t),

Q = pumping rate (L^3/t),

Δs = drawdown per log cycle of time (L),

S = storativity (dimensionless),

r = radial distance to the well (L),

t_o= time, where the straight – line intersects zero – drawdown axis (T, d).

For distance-drawdown plots the equations are modified as follows:

$$T = \frac{2.3Q}{2\pi\Delta S} \qquad \text{Equation 6}$$

and

$$S = \frac{2.25Tto}{r^2o} \qquad \text{Equation 7}$$

Where,

t = time (in days or minutes),

r_o= distance at which the straight –line intercepts the zero-drawdown axis (L)

The results from the Cooper – Jacob solution and Theis solution are generally comparable; however, the former is much easier to plot in the field and does not involve any curve matching techniques.

2.1.2.3 Hantush – Jacob's method

It is seldom in nature that aquifers are perfectly confined; instead leaky aquifers occur more frequently, which implies that confining layers overlying or underlying a particular aquifer are hardly ever completely impermeable (Kruseman and de Ridder, 1991). Hantush and Jacob, (1955) presented the solution for drawdown in a pumped aquifer that has an impermeable base and a leaky confining unit above. Conceptually, this would be regarded as a four – layered system, from top to bottom, a water table aquifer, a leaky confining unit, a confined aquifer, and extremely low permeability bedrock. During early pumping time, water is coming out of storage from the pumped aquifer and the leaky confining unit. Eventually, the drawdown comes into equilibrium with the leakage through the confining unit from the unstressed aquifer and the system achieves

steady – state. Once equilibrium is reached, the aquitard merely serves as a water transmitting medium, and the water contributed from its storage can be neglected (Kruseman and de Ridder, 1991). The assumptions and conditions underlying this method are:

1. Aquifer is leaky, horizontal flow in stressed aquifer and vertical flow through the aquitard.
2. The aquifer is pumped at a constant discharge rate.
3. Pumping well is fully penetrating.
4. Aquitard is overlain by an unconfined aquifer, known as the source bed.
5. Water table in the source bed is initially horizontal and does not fall during pumping of the aquifer.
6. Aquifer is compressible, and water drains instantaneously with a declining head.
7. Aquitard is incompressible; no water is released from storage in the aquitard when the aquifer is pumped.

The Hantush – Jacob formula for drawdown of a pumped borehole at a constant discharge in a leaky aquifer is:

$$s = \frac{Q}{4\pi T} W\left(u, \frac{r}{B}\right) \qquad \text{Equation 8}$$

$$u = \frac{r^2 s}{4Tt} \qquad \text{Equation 9}$$

$$B = \left(\frac{Tb'}{K'}\right)^{1/2} \qquad \text{Equation 10}$$

Where,

Q = pumping rate (L^3/t),

s = drawdown (L),

T = transmissivity (L^2/t),

W (u, r/B) = leaky artesian well function,

r = distance from pumping borehole to observation borehole (L),

S = storativity (dimensionless),

t = time (in days or minutes),

B = leakage factor (L),

b' = aquitard thickness (L),

K' = hydraulic conductivity of the aquitard (L/t).

It is important to take cognisant of the fact that, up until now we have considered steady state conditions, whereby storage in the aquitard is considered to be negligible. However, when flow is unsteady the effects of aquitard storage cannot be neglected. Two useful methods that accounts for the aquitard storage capacity are the Hantush – curve fitting method and the Neuman – Witherspoon method (Fetter, 1999).

2.1.2.4 Barker's method

The inherent complexity of flow through fractures makes the use of classical techniques (Theis and Cooper – Jacob) inaccurate for calculation of aquifer constants (Marechal et al., 2004). The problem that generally arises when conducting hydraulic tests in fractured-rock aquifers is being able to choose an appropriate geometry for the fracture system through which flow occurs. Barker, (1988) proposed a model, commonly referred to as the generalized radial flow (GRF) model, which is based on the generalization of the flow dimension to non – integral values. The reason for proposing the GRF model is that it contains relatively few parameters, making it suitable for data analysis. Secondly, it is much easier to generalize the dimension of the flow system as it is often difficult to choose an appropriate dimension (Barker, 1988). The model is usually applied to aquifers with complex geometry and heterogeneous properties. The GRF model is based on the following assumptions:

1. Flow is radial and Darcy's law applies throughout the system.
2. The source is an n – dimensional sphere (projected through three – dimensional space e.g. finite cylinder in two dimensions) with a radius rw and storage capacity Sw.
3. The source has infinitesimal skin which is characterised by a skin factor Sf; the head loss across the surface of the source is proportional to Sf and the rate of flow through the surface.
4. Any piezometers in the fracture system have negligible size and storage capacity.

The following equations of the GRF model shows the relationship between cross – sectional area of flow and distance from the source (Walker and Roberts, 2003):

$$A(r)=\partial_n r^{n-1} \qquad \text{Equation 11}$$

Where the surface area of a unit sphere in n dimension is

$$\partial_n = b^{3-n}\frac{2\pi_2^n}{\Gamma\left(\frac{n}{2}\right)} \qquad \text{Equation 12}$$

Where,

A(r) = is the cross – sectional area of flow (L^2),

r = radial distance from the borehole (L),

b = is the extent of the zone (L),

n = flow dimension,

Γ = gamma function.

The governing equation for the GRF model is given by:

$$Ss\frac{\partial h}{\partial t}=\frac{K}{r^{n-1}}\frac{\partial}{\partial r}\left(r^{n-1}\frac{\partial h}{\partial r}\right)$$ Equation 13

Where,

h (r,t) = change in hydraulic head from h(r,0) = 0 (L),

K = hydraulic conductivity (L/T),

Ss = specific storage (1/L).

The Barker method takes into account the dimension of the flow, which results from the distribution and connectivity of the conductive fractures (Marechal et al., 2004). This theory is a generalization of the Theis theory, which considers radial flow, into a homogeneous, confined and isotropic fractured medium characterised by a hydraulic conductivity *Kf* and specific storage *Ssf*. The model introduces the fractional dimension of flow, n, which characterises the variation of flow section according to distance from the pumping borehole. Values of n generally vary from 0 to 3, whereby n = 3 indicates spherical flow, n = 2 cylindrical and linear where n = 1 (Figure 2.2).

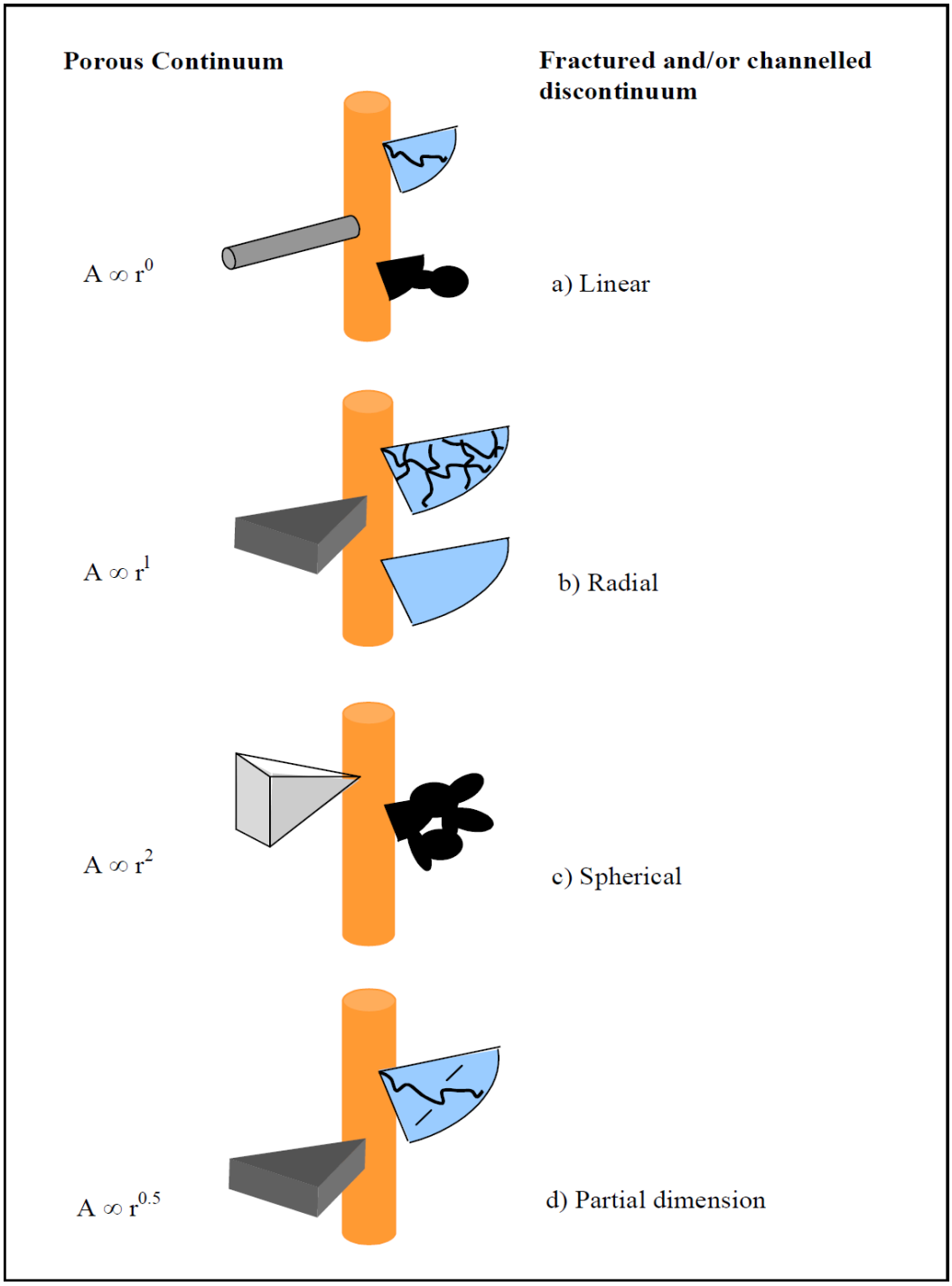

Figure 2.2 Flow dimensions and their practical approach in porous continuum and fractured discontinuum (Black, 1994).

2.1.3 Tracer Tests

Tracer testing can provide insight into groundwater flow characteristics and contaminant transport processes that are not provided by conventional aquifer testing methods. These insights generally complement those gained by conventional methods, and are best suited for assessing water quality issues associated with contaminant migration. Choosing the appropriate tracer can help identify the dominant transport mechanisms. Ideally, one of the tracers should move at the same velocity as the water. The tracer under consideration should not decay, adsorb onto the rock or react with other tracers (i.e. it should be chemically inert) (National Research Council, 1996).

One of the critical issues in planning a tracer test is determining what mass of tracer to inject, and as a result a number of empirical equations have been developed for this purpose (Käss, 1998). The following formula is one of many used to estimate the tracer quantity:

$$M = Q \,.L\,.k\ (kg\ ) \qquad \text{Equation 14}$$

Where Q = discharge or pumping rate of the well (m^3/s),

L = distance (km),

k = coefficient of the tracer

Forced-gradient cross-hole tracer tests, in which tracers are injected into one or more boreholes and recovered by pumping a nearby borehole, provide estimates of effective flow porosity of the aquifer system. Cross-hole tracer tests can also be conducted under natural-gradient conditions (i.e. without pumping) to obtain direct estimates of both ambient groundwater flow velocities and solute dispersivity (longitudinal and transverse) in the aquifer (Käss, 1998). These tests are generally conducted with one or more injection boreholes and several down gradient observation boreholes that are passively sampled for tracers. Single - well tracer tests can also be used, with different rest periods, or times that tracers are allowed to drift in the aquifer before being pumped back, are probably a more practical, though less direct, method of obtaining estimates of

ambient groundwater flow velocities in an aquifer than natural-gradient cross-hole tracer tests. Both cross-hole and single-well tracer tests should always be conducted by simultaneously injecting several inert tracers that have different diffusion coefficients so that the effects of diffusion, advection, and hydrodynamic dispersion can be distinguished from one another and deconvoluted to obtain more constrained estimates of transport parameters describing the three processes (National Research Council, 1996). It is also helpful to add reactive tracers to the mixture of nonreactive tracers, which will provide additional information on diffusion and sorptive processes in retarding the transport of contaminants in the aquifer. The effect diffusion has on the overall movement of tracers in the subsurface cannot be underestimated. This is particularly true for tracers that have large diffusion coefficients as apposed to those with smaller diffusion coefficients. Extensive diffusive mass transfer between flowing and near stagnant water in the aquifer will slow the migration of contaminants, but will also make it much more difficult to remediate the aquifer afterwards once contaminants diffuses from fractures into the adjacent porous matrix. Maloszewski and Zuber, (1990) developed the single fissure dispersion model (SFDM) to incorporate sorbable substances by coupling an instantaneous equilibrium reaction governed by a linear adsorption isotherm with a nonequilbrium kinetic reaction of the first order. The model is based on the assumption that the fracture system can be substituted by a single fracture and accounts for diffusion processes into an adjacent infinitely extended matrix. The concentration C at the pumping borehole can be expressed in terms of mean residence time t_o , Peclet number, *Pe*, and a third fitting parameter, a, that incorporates matrix diffusion:

$$C(t) = \frac{a\,M}{2\pi\,Q}\sqrt{Pe\,t_o}\int_0^t \exp\left[-\frac{Pe\left(t_o-\tau\right)^2}{4t_o\,\tau}-\frac{\left(\tau a\right)^2}{\left(t-\tau\right)}\right]\frac{d\,\tau}{\sqrt{\tau\left(t-\tau\right)^3}}$$

Equation 15

Where M = injected tracer mass

Q = flow rate

The three fitting parameters of the SFDM (a, Pe, T_0) combine several physical parameters. For non – reactive tracers the diffusion parameter a is given by (Maloszewski and Zuber, 1990):

$$a = \frac{\eta\sqrt{D_p}}{2b} \qquad \text{Equation 15.1}$$

Where 2b is the mean fracture aperture (m), η the effective matrix porosity (m^3/m^3) and D_p the pore diffusion coefficient (m^2/s). The Peclet number Pe is defined by:

$$Pe = \frac{vX}{D} \qquad \text{Equation 15.2}$$

Where v is the mean flow velocity, and X is the distance along the flow direction between the injection and extraction borehole (m). The mean travel time t_o of a non-sorbing tracer in the fracture is given by:

$$t_0 = \frac{X}{v} \qquad \text{Equation 15.3}$$

The relative recovery can be calculated from both, the experimental and theoretical tracer curve as a function of time. According to Käss, (1998), the comparison of the above curves improves the inverse fitting procedure, because it is very sensitive for diffusion processes affecting the tailing of the breakthrough curve. The relative recovery is defined as follows:

$$RR(t) = Q\int_0^t C_f(t)\,\delta t \,/\, M \qquad \text{Equation 15.4}$$

Where RR = recovered tracer mass

M = injected tracer mass

Q = flow rate

t = DIRAC delta function

cf = tracer concentration in the fracture

The application of the SFDM by Maloszewski et al., (1999) to two multi-tracer tests performed in one of the major cross – fault zones of the Lange Bramke basin (Harz Mountains, Germany), have shown that at least one of the injected tracers should be conservative, otherwise it would not be possible to effectively distinguish sorption from diffusion processes and the influence of diffusion exchange between mobile water in the fractures and immobile water in the rock matrix. This particular model has also been applied successfully in related studies at the Lindau rock tests site (Himmelsbach et al., 1995 and Witthüser et al., 2003).

2.2 TRANSPORT MECHANISMS IN FRACTURED ROCKS

Over the last two decades major efforts have been devoted to the development of realistic theoretical models capable of simulating flow and transport processes in fractured and heterogeneous porous formations (Berkowitz et al., 1999). These models have consequently led to a significantly improved understanding of the dynamics of flow and transport processes. The most common model for flow in a single fracture is the cubic law, in which two parallel plates separated by a constant distance (aperture), represents the fracture being used. This is commonly referred to as the parallel plate model of groundwater flow, considered as a system of one or several planar, parallel fractures in an impermeable rock matrix. The equation for one – dimensional flow between two parallel plates is given by the cubic law (National Research Council, 1996):

$$Q = \frac{b^3}{12\gamma}\Delta p \qquad \text{Equation 16}$$

Where:

Q = volumetric flow rate (L^3/T),

b = distance between the plates or the aperture (L),

Δp = pressure gradient

γ = dynamic viscosity.

It is normally assumed that fracture walls are smooth and that flow is in the laminar range, although it is not the case in reality (Bear et al., 1993).The influence of fracture roughness on the laminar flow rate was investigated and the following relationship was identified:

$$\Psi = \frac{96}{\mathrm{Re}}\left[1+6.0\left(\frac{\varepsilon}{2b}\right)^{\frac{3}{2}}\right] \quad \text{valid for } \frac{\varepsilon}{b} > 0.0065 \qquad \text{Equation 17}$$

Where:

Ψ = friction factor
Re= Reynolds number
ε = fracture roughness
b = aperture (L)

Generally laminar flow between parallel plates is expressed as:

$$\Psi = \frac{96}{\mathrm{Re}} f \qquad \text{Equation 18}$$

Where:

f= friction factor
f = 1 for smooth walls
f > 1 for rough walls.

To predict flow in a real fracture with rough walls, the difficulty in applying the cubic law comes about in defining a representative distance between the fracture walls. Equation.16 can be corrected by a friction factor f to account for the roughness of the fracture surfaces (Witherspoon et al., 1980):

$$Q = \frac{1}{f}\frac{b^3}{12\gamma}\Delta p \qquad \text{Equation 19}$$

Where:

Q = volumetric flow rate (L^3/T),
b = distance between the plates or the aperture (L),
Δp = pressure gradient
γ = dynamic viscosity.
f = friction factor

The validity of this modified cubic law was discussed by Witherspoon et al., (1980) based on their experimental measurements of radial and straight flows through artificially induced tensile fractures in different rock types (granite, basalt and marble) with normal stresses up to 20 MPa and apertures ranging from 250μm down to 4μm. The results showed that the cubic law was found to hold whether the fracture surfaces were open or closed due to asperities or contact points and was independent of the rock type. In that particular investigation *f* was allowed to vary between 1.04 and 1.65. Raven and Gale, (1985) made measurements of fluid flow at different normal stresses with natural fractures in granite specimens of different sizes (ranging from 100mm to 294mm in diameter). The results obtained showed that the deviation from the cubic law increased with increasing loading cycles and specimen sizes. These effects are a direct result of the roughness or asperity characteristics of fracture surfaces.

The concept of channeling also became an increasingly important phenomenon in fractured porous media and was found to have a substantial effect on solute transport in such media (Tsang and Tsang, 1989). The wide range of aperture values in a single fracture gives rise to a very heterogeneous two-dimensional flow system. Thus the whole fracture plane is not uniformly conductive to water and the majority of flow occurs in flow paths of least resistance or more commonly referred to as channels (Tsang and Tsang 1989; Tsang et al., 1991) (Figure 2.3). Abelin et al., (1994) conducted channeling experiments to study the transmissivity and aperture variations in fractures in crystalline rock at the Stripa experimental mine in mid –Sweden. Two types of experiments were designed; however, both tests could not prove the transmissivity or aperture variability with any accuracy as explained below. In the single-hole test no obvious correlation between the observed aperture and the injected flow rate was observed. This was mainly attributed to the rough and undulating fracture surface. In the case of double-hole and tracer tests, the investigated fractures were intersected by other fractures, which basically diverted the flow in a manner similar to a porous medium in radial flow. The observations of the tracer movements lead to the conclusion that there exist dead end channels and that the aperture can be of the order of several hundred μm.

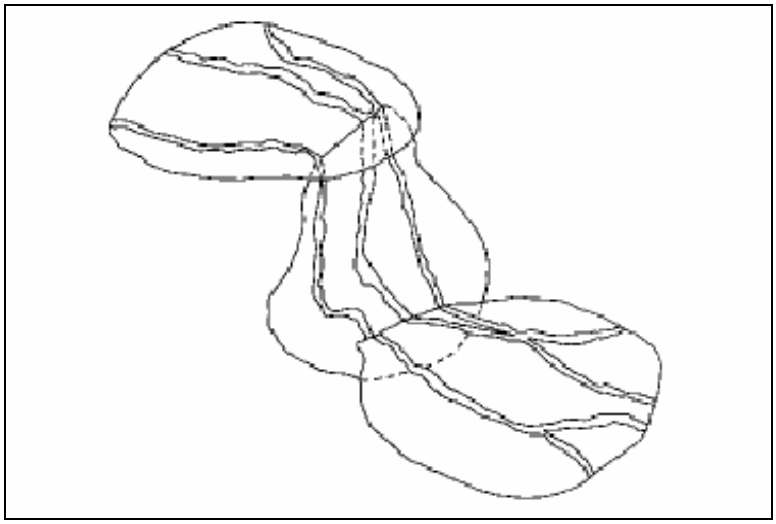

Figure 2.3 Illustration of tortuous channels of flow paths within a fracture (Tsang et al, 1991)

Transport and retardation in a single fracture can occur either by way of advection, hydrodynamic dispersion, matrix diffusion, sorption and decay. The solution of mass transport in fractured rocks with an impermeable matrix is governed by what is known as the advective – dispersion equation (Bear et al., 1993), assuming no advective transport in the rock matrix. The equation is:

Fracture	$\underbrace{R_f \frac{\partial c}{\partial t}}_{\text{Temp change of concentration}} = \underbrace{-v \frac{\partial c_f}{\partial x}}_{\text{Advection}} + \underbrace{D_L \frac{\partial^2 c_f}{\partial x^2}}_{\text{Dispersion}} + \underbrace{\frac{u_p . D_p}{b} \frac{\partial c_p}{\partial \gamma}}_{\text{Diffusion}} - \underbrace{\lambda R_f c_f}_{\text{Transformation}}$	Equation 20

Matrix	$\underbrace{\frac{\partial c_p}{\partial t}}_{\text{Temp change of concentration}} = \underbrace{\frac{D_p}{R_p} \frac{\partial c_p}{\partial \gamma^2}}_{\text{Matrix Diffusion}} - \underbrace{\lambda c_p}_{\text{Transformation}}$	Equation 21

Where

R_f = retardation coefficient of fracture surface [-]
c = concentration in the mobile (fracture) zone [ML-3]
v = average solute velocity in the fracture [LT-1]
Dh = hydrodynamic dispersion coefficient [L_2T-1]

2.2.1 Advection

Advection describes the movement of solutes and suspended matter with the pore water flow velocity. The amount of solute transported is a function of its concentration in the groundwater and the groundwater flow rate. In a saturated medium, this velocity can be calculated from Darcy's law (Fetter, 1999):

$$vx = \frac{K}{\eta_e}\frac{dh}{dl} \qquad \text{Equation 22}$$

Where

vx = average linear velocity (L/T)
K = hydraulic conductivity (L/T)
η_e = effective porosity (dimensionless)
$\frac{dh}{dl}$ = hydraulic gradient (L/L)

2.2.2 Matrix Diffusion

Matrix diffusion is a transport mechanism by which solutes are transferred from the water-flowing portions of permeable media to the non–flowing portions (matrix) and vice versa through molecular diffusion (Carrera et al., 1998). Diffusion will occur as long as concentration gradients exist, and can be expressed by Fick's first law in one dimension and under steady state conditions as (Fetter, 1999):

$$F = -D\frac{dC}{dx} \qquad \text{Equation 23}$$

Where

F = mass flux of solute per unit area per unit time
D = diffusion coefficient (L^2/T)
C = solute concentration (M/L^3)
$\frac{dC}{dx}$ = concentration gradient (M/L^4)

Systems in which concentrations are changing with time (unsteady state); Fick's second law applies (Drever, 1988):

$$\frac{\partial C}{\partial t} = D\frac{\partial^2 C}{\partial x^2} \qquad \text{Equation 24}$$

Where

$\frac{\partial C}{\partial t}$ = change in concentration with time ($M/L^3/T$)

The molecular diffusion coefficient in porous media, D, will be small as compared with that in water due to the resistance in the porous medium by the length and tortuosity of the flow paths (Drever, 1988). To account for this effect an effective diffusion coefficient must be used:

$$D' = \frac{D\phi}{\theta^2} \qquad \text{Equation 25}$$

Where

D' = effective diffusion coefficient,
D = diffusion coefficient in solution
ϕ = porosity
θ = tortuosity

The tortuosity factor (τ), which is a geometric parameter to account for the increased distance of transport, is expressed as the square of the ratio of the effective path length (l_e) to the shortest distance l. Hence, $l_e > l$ for porous media and τ is always greater than 1. At a microscale, the pore diffusion coefficient D_p includes the resistance to diffusion from the pore geometry $\frac{\delta}{\tau^2}$, where δ is the constrictivity of pores, which describe the cross-section variation in pore space and depends on pore and diffusing component sizes.

$$\tau = \left(\frac{l_e}{l}\right)^2 > 1 \qquad \text{Equation 26}$$

Over the last two decades many theoretical and experimental studies have shown the great influence matrix diffusion has on transport (Tsang and Tsang 1989; Tsang et al, 1991; Moreno et al., 1997). It is well documented in the literature that matrix diffusion is an important process for retarding solute transport in fractured rock, by allowing for solute storage within the often-large void space of the matrix. The matrix diffusion coefficient is a key parameter for describing the diffusion process in the rock matrix and the diffusive mass transfer between the fractures and the matrix. Laboratory experiments on rock matrix cores and field tracer tests at a larger scale have often been employed to estimate the matrix diffusion coefficient (e.g. Witthüser et al., 2003, et al., 2006 and Shapiro et al., 2007). Another feature of matrix diffusion is tailing effects observed in breakthrough curves, where solutes take a long time to diffuse out of the matrix. (Figure 2.4) shows an example of breakthrough curves with extensive tailing resulting from matrix diffusion (Bodin et al., 2003).

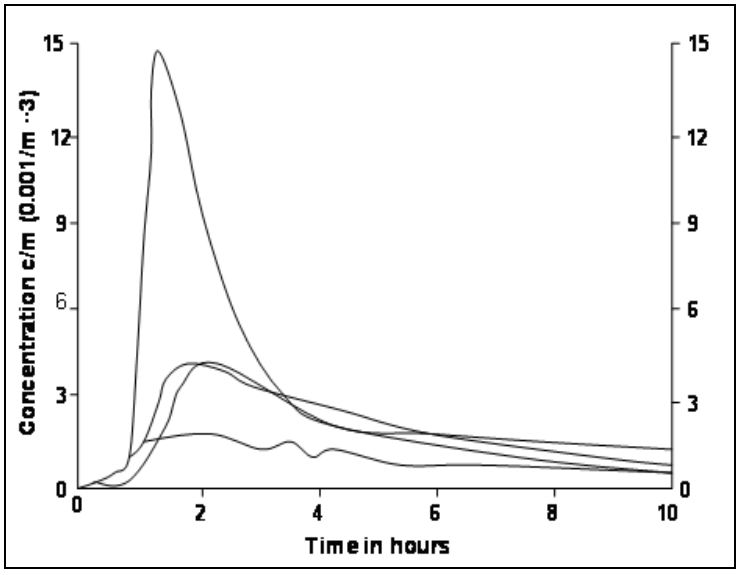

Figure 2.4 Tracer concentration curves in a multitracer experiment conducted in Chalk formation (Bodin et al., 2003).

This tailing effect, which is common to both channeling and matrix diffusion effects, emphasises possible problems in the interpretation of tracer experiments. It can be difficult to determine which mechanism the observed tailing represents. Tracer tests conducted by Becker and Shapiro (2000) proved that the tailing effect of breakthrough curves is not always as a result of matrix diffusion processes. It's been shown that tracers of varying diffusion coefficients produced identical late time breakthrough. This would imply that the tailings were not caused by any purely diffusive transport mechanism rather; this tailing resulted from hydrodynamic transport mechanisms such as advection and dispersion. The above authors hypothesise that this advection-dominated tailing results from the highly heterogeneous spatial and temporal nature of transport in fractured rocks. Based on laboratory experiments from rock matrix cores and field tracer tests to determine diffusion and distribution coefficients Witthüser et al., (2003) have shown that, due to the high matrix porosity of the chalk diffusion controlled tailing can be expected even for short distance tracer tests. A diffusion determined tailing can be identified by a decrease in the concentration of the tailing according to $t^{-1.5}$ as a criterion. This allowed a distinction to be observed between an injection/dispersion and diffusion determined tailing.

2.2.3 Mechanical dispersion

Mechanical dispersion describes the macroscopic phenomenon whereby dissolved constituents as well as suspended particulates and colloids are transported with different velocities and in different directions along the flow path as a result of inhomogeneities in porous media and variations in pore water velocity. Dispersion in general is caused by a number of factors including:

1. Pore size – whereby, some pores are larger than others and allow fluid to move faster,
2. Path length – some solute particles travel along longer flow paths to go the same linear distance,
3. Friction in pores – fluids move faster through the centre of pores than along the edges.

Mixing that occurs along and perpendicular to the direction of the flow path is termed longitudinal and transversal dispersion. In the case of an advancing solute front, spreading will occur in directions normal to the direction of flow because at the pore scale the flow path can diverge (Fetter, 1999). This type of mixing in the direction normal to the flow path is called transverse dispersion. Mechanical dispersion due to the preceding factors is equal to the product of the average linear velocity and the dynamic dispersivity (α).

Mechanical dispersion = $\alpha_L \, v_X$	Equation 27

Dispersion is generally higher in the flow direction (longitudinal) than in the direction perpendicular to the flow (transversal and vertical). It is scale dependent and increases with the scale of measurement, due to the heterogeneous nature of the aquifer material (Berkowitz, 2002). Flow channeling within the fracture is widely recognised to have a huge effect on dispersion (Berkowitz, 2002).

2.2.4 Hydrodynamic dispersion

Hydrodynamic dispersion is the flux of solute due to the combined effect of molecular diffusion and mechanical dispersion, described by the following equation (Fetter, 1999):

$D_L = \alpha_L \; v_X + D^*$	Equation 28

Where

D_L = the longitudinal coefficient of hydrodynamic dispersion (L^2/T)
α_L = the dynamic dispersivity (L)
v_X = the average linear groundwater velocity (L/T)
D^* = the effective molecular diffusion coefficient (L^2/T)

The effects of mechanical dispersion are generally much greater than those of molecular diffusion, and except at low groundwater velocities; the contribution of molecular diffusion is almost negligible (Berkowitz, 2002).

2.2.5 Sorption

In most cases transport can be strongly affected by interactions between the solutes and the rock minerals. Various kinds of mechanisms can be involved (Bodin et al., 2003):

1. Electrostatic interactions, generally between negatively charged mineral surfaces and cationic species in solution.
2. Electromagnetic interactions (Van Der Waal's forces).
3. Chemical interactions i.e. chemical bonds between the solute and the grain surface.

Most sorption reactions are considered instantaneous and reversible. Diffusion and sorption reactions play a major role in the retardation of solutes in geological formations. Due to matrix diffusion being a relatively slow mechanism, solute sorption mainly occurs at the fracture surface when flow is fast. For long residence times, sorption reactions mainly occur within the matrix because the available exchange surfaces in the matrix are much more important than those in the fracture (Bodin et al., 2003). The experimental method commonly used to characterise the sorption properties of a rock is the batch technique. It consists of generating an equilibrium condition between a solution of known initial concentration and crushed rocks and calculating the fraction of mass adsorbed at the grain surface. However, sorption parameters inferred from such experiments should be treated with vigilance as rock crushing can increase the surface area available for solute sorption (Bodin et al., 2003). A plot of adsorbed contaminant concentration C^* fixed on solid surfaces, as a function of contaminant concentration C in the liquid phase is known as an adsorption isotherm (Figure 2.5). The most common sorption isotherms are linear (Henry), Freundlich and Langmuir (Domenico and Schwartz, 1998).

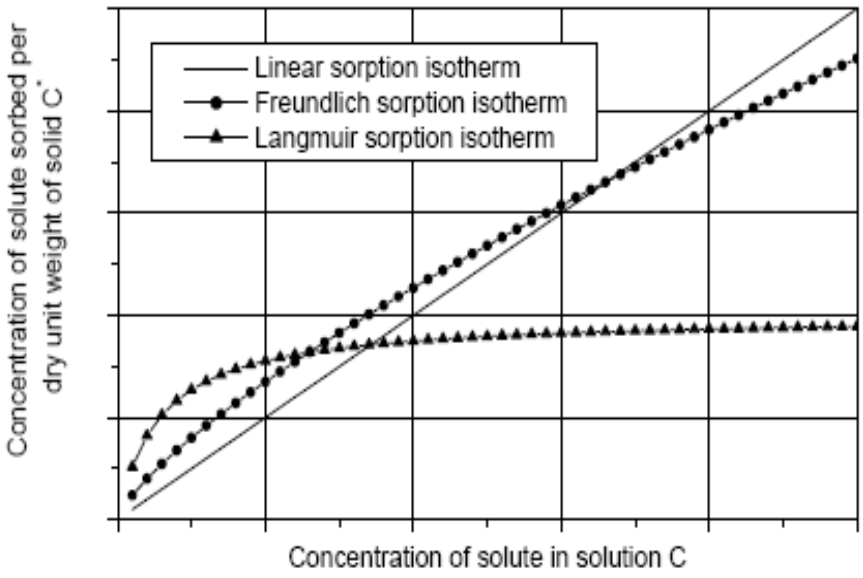

Figure 2.5 Sorption Isotherms (Domenico and Schwartz, 1998)

Linear (Henry) sorption isotherm

A linear relationship between the amount of a solute sorbed onto solid C* and the concentration of the solute C, the adsorption isotherm of C, as a function of C* will plot as a straight line (Figure 2.5). The equation for a linear (Henry) isotherm is given by:

$$C^* = K_d C \qquad \text{Equation 29}$$

Where

C^* = mass of solute sorbed per dry unit weight of solid (mg/kg)
C = concentration of solute in solution in equilibrium with the mass of solute sorbed onto the solid (mg/L)
K_d = distribution coefficient (L/kg)

Attenuation due to sorption can be described by the retardation equation as follows:

$$1+\frac{B_d}{\theta}K_d = R_f \qquad \text{Equation 30}$$

Where

B_d = bulk density of the aquifer (M/L^3)
θ = volumetric moisture content or porosity for saturated media (dimensionless)

R_f = retardation coefficient

This dimensionless retardation factor (R_f), is a measure of the attenuated transport of a reactive contaminant species compared to the advective behavior of groundwater (Hiscock, 2005).The major drawback associated with this particular isotherm is that there is no limit to the amount of solute that can be sorbed onto the sorbent (Fetter, 1999).

Freundlich sorption isotherm

The Freundlich isotherm is a non linear isotherm and is described as follows (Fetter, 1999):

$$C^* = KC^N \qquad \text{Equation 31}$$

Where K and N are constants.

When C is plotted as a function C* the data will be curvilinear (Figure 2.5), however the data can be linearised by using the following equation:

$$\log C^* = \log K + N \log C \qquad \text{Equation 32}$$

Langmuir sorption isotherm

This isotherm was developed with the concept that the solid surface possesses a finite number of sorption sites. When all the sorption sites are filled, the surface will no longer sorb solute from solution. The equation is given by (Fetter, 1999):

$$\frac{C}{C^*} = \frac{1}{\alpha\beta} + \frac{C}{\beta} \qquad \text{Equation 33}$$

Where

α = adsorption constant related to the binding energy (L/mg)

β = maximum amount of solute that can be absorbed by the solid (mg/kg)

Important to note is that when the Langmuir sorption isotherm is plotted it will give a curved shape that has a distinctive upper limit, referred to as the sorption capacity (Figure 2.5).

2.2.6 Decay/Transformation

The rate of decay of a radioactive parent nuclide to a stable daughter product is proportional to the number of atoms, *n*, present at any time *t* (Dickin, 2005). If radionuclides enter the groundwater system the cations and to a lesser degree anions will be subjected to retardation processes on soil surfaces. Furthermore, radionuclides undergo radioactive decay, reducing the concentration in both the dissolved and sorbed phases (Fetter, 1999). Some solutes can also be adsorbed onto the fracture walls and undergo biodegradation reactions. Generally decay reactions obey first order kinetics, given as (Bodin et al., 2003):

$$\frac{\partial c}{\partial t} = -\lambda c \qquad \text{Equation 34}$$

Where

λ (T^{-1}) = decay constant (T^{-1})

The decay constant states the probability that a given atom of a radionuclide will decay within a stated time.

A useful way of referring to the rate of decay of a radionuclide is the half – life, $t^{1/2}$, which is the time required for half of the parent atoms to decay (Dickin, 2005):

$$t^{\frac{1}{2}} = \frac{\ln 2}{\lambda} \qquad \text{Equation 35}$$

2.3 CHEMICAL PROPERTIES OF URANIUM AND THORIUM

Martin H. Klaproth whilst experimenting with pitchblende in 1789 discovered uranium (Kotz and Treichel, 1999). Uranium is in the actinide series, corresponding to the filling of the 5f electron orbital subshell. When it is refined its a dense silvery white weakly radioactive metal that is slightly softer than steel and has an atomic number of 92 and a relative atomic mass of 238.03 g/mol.

The element is weakly radioactive and contributes to natural background environmental radiation. Thorium was discovered later in 1828 by a Swedish chemist named Jöns Jacob Berzelius (Kotz and Treichel, 1999). It occurs also in the actinium series with an electron configuration of $6d^2\ 7s^2$ and has a silvery white metallic appearance with an atomic number of 90 and a relative atomic mass of 232.03 g/mol. In groundwater, the weathering of uranium bearing rocks and minerals is the main source of dissolved uranium. Uranium in particular is very mobile and soluble under oxidising conditions, whereas thorium is rather immobile and insoluble under similar conditions (Giammar, 2001). As a result uranium can be a major pollutant in the subsurface, where it occurs predominantly as the uranyl dioxo ion (UO_2^{2+}).

2.3.1 Modes of Radioactive Decay

Some radioisotopes are known to decay by more than one mechanism. For instance, isotopes in the U^{238} decay series (as will be shown later) decay by emitting α or β particles, with a simultaneous emission of γ - radiation (Ivanovich and Harmon, 1982). Naturally occurring uranium is a mixture of three isotopes and contains about 99.27% U^{238}, 0.72% U^{235} and 0.0054% U^{234} with each one beginning a cascade of daughter products referred to as a radioactive decay series (Ivanovich and Harmon, 1982). The uranium series is also the longest known series, which ends with the stable isotope of Pb^{206}. U^{238} is the chief constituent of natural U (99.27%) and is the progenitor of the (4n +2) series of radioactive elements (Ivanovich and Harmon, 1982).

According to Langmuir (1997), there are three modes of radioactive decay, denoted by, α, β and γ. Alpha (α) particles are identical to the nuclei of helium atoms, with a mass of 4 atomic mass units (1amu = 1.661 x 10^{-27}kg) and a charge of +2. Following α decay, the α particle accumulates two electrons from its surrounding environment, thereby balancing its charge and becoming a helium atom ($\frac{4}{2}He$). When α - decay occurs, a daughter element is produced along with a α particle and this occurs with the conservation of momentum. Therefore, the newly produced daughter element recoils in the opposite direction from that in which the α particle was emitted. This concept is known as alpha recoil, with recoil distances in water and air being significantly larger than in solids (Langmuir, 1997). Alpha particles have limited penetrating power and can easily be stopped by several sheets of ordinary paper or clothing (Kotz and Treichel, 1999). Beta (β) particles are identical to electrons emitted from the nucleus, with a mass of 5.49 x 10^{-4} amu and a charge of -1. The β particles are electrons ejected at high speeds from some radioactive nuclei. They are more penetrating than alpha particles and thus require a piece of aluminum to be stopped (Kotz and Treichel, 1999). Gamma rays (γ) are electromagnetic radiation with wavelengths shorter than those of X – rays (Langmuir, 1997). Gamma (γ) rays have no electrical charge and are not

affected by an electric field. Gamma (γ) radiation is the most penetrating radiation because it passes completely through the human body.

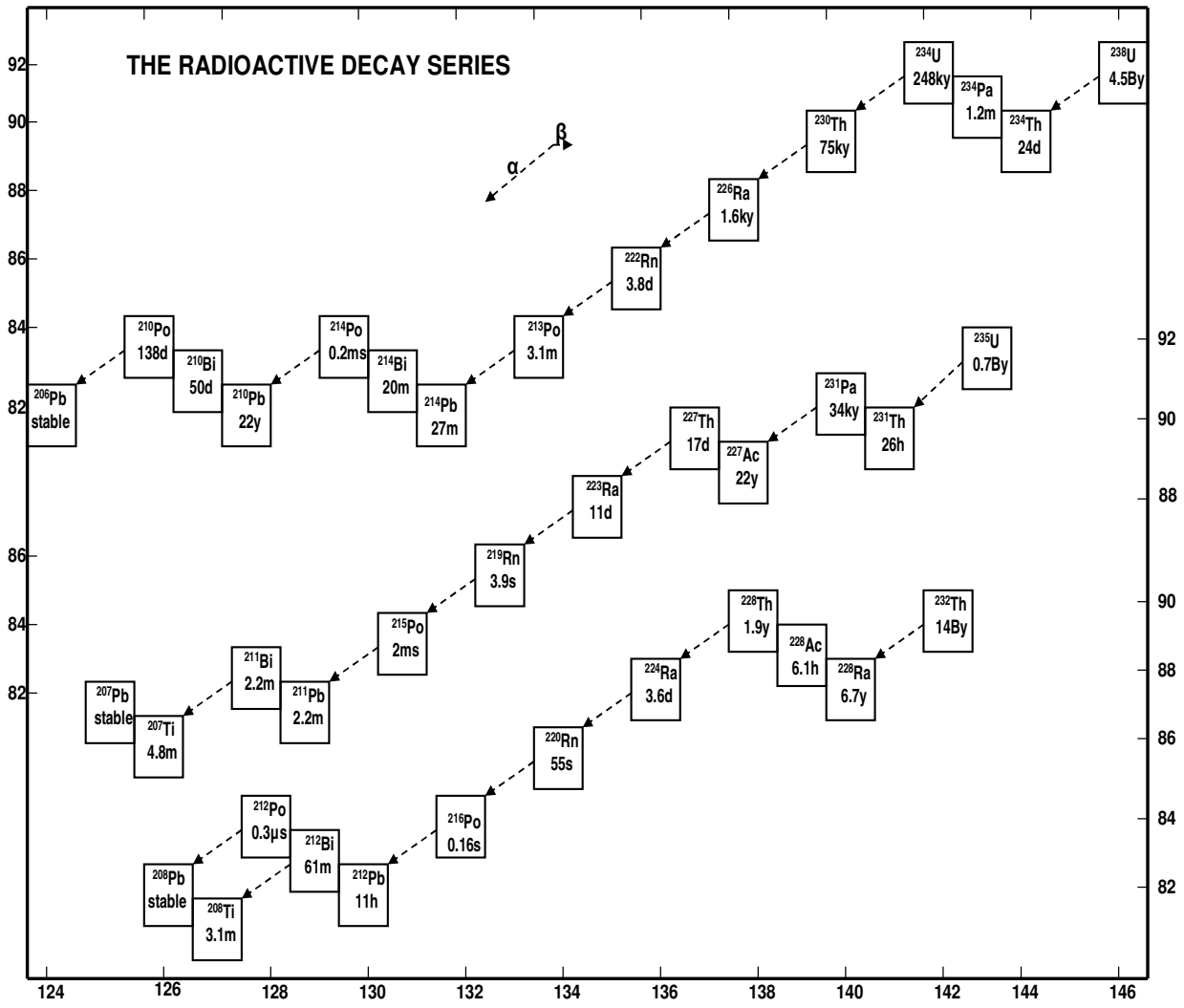

Figure 2.6 The Uranium decay series (modified from Dicken, 2005).

U^{238} is an alpha emitter with a half -life of 4.51 x 10^9 years corresponding to a specific activity of 0.747 disintegrations per minute. The actinium series (4n + 3) begins in nature with the radionuclide of U^{235} and ends with the stable lead isotope Pb^{207} (Ivanovich and Harmon, 1982). U^{235} has a half – life of 7.1 x 10^8 years and is also an alpha emitter with a very much complex alpha spectrum and a correspondingly complex gamma spectrum (Figure 2.6). Th^{232} is the third decay series of the three naturally occurring series of radioactive elements and is the longest lived member of the (4n) series with a half – life of 1.4 x 10^{10} years (Figure 2.6).In this particular decay series a significant branch at

Bi^{212} occurs , which undergoes either α or β decay. The half – lives of the two decay modes of Bi^{212} are given as 1.15 x 10^{-4} years, indicating the cumulative half – life of both types of decay (Langmuir, 1997).

2.3.2 Aqueous Uranium Geochemistry

Uranium occurs naturally in oxidation states 4+, 5+, and 6+, which are usually written as U(IV), U(V) and U(VI) (Langmuir, 1997). However, under environmental conditions, only the tetravalent and hexavalent states are known to be stable. According to (Giammer, 2001), the solubility of uranium in aqueous systems is controlled by three factors, oxidation – reduction potential, pH and dissolved carbonate content. Uranium (VI) is considerably more soluble than uranium (IV) and under reducing conditions uranium (IV) forms complexes with hydroxides or fluorides as the only dissolved species.

A study conducted by Vogel et al., (1999), who evaluated the rate of migration of a uranium deposition front within the Uitenhage aquifer (Cape Province, South Africa), clearly showed that the solubility of uranium in groundwater is very sensitive to changing redox conditions. U^{238} isotopes were employed to study the historical evolution of the reducing barrier. Radium and radon were then used to evaluate the path of migration that the front of the oxygen depletion zone has taken over the past 10^5 years. Uranium was reduced and found to precipitate as it flowed into the oxygen depleted front. This process is often referred to as roll-front or tongue-type deposits, which is an example of epigenetic deposits (Hobday and Galloway 1999). Coupled with this decrease was a rise in the U^{234}/U^{238} activity ratio indicating that the U^{234} isotope has been injected into the water by the process of alpha recoil. In pure water and under oxidising conditions the U(VI) species exists as the soluble uranyl (UO_2^{2+}) species along with the U(IV) species or uranous ion and their respective hydrates. The uranous species is insoluble; hence the U(VI) species is most commonly encountered as (UO_2^{2+}) and UO_2CO_3 species under normal groundwater conditions. Under very low pH conditions(<3) and oxidising conditions uranium occurs as the free ion U^{4+} and as UOH^{3+}, which is typical of acid mine drainage waters (Figure 2.7). Bain et al., (2001) developed a reactive transport model (MIN3P) to evaluate the potential effects of mine closure on the geochemical evolution in an aquifer down gradient from the Konigstein uranium mine

located in Saxony, Germany. It was shown that at lower pe values, the reduction of infiltrating dissolved U(VI), the precipitation of uraninite and removal of uranium from solution occurred. The ability of uranium to exist in either it's oxidised or reduced state is a function of both the pH and Eh (Figure 2.7).

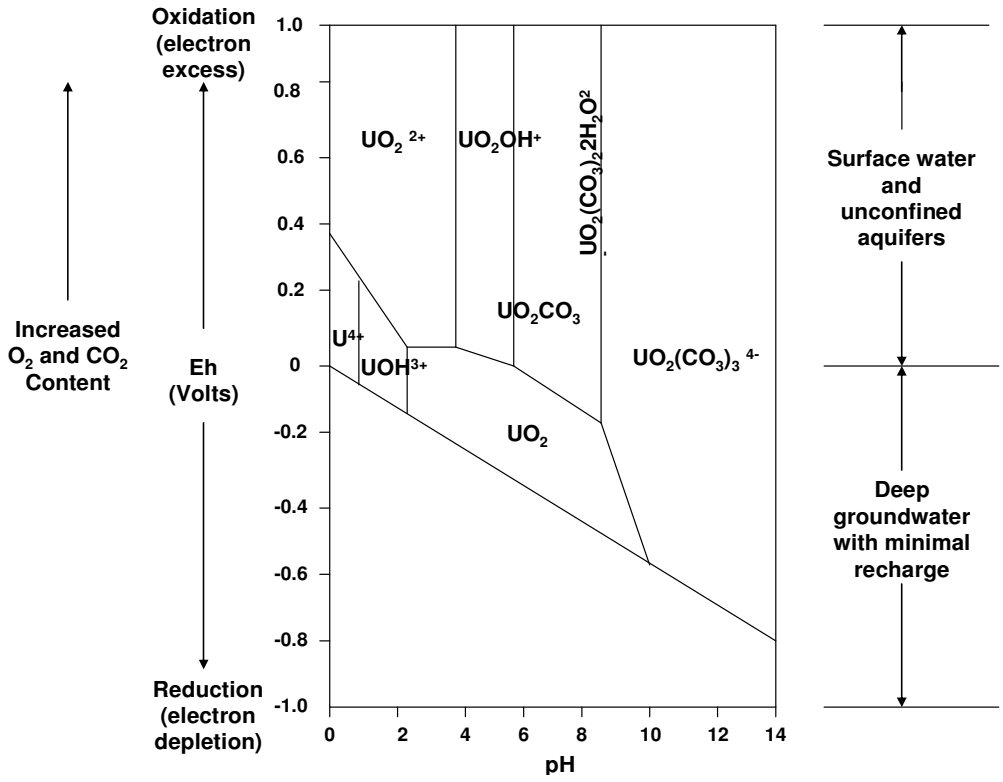

Figure 2.7 Phase diagram of uranium speciation (Grainger, 1985).

The uranyl species normally occurs only at very low pH (<5), however under normal pH conditions (6 – 9) the U(VI) hydroxyl form of $(UO_2)_3(OH)_5^-$ is the dominant species of UO_2CO_3 and $UO_2(CO_3)_2$ in the presence of dissolved oxygen and carbon dioxide (Figure 2.8). It is important to note that although the speciation of dissolved uranium (VI) is likely to be dominated by hydrolysis and carbonate complexes, sulphate, fluoride and organic ligand complexes may also occur in environmental systems (Giammar, 2001). Amongst the complex uranium ions, uranyl carbonate ions are the most stable and will predominate not only in the bicarbonate, but also in the neutral sulphate, chloride, weakly acidic and weakly alkaline groundwaters. Ivanovich and Harmon, (1982), pointed out that normal groundwaters with pH values of 4.5 – 8 and under

anoxic conditions, uranium will be mobilised as the hydroxyl complex $U(OH)^{5-}$, whereas it is immobile under most anoxic conditions and usually precipitates a urananite.

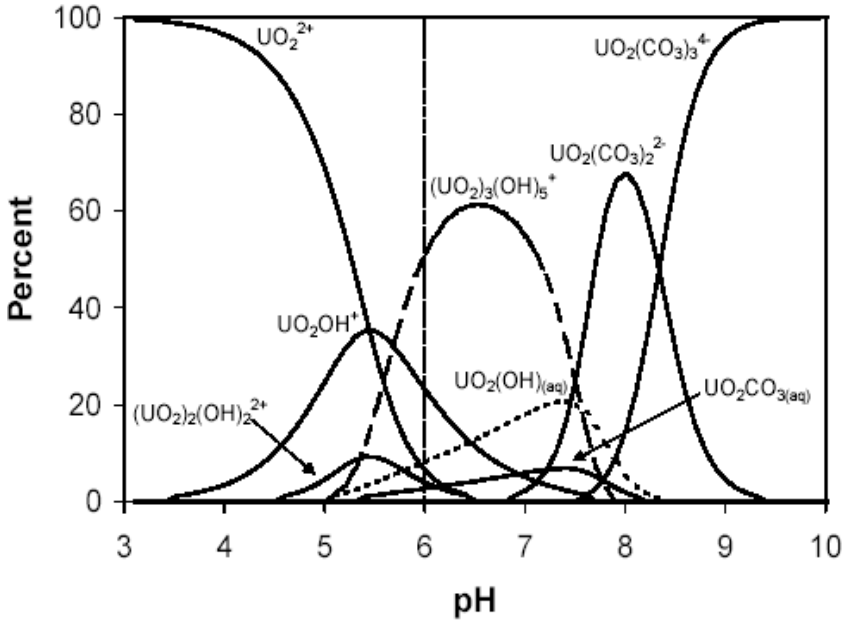

Figure 2.8 Speciation of dissolved uranium as a function of pH for (U) tot = 5µM, 1 = 0.1M, and $P_{CO2} = 10^{-3.5}$ atm. The calculations were made without considering the precipitation of any solid phases (Giammer, 2001).

2.3.3 Water Quality Guidelines

Environmental radiation originates from a number of naturally occurring and anthropogenic sources (WHO, 2005). By far the largest proportion of human exposure to radiation comes from natural and external sources of radiation, including cosmic and terrestrial radiation and from inhalation or ingestion of radioactive materials. The contribution of drinking water to total exposure is typically very small and is largely due to naturally occurring radionuclides in the uranium and thorium decay series. On average our radiation exposure due to all natural background sources amounts to approximately 2.4mSv/year (WHO, 2005). However, this figure can vary depending on the geographical location by several hundred percent (DWAF, 2002). The (WHO, 1993) guidelines for drinking-water quality recognised uranium as a potential chemical risk but concluded that insufficient data were available to derive a realistic guideline value at the time. The (WHO, 1998) addendum to the guideline incorporated a provisional value of 2µg/l based on a tolerable daily intake by ingestion of 0.5 µg per kg body weight (soluble uranium). On the basis of currently-available data for sources of uranium in the human diet, WHO has recently revised the standard for drinking water and as a result the (WHO, 2005) guidelines specify a provisional guideline value of 15µg/l. For comparison purposes the US-EPA in 2006 introduced a maximum contaminant level (MCL) for uranium in drinking water of 30µg/l. This is applicable to public supplies in the USA. The level set followed an initial proposal of 20 µg/l set in 1991 with the drinking water standard in Canada being the same.

It has been noted that in certain parts of the world, such as the Kerala state in India and the Pocos Del Caldas in Brazil, levels of background radiation are relatively high (WHO, 2005). The levels of exposure for the general population in such areas may be up to 10 times higher than the average background level of 2.4mSv/year given above. In the case of uranium, chemical toxicity is of more concern than the actual radiological risk of cancer (DWAF, 1996). In recent years, there has been increasing concern that the chemical effects of uranium may also pose a potential hazard to exposed populations. Toxic effects of exposure include nephritis (kidney disease) and other organs at risk from chronic radiological toxicity include the lymph nodes and the bone. A study

conducted by Kurttio et al., (2002) on the renal effects of uranium in drinking water, whereby measurements of uranium concentrations in drinking water and urine of 325 persons using drilled boreholes for drinking purposes showed significantly altered tubular function with uranium concentrations exceeding 300µg/l. This is far above the recommended guideline values given above WHO (15µg/l) and the US-EPA (30µg/l) respectively (U.S. EPA, 2006). From a local perspective the South African water quality guidelines for domestic use are shown in (Table 2.1), along with the radiological dose calculations and water quality evaluation guidelines for domestic water use given in (Table 2.2).

Table 2.1 Effects of uranium-238 on human health (DWAF, 1996).

U-238(mg/l) (mg/l)	U-238 (Bq/L)	Colour Class	Effects
Target water quality range 0 - 0.070	Target water quality range 0 - 0.070	Blue,Ideal (<0.25Bq/l)and Green (0.25 to 0.89 Bq/l)	No Significant risks.Annual cancer risk less than one in four million
0.070 - 0.284*	0.89 - 3.6	Yellow	Annual risk < one in a million May potentially be a slight risk of renal toxicity in sensitive individuals where renal functions is impaired, but unlikely to have demonstrable renal toxicity in healthy individuals.
If 0.284 mg/l is exceeded, human health may be at risk due to chemical toxicity.			
0.284 - 1.42	3.6 - 18	Red	Annual cancer risk less than one in 200 000 but significant risk of chemical toxicity with renal damage
> 1.42	>18	Purple	Increasing cancer in long term. Increasing risk of renal damage in short term.

Table 2.2 Different ranges of water quality (DWAF, 2002).

Class /Colour	*Dose range; mSv/a*	*Health Effects and Typical Exposure Scenarios*	*Intervention Decision Time Frames*
Class 0 (Blue - Ideal water quality)	0.01 – 0.10	• There are no observable health effects. • This is the range of exposure from ideal quality water sources. • Most treated water falls in this water quality range. • Additional doses that result from human activities that fall within this range are difficult or impossible to determine and/or to distinguish from variations in background doses with sufficient confidence.	Intervention not applicable for this class of water.
Class 1 (Green - Good water quality)	> 0.10 – 1	• There are no observable health effects. • It is the range of exposure from some natural and untreated water sources (e.g. ground water / wells) as well as water sources that could be influenced by mining and mineral processing activities. • A dose between 0.2 to 0.8 mSv/a is the typical worldwide range of ingestion radiation dose resulting from water as well as food. • A dose equal to 1 mSv/a corresponds to the regulatory public dose limit for human activities involving radioactive material.	No intervention is required although ALARA principles apply.
Class 2 (Yellow - Marginal water quality)	> 1 – 10	• A small increase in fatal cancer risk associated with this dose range. • Probably only a small number of natural water sources of this quality exist, resulting from exceptional geological conditions. • Abnormal operating conditions at some nuclear certified mineral and mining processes may result in a dose in this range when a person drinks the untreated water. Intervention will most likely be required to improve the quality of water that is released into the public domain. • The total natural background radiation from all exposure pathways, not only water, falls in this range.	Intervention considerations within 2 years.
Class 3 (Red - Poor water quality)	> 10 – 100	• Health effects are statistically detectable in very large population groups. • This range represents excessive exposure. • It is highly unlikely to find water of this poor quality in the natural environment.	Intervention is required in less than 1 year.
Class 4 (Purple - Unacceptable water quality)	> 100	• Health effects may be clinically detectable and a significant increase in the fatal cancer risk (greater than one in a thousand). • A dose greater than 100 mSv can usually only occur during a major accident at a nuclear facility. These facilities have to demonstrate that such an accident cannot happen with a frequency of more than once in a million years.	Immediate intervention is required.

2.4 BEHAVIOUR OF RADIONUCLIDES IN FRACTURED AQUIFERS

Numerous studies dealing with the transport mechanisms of U-Th series radioisotopes have been discussed at length in the literature (Rama and Moore 1984, Folger et al., 1997, Przylibski, 2000 and Wood et al., 2004) to determine exactly which of these mechanisms play a dominant role in aiding the release of radon, which is the daughter isotope of uranium to groundwater. Radon (Rn^{222}, half – life 3.84 days) is a colorless, odorless, tasteless, chemically inert, radioactive and volatile noble gas, which is continuously produced in rocks and soils through α- decay of Ra^{226} (Bonnoto and Mello, 2006). Some atoms of Rn^{222} escape from rocks and soils into the surrounding

phases, such as groundwater or air. Most groundwater contains readily detectable quantities of radon, which occur in greater amounts in comparison to the dissolved radium concentration. A simple method for estimating the coefficient of radon emanation from crystalline rocks in the Sudety Mountains (SW Poland) into groundwater was proposed by (Przylibski, 2000). The method took into consideration the important petrophysical factors of the source rock, particularly the content of parent isotopes of radon, the effective porosity and its permeability as this would have a direct influence on the radon concentration in groundwater. The highest values of emanation coefficients (41, 33 and 21%), were obtained in areas of tectonic dislocations (faults) and the lowest ones where rocks are sparsely fissured or cracked just outside the major dislocation zones of (9 and 7%).The high variability of dissolved Rn^{222} in water of fractured rocks was proposed with a physically based surface area to water volume model (Folger et al., 1997). As with uranium – mineralisation models, alpha recoil along with matrix diffusion from the matrix to the fractures provides the means for Rn^{222} to enter the groundwater system. Rama and Moore, (1984), argued that there is a problem with the basic assumption regarding the release of Rn^{222} and non gaseous isotopes into the groundwater directly and dominantly by recoil mechanisms, and proposes another model to explain the variable Rn^{222} activities in groundwater.

This model relies on the presence of nanopores within the rock, which act as intermediary channels for Rn^{222} transport after being generated predominantly within the solid matrix of the rock itself (Figure 2.9). Wood et al., (2004), state that the above model does not explain how or why these nanopores are formed and does not require the existence of chemical or weathering produced substrates for the accumulation of Rn^{222} precursors. It therefore remains unclear why most of the groundwater should not contain very high activities contrary to observations or why elevated Rn^{222} activities seems to be found more often in water from fractured – rock aquifers rather than primary porosity aquifers, given the similar uranium activity in both rocks. A chemically based model that provides an explanation for the high radon activity in groundwater in fractured rocks was proposed by Wood et al., (2004). In their chemically based model, Ra^{226} (half–life 1601years) is transported by Fickian diffusion from the matrix to the fracture surface, where it is sorbed on ion exchange minerals formed from weathering of

the fracture surfaces. Due to the fact that Ra^{226} is sorbed on the fracture surface, this sorption removes it from the matrix, thus ensuring an activity gradient towards the fracture and in turn providing a continuous supply of Ra^{226} to the fracture surface (Wood et al., 2004). It is important to note that radium, unlike uranium, is not redox –sensitive and can therefore diffuse readily in oxygen depleted environments typical of matrix blocks between fractures. The decay of radium is what provides Rn^{222} to the adjacent water filled fracture via diffusion and alpha recoil. The fundamental difference between this diffusion/ion exchange model and the other models mentioned thus far is that it predicts the presence of Ra^{226} sorbed on or near the fracture surface without significant amounts of its parent radionuclide U^{238}. The model also provides a mechanism for both chemical and isotopic separation missing in the previous models.

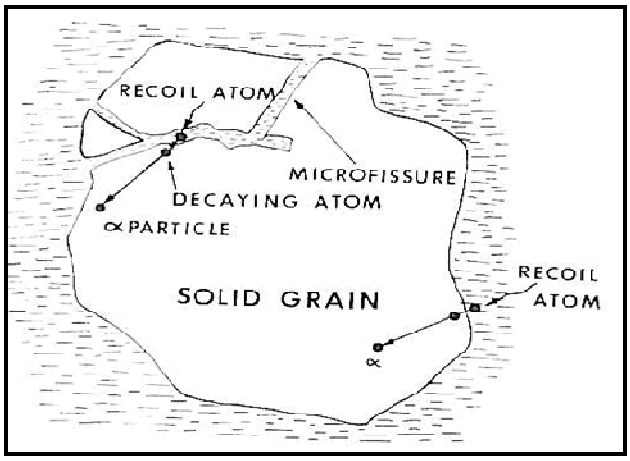

Figure 2.9 Illustration of how Radon and other U – Th series isotopes enter the nanopores by recoil in approximately equal quantities. Radon diffuses out of the nanopores, while others are adsorbed on the walls of these nanopores (Rama and Moore, 1984).

CHAPTER 3- STUDY AREA

3.1 INTRODUCTION

Historically, uranium mineralisation in the Karoo Basin was first reported in 1964, during the search for onshore oil and gas (Hoadley, 2007). This gave impetus to several international companies developing a keen interest in the Karoo sequences, based on similarities noted with the deposits of the Colorado Plateau in the USA (Cole et al., 1991). By the mid-seventies no less than eleven private companies as well as the former Geological Survey of South Africa and the Nuclear Development Corporation of South Africa (Pty) Ltd were vigorously engaged in uranium exploration and geological studies in the Karoo basin (Cole et al., 1991). Sandstone-hosted uranium was first discovered in the Karoo on the farm Grootfontein, some 20km west of Beaufort West in 1969. Eventually, more than two hundred sandstone –hosted uranium occurrences were discovered of which Ryst Kuil proved to be the most successful (Van der Merwe and de Beer, 2006). Esso Minerals Africa Inc. (ESSO), by far the most committed and successful exploration company active in the Karoo at the time, started their exploration programme in 1974. By 1976, they had located outcropping mineralisation on the farm Ryst Kuil, and following an intense drilling campaign, had defined the extent of an approximately 70km strike length subsurface fluvial sandstone channel and several large, discontinuous, uranium-molybdenum deposits. Most of their effort was focused on the deposits of the “Western Sector” where they established a uranium deposit of 10,997,000 t, containing in excess of 25 Mlbs[2] U_3O_8 at a grade marginally greater than 1,000 ppm (Hoadley, 2007).

3.2 SITE LOCATION

The study area is situated approximately 450 kilometers northeast of Cape Town along the N1 route, which connects Cape Town with cities like Kimberley, Bloemfontein and Johannesburg between 32° 0' 10" S and 32° 5' 27" S and 22° 4'40" E and 22° 9'15" E. Immediately north of Beaufort west, the Nuweveld Mountains rises up to a plateau of approximately 1450m above mean sea level. The Nuweveld Mountains are characteristically flat-topped, being capped by thick sheets of erosion-resistant dolerite. Beaufort West lies at the base of the escarpment, which acts as a watershed between the north and south-flowing rivers (Figure 3.1).

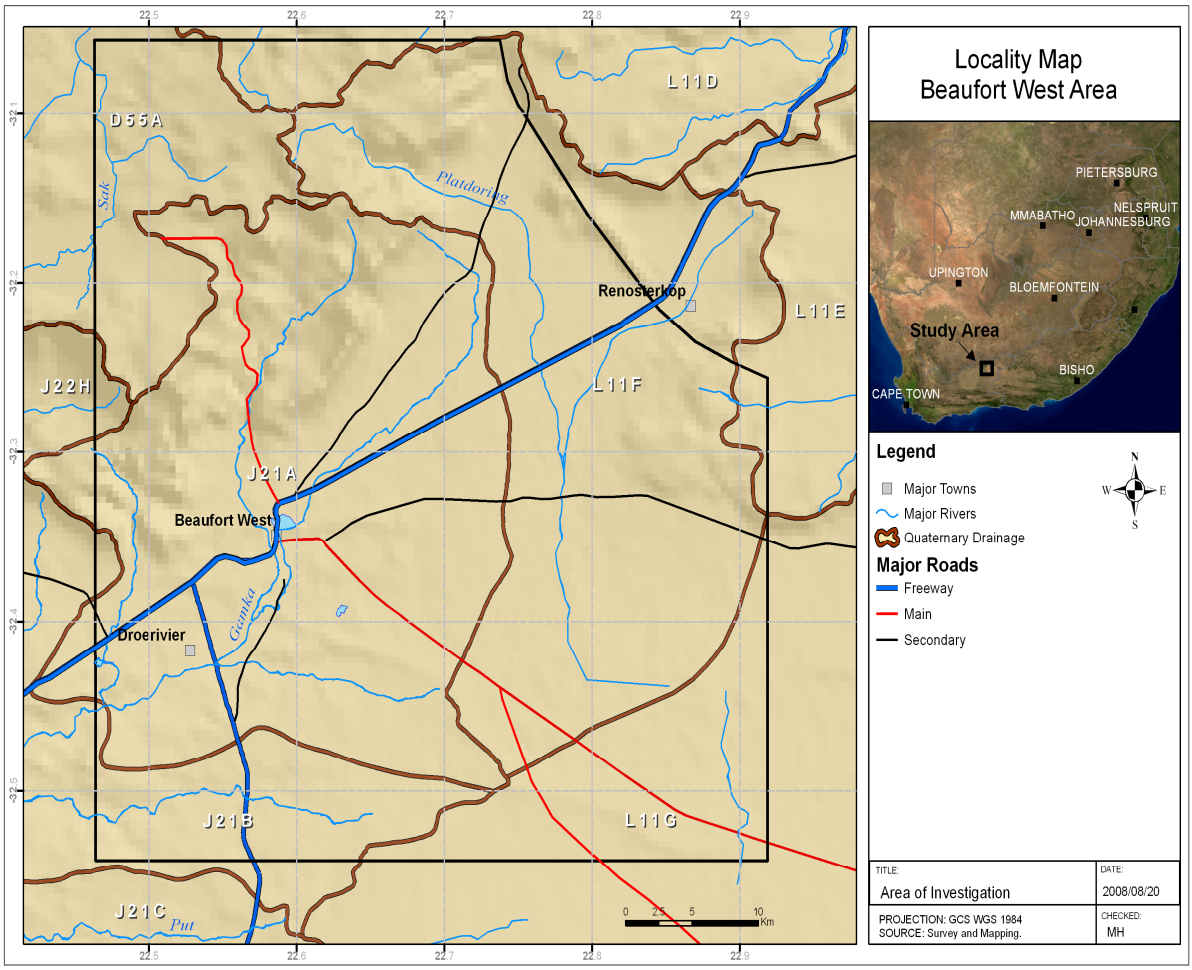

Figure 3.1 Location of the study area in Beaufort West.

3.3 CLIMATE AND PHYSIOGRAPHY

Beaufort West falls in a late summer rainfall area (Oct-March) with an average rainfall of 236mm/annum, however this value can increase to 400mm in the high mountainous terrain and as low as 100mm in the flat lying plains. Continuous long term rainfall data for the past thirty eight years was obtained from the Beaufort West municipality and is illustrated in (Figure 3.2). The position of the Beaufort West rain gauge of the Weather Bureau (rain gauge no.00921414) has varied considerably over the past years, and is the only reliable long-term rainfall record available.

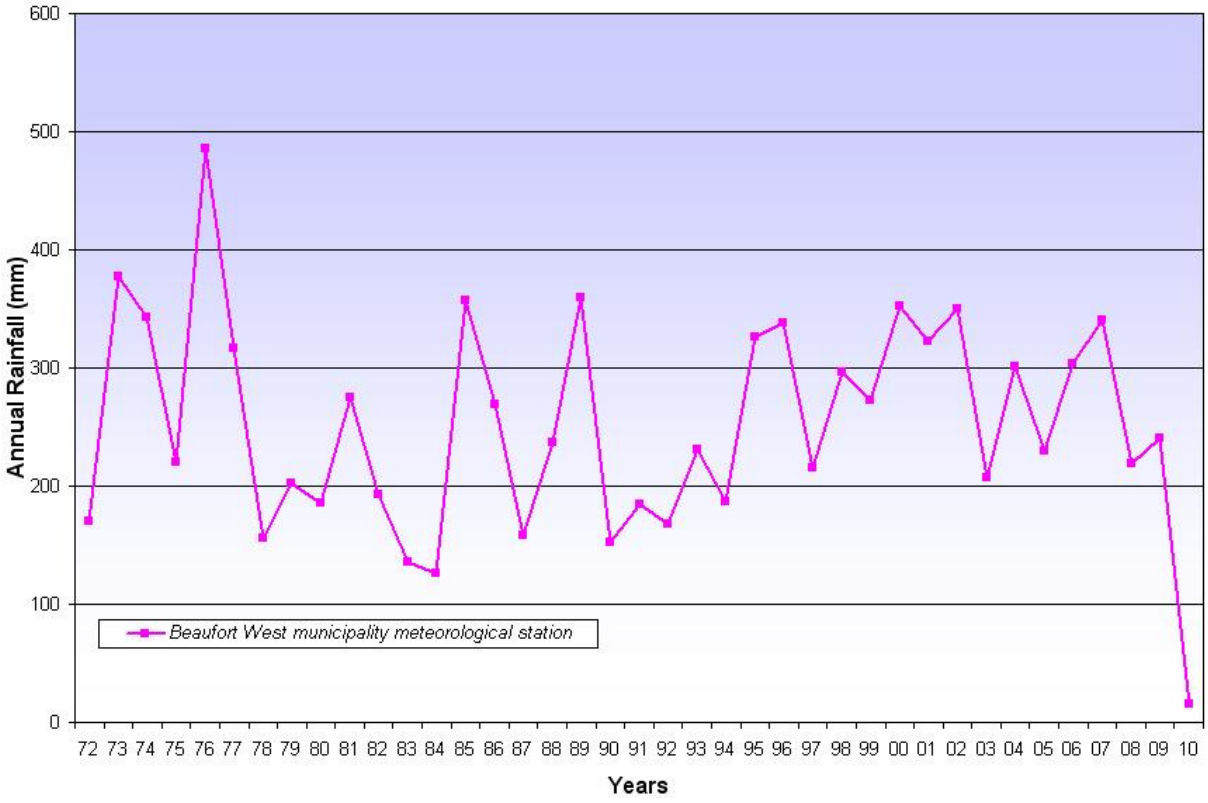

Figure 3.2 Long-term annual rainfall for Beaufort West.

The mean annual potential evaporation (MAPE) generally exceeds 2400mm/annum, with an average of 2445mm/annum (Woodford and Chevallier, 2002).The average daily temperature variations is 10℃ to 25℃ with the highest recorded in November to February of 41℃ and the lowest from June to August of -5℃ to -6 ℃ (Van der Merwe and de Beer, 2006)**.** The area is reported to be extremely windy with most northwesterly winds attaining maximum speeds during the afternoon. Surface water bodies are made up of two main perennial rivers, the Gamka and Kwagga rivers. In addition to these two perennial rivers there are three main dams, namely the Beaufort West dam, walker's dam and the pap dam. These open water bodies are subjected to extreme temperatures ranging from 32℃ to as low as -4 ℃.The dominant veld type is that of the central upper Karoo (as described by Acocks, 1988) and the upper Nama Karoo. Arid shrublands have developed on the sandstone-derived soils. This vegetation type includes dwarf shrub species and perennial grasses. The river beds and protected cliffs and ravines often contain denser and taller growing shrubs and trees consisting predominantly of Acacia karroo, Euclea undulate, Rhus burchellii and Rhigozum obovatum. Extensive short grasslands occur in places on the plains and flat mountain areas.

3.4 GEOLOGY

The Karoo Basin is a Late Carboniferous–Middle Jurassic retroarc foreland basin developed in front of the Cape Fold Belt (CFB) in relation to subduction of the palaeo-pacific plate underneath the Gondwana plate (Catuneanua, Hancox and Rubidge 1998). These were infilled with up to 12 km of sedimentary strata of the Karoo Supergroup (Figure 3.3).The sedimentary succession reflects changing environments from glacial to deep marine, deltaic, fluvial and aeolian and is subdivided into five main groups, i.e. the Dwyka, Ecca, Beaufort (comprising the Adelaide and Tarkastad subgroups), Stormberg and Drakensberg.

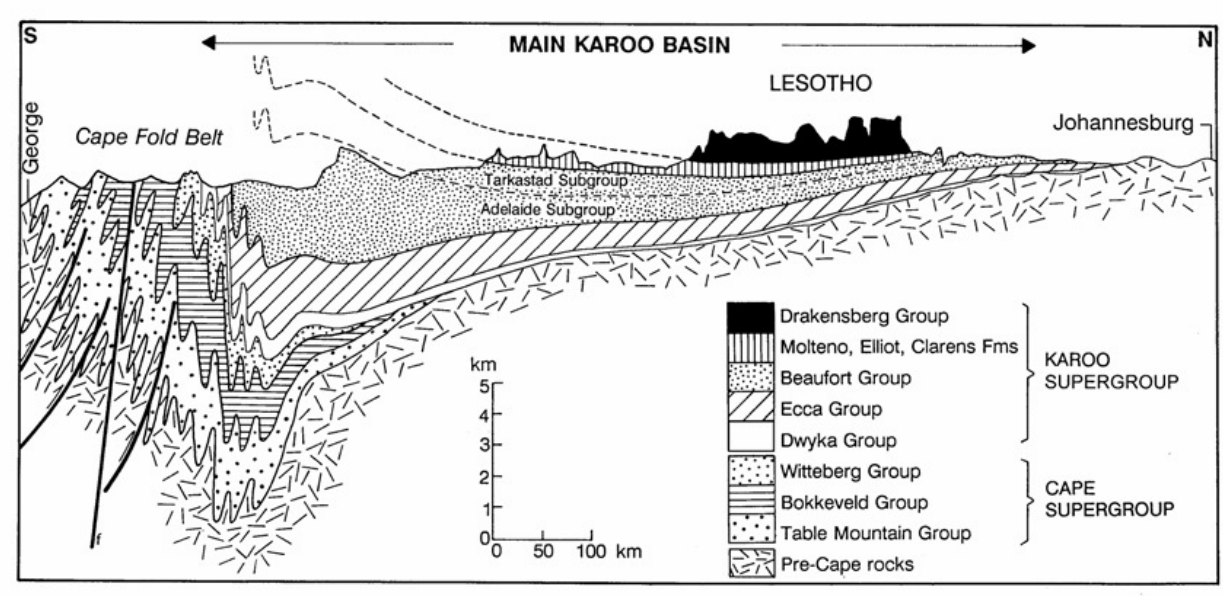

Figure 3.3 Cross-section of the main Karoo basin (Woodford and Chevallier, 2002).

The Beaufort group of the Karoo Supergroup is subdivided into the lower Adelaide and upper Tarkastad subgroups, of which only the former is present in the study area (Figure 3.4). The Adelaide subgroup of late Permian age (i.e. 260 Ma) attains a maximum thickness of 2000m and consists of the older Abrahamskraal and younger Teekloof formations of alternating bluish-grey mudstone and grey very fine to medium grained sandstone (Woodford and Chevallier, 2002). The Abrahamskraal formation represents a high-sinuosity fluvial environment and was deposited mainly by overbank flooding from meandering rivers flowing across an extensive alluvial plain towards the receding Ecca sea. The overlying Teekloof formation differs from the Abrahamskraal formation in the respect that it is dominated by green, grey and maroon mudrocks with minor, laterally accreted channel sandstones (Figure 3.5). The Teekloof formation represents a typical floodplain environment.

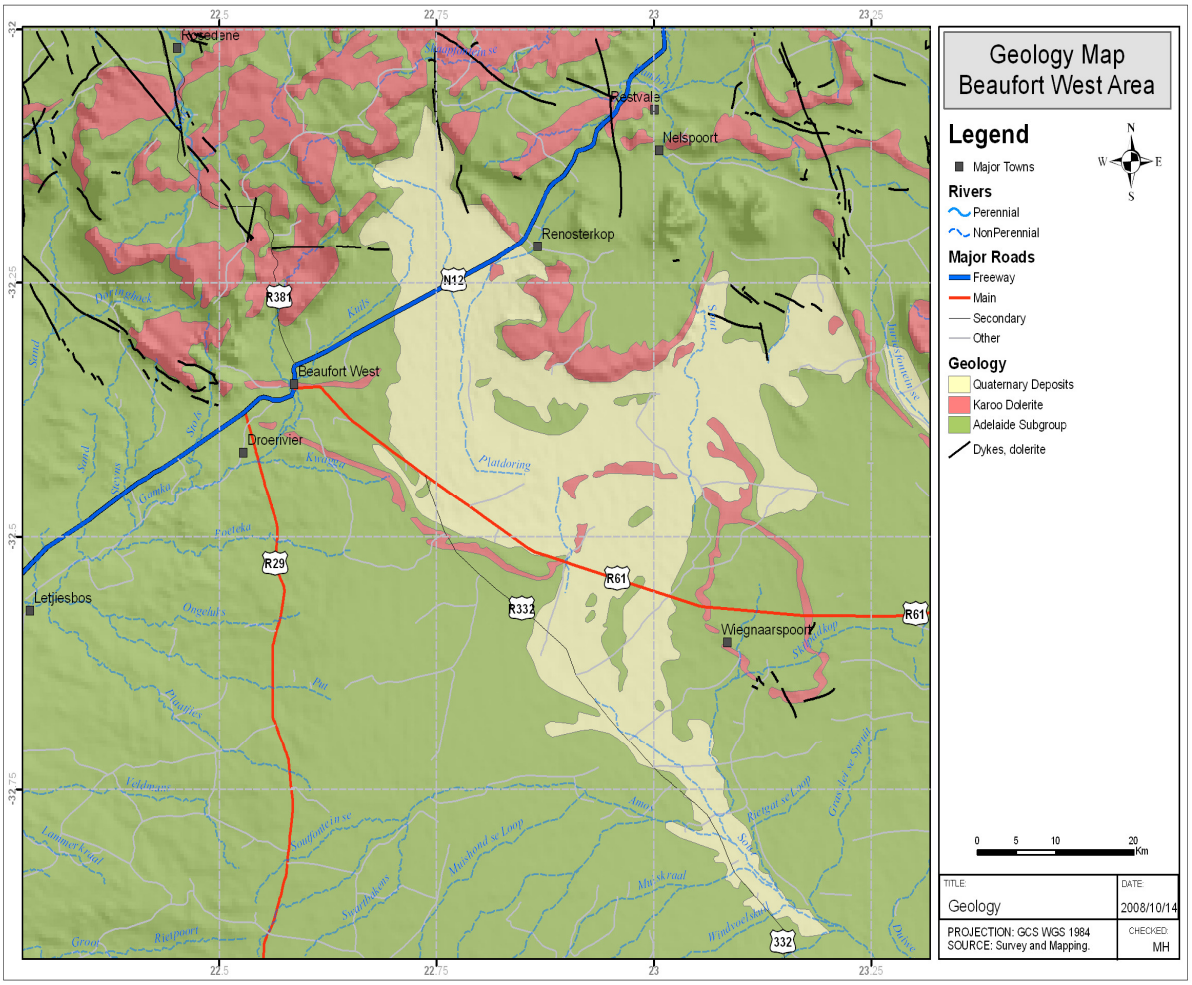

Figure 3.4 Simplified geological map of the Beaufort West area.

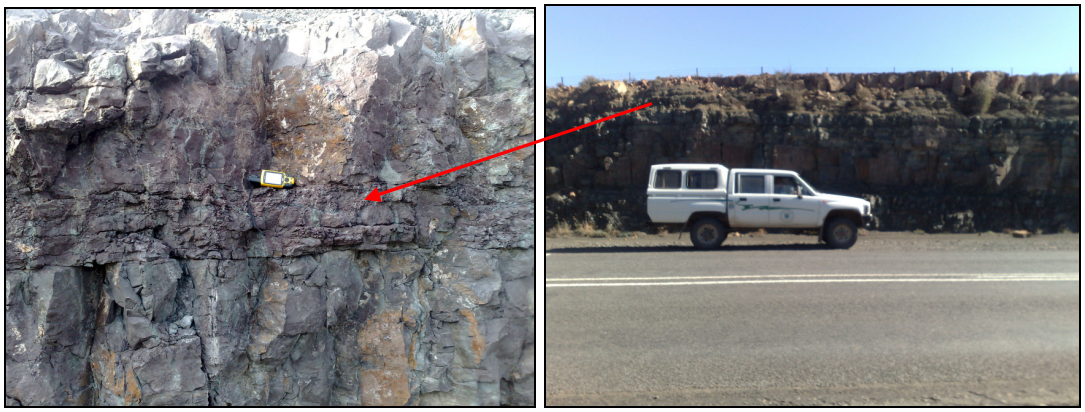

Figure 3.5 Lenticular channel mudstone in the Adelaide subgroup at Beaufort West.

3.4.1 Stratigraphy

Several upward-fining megacycles, up to 400m thick, have been recognised in the Beaufort group. Each megacycle consists of several sandstones in the lower portion and a mudstone-dominated sequence in the upper portion. From bottom to top, the sandstone-rich parts of the upper three megacycles have been named the Moordenaars sandstone (Moordenaars member), Poortjie member and Oukloof sandstone (Oukloof member). Most of the uranium occurrences are restricted to these three units (Van der Merwe and de Beer, 2006). The lithostratigraphy of the Beaufort group is illustrated in (Figure 3.6). North of the Nuweveld escarpment the Karoo Supergroup has been intruded by dolerite dykes. These dykes have been radiometrically dated between 150 and 190Ma, i.e. Jurassic in age (Johnson et al., 2006).

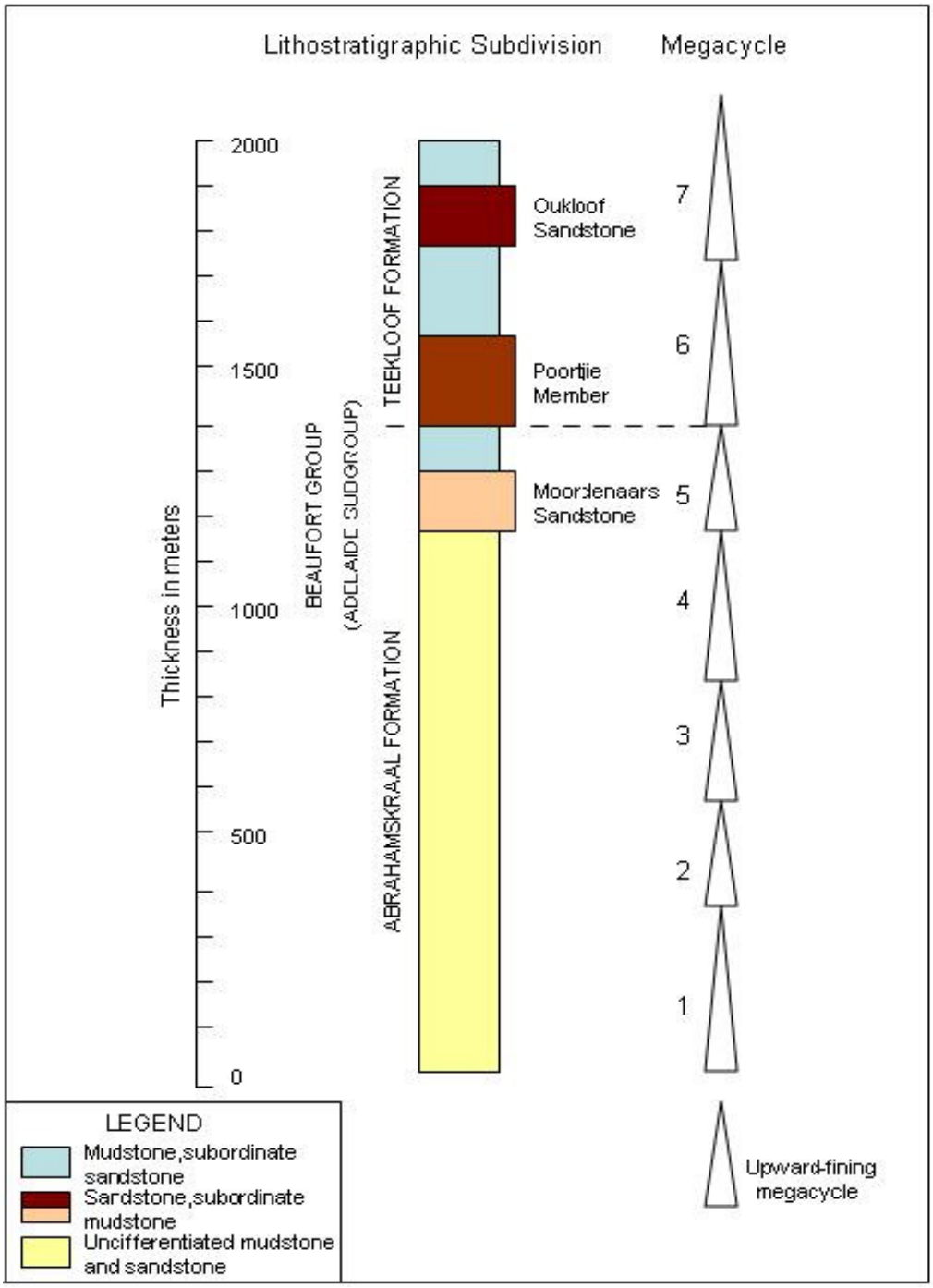

Figure 3.6 Lithostratigraphic subdivision of the Beaufort Group in the south-western Karoo (modified from Van der Merwe, A.J. and De Beer, J.H, 2006).

The Karoo dolerites form generally concordant sills varying a few meters up to 900m in thickness, and feeder dykes of less than a meter to several tens of meters thick. The two main dykes in the study area are the east-west trending dyke stretching from the Nuweveld Mountains north of the Gamka dam in an easterly direction cutting across the farms Tweeling, Brandwag and Renosterkop (TBR), and terminating into an interpreted dolerite ring structure on the farm Renosterkop (Rose, 2008). The other east-west trending dyke cuts through the town and is termed the town dyke. The other dykes in the area are the droerivier dyke (i.e. southeast-northwest trending) and the Hansrivier dyke (north-south trending) as shown in (Figure 3.7). The interpreted dolerite ring structure on the farm Renosterkop was described by Woodford and Chevallier, (2002) as saucer-like inclined dolerite sheet. A large part of the area especially in the lower lying regions is covered by calcrete and hardpan deposits, possibly as a result of secondary weathering of the Karoo sediments.

Figure 3.7 Contact between Hansrivier dolerite dyke and host rock (tape measure as scale).

3.4.2 Uranium mineralisation in the Karoo

The Karoo uranium Province is a typical example of an epigenetic deposit, where the concentration of uranium in the sandstone bodies of the Karoo Sequence was controlled by both sedimentary and geochemical processes (Cole et al., 1991). Most sandstone-type deposits are in fluvial and lacustrine sediments in either continental or marginal marine environments. Where lacustrine rocks dominate, very fine grained organic-rich hosts are more abundant and the uranium deposits may be in part syngenetic. The geochemical environment of mineralisation determines the mineralogy and form of a deposit (Van der Merwe and de Beer., 2006). Uranium mineralisation is almost entirely confined to the fluvial channel sandstone and is best developed in the thicker sandstones. In particular, the possibility of uranium mineralisation is highest where the sandstone (siltstone + mudstone) ratio exceeds 50 (Brunke, 1977). The uranium occurrences within the channel sandstones form discrete pods and lenses, peneconcordant to the bedding. The discrete pods and lenses within channel sandstones are by far the most common uraniferous host rock. It is readily recognised in outcrop areas around Beaufort West, where it occurs as thin surface coatings of dark-brown manganese oxide, locally known as “Koffieklip” (Figure 3.8).

Figure 3.8 Typical outcrop of dark-brown calcareous sandstone (Koffieklip).

(Cole and Wipplinger, 2001) identifies two main styles of mineralisation in the area of interest:

- laminated, non calcareous sandstone containing high molybdenum (Mo) and high uranium (U) values, and
- Carbonate-cemented sandstone containing low (Mo) and high (U) values.

Coffinite ($U(SiO_4)_{0.9}(OH)_{0.4}$) and uraninite (UO_2) are the primary uraniferous minerals and are associated with carbonaceous debris and sulphides. Both minerals are very fine-grained and commonly intergrown with coal macerals. Yellow and green secondary uranium minerals, which include torbernite, sabugalite and uranium-arsenates, phosphates and silicates, occur along joints, fractures and bedding planes in sandstones. Uraniferous ore-forming fluids presumably derived either from volcanic tuff fragments, which were laid down contemporaneously with the fluvial sediments and/or from detrital material transported from a granitic provenance. There remains much speculation as to which of the two processes are more plausible. In the broader context, the consensus reached amongst workers relating to Karoo geology and the uranium occurrences fits the outline of a sandstone-type uranium model (Cole et al., 1991).

3.5 HYDROGEOLOGY

In general, the sandstone and mudstones of the Beaufort group are characterised by the virtual absence of primary porosity and permeability due to diagenesis. As a result the secondary hydrogeological properties of the rocks, such as the degree, density, continuity and interconnection of fracturing control the occurrence, storage and movement of groundwater (Kotze et al., 1997). According to Botha et al., (1998) Karoo fractured – rocks are multi-layered, highly heterogeneous and isotropic with relatively low and variable permeability. Based on the 1:500 000 hydrogeological map sheet 3122 of Beaufort West it can be seen that fractured-rock aquifers cover most of the study area. A combination of intergranular and fractured-rock aquifers also exist as a result of alluvium and/or deeply weathered Beaufort sediments overlying much younger Karoo sediments. Fractured- rock aquifers also tend to produce higher yielding boreholes in excess of 5l/s, whereas those with dual porosities produce yields of between 0.1 – 0.5l/s (Rose, 2008).

Nhleko and Dondo, (2008), divided the Beaufort west area into three aquifer systems based on aquifer mapping. The top aquifer, extend to a depth of 10m is characterised by weathered intergranular material consisting of primary sandstone, mudstone, siltstone and dolerite. It is postulated that this aquifer is recharged directly by precipitation and surface water sources such as rivers and pans where connectivity exists. The sustainability of this aquifer remains questionable due its low storage capacity. The middle fractured-rock aquifer is characterised mainly by thick sandstone and mudstone with associated dolerite intrusions. The aquifer occurs at a depth of 50m and is regarded as the most extensive aquifer in the study area (Nhleko and Dondo, 2008). Recharge occurs along bedding planes as well as from runoff and leakage albeit at a much slower rate. Due to the large scale connectivity of fractures, the aquifer is highly transmissive. A deeper aquifer exists at a depth of around 80-90m, and due to dolerite intrusions the surrounding sandstone are heavily fractured.

3.5.1 Aquifer properties

(Table 3.1) gives the average horizontal transmissivity and storativity values at the respective localities. Due to the fact that limited data exist to the south of Beaufort west, the current dataset is restricted mainly to the municipal well fields situated to the north of the town. This reflects the areas most extensively explored over the past twenty years (Rose, 2008).

Table 3.1 Summary of fracture T and S values for high yielding boreholes along lineaments in the study area (Rose, 2008)

Subarea	Transmissivity (T in m^2/day)	Storativity (S dimensionless)	Yield (l/s)
Brandwag east	>200	0.01 - 0.001	15
Brandwag west	<200	0.0001 - 0.00001	5
De Hoop	30 - 300	0.001 - 0.00001	5
Platdoorns	<10 - >200	0.00001	2
Lemoenfontein	100 - 250	0.0001-0.00001	8
Town well	40 - >400	0.001 - 0.0001	5
Droerivier	<10	0.001 - 0.0001	2
Hansrivier	>300	0.001 - 0.0001	18
Sunnyside	100 - 360	0.00001 - 0.000001	6

According to Rose, (2008) there is a strong correlation between borehole yields and transmissivities, whereby areas with high transmissivities >100m^2/day is generally associated with borehole yields greater than 5l/s. The influence of dolerite dykes on the yields of boreholes can be seen by the large amount of boreholes drilled in close proximity to these geological structures. Pumping test data from Rose and Conrad, (2007) indicated that boreholes drilled on the farm Hansrivier (south east of Beaufort West) on a contact zone between the dolerite dyke and fractured Teekloof Formation produced sustainable yields in excess of 10l/s.

CHAPTER 4 - RESULTS AND DISCUSSIONS

4.1 INTRODUCTION

An initial hydrocensus of the study area in Beaufort West was conducted from the 6-18th May 2008, to asses the water resources utilisation of the town and its surroundings. This was done by surveying available boreholes in the area and where possible measurements of physico-chemical properties and water levels were taken. Communication with farmers and the local municipality formed an integral part of the hydrocensus, which assisted in determining the historical and current status of groundwater in the area. A follow-up hydrocensus was carried out in June 2009 focusing predominantly to the south of Beaufort West in the vicinity of the proposed new uranium mine, to gain a better understanding of the regional flow and transport processes in Karoo sedimentary rocks with relatively low permeability.

The main focus was to add more groundwater sampling points, especially to the north and south of the study area to form a more comprehensive monitoring network. The concluding fieldwork was undertaken between the 7th and 14th of February 2010, to identify the aquifer boundaries and to characterise the anisotropy of Karoo aquifers by conducting an aquifer and radially-convergent tracer test on the farm Hansrivier. This information was then utilised to conceptualise the flow dynamics and contaminant processes of the system under investigation. The boreholes sampled during the hydrocensus are shown in Appendix A. Figure 4.1shows the boreholes sampled for major cations/anions, in total 10 additional samples were collected.

Borehole sampled for Cation/Anion analysis

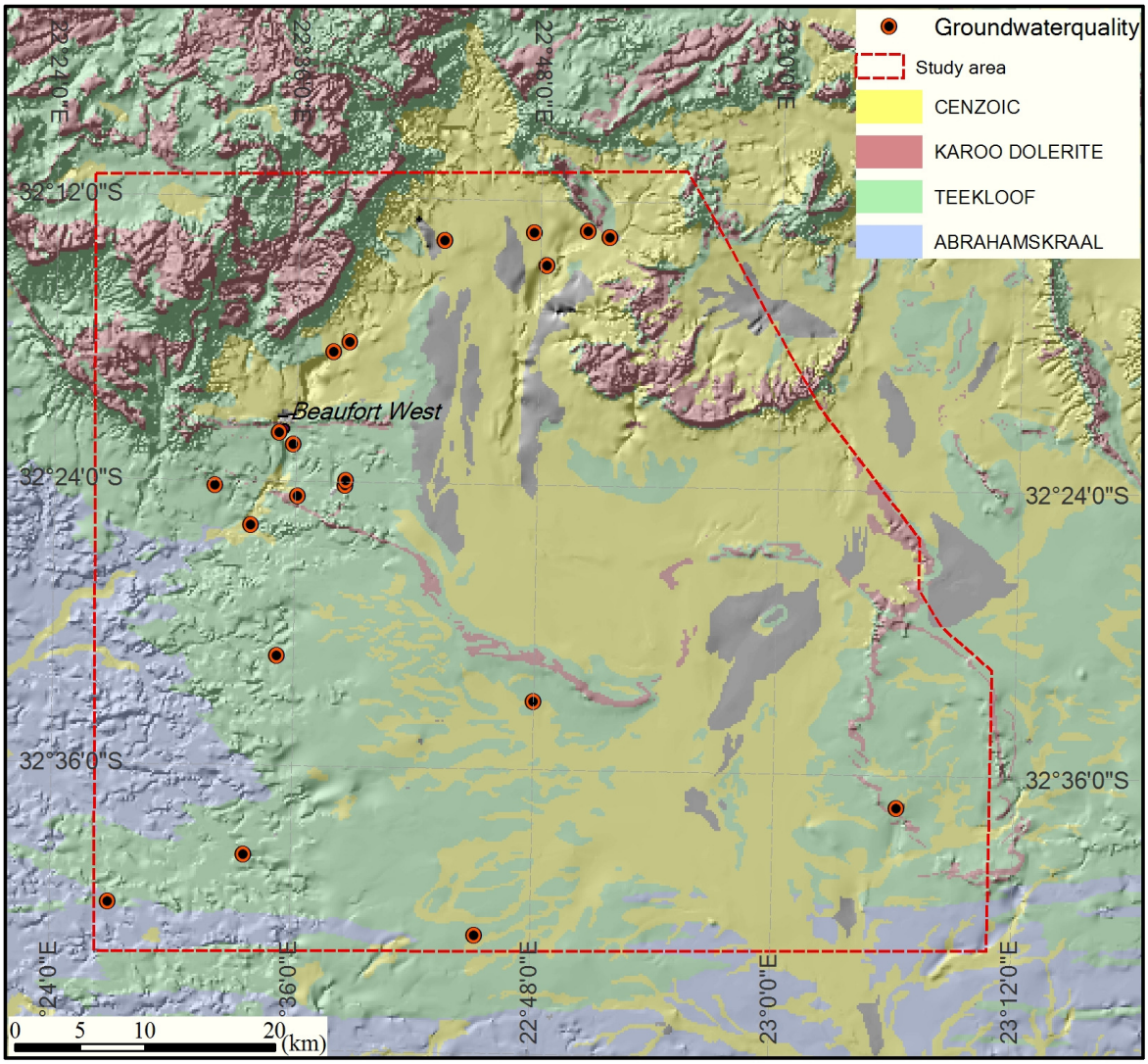

Figure 4.1 Map of Beaufort West indicating boreholes sampled for major cations and anions

4.1.1 Description of the Hydrochemical dataset

The water chemistry data was collated from the previous sampling run in 2008 and compared to the present results. The macro – chemical laboratory results were used to construct the various chemical plots. Figure 4.2 shows the piper diagram of boreholes sampled during the May 2008 fieldwork.

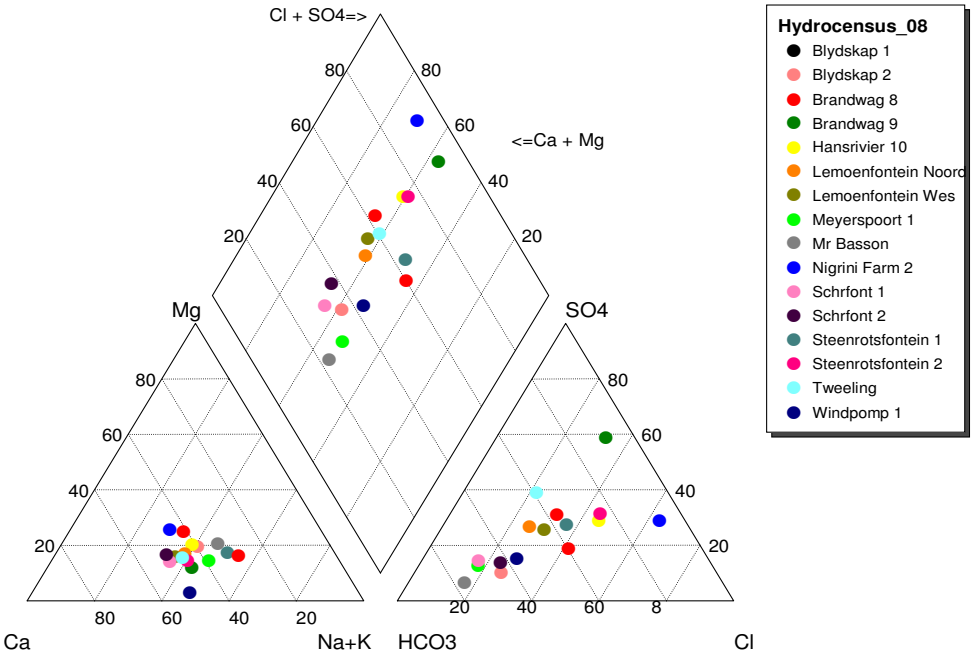

Figure 4.2 Piper diagram of boreholes sampled in Beaufort West (May, 2008).

The hydrochemical facies shows a Ca-Na-HCO_3 type water evolving into a Ca-Mg-SO_4-Cl type groundwater. Thus, indicating relatively fresh shallow groundwater with little chemical alteration from recharge to discharge. However, Brandwag.9 has a distinctively different hydrochemical facies Ca-Na-SO_4-Cl, probably as a result of its close proximity to the TBR dyke, which cuts across the Brandwag wellfield north of the town. The higher SO_4^{2-} concentration of this sample could also be due to either the dissolution of sulphides from rocks or calcium being removed from the solution, most likely by the precipitation of calcite or by ion exchange reactions (Hounslow, 1995).

Figure 4.3 shows the results for the 2009 sampling run with a reduced number of sampling sites. The major water chemistry is almost identical to the May 2008 sampling run, with most of the samples showing a fresh Ca-HCO_3 type facies evolving towards a Ca-SO_4 type hydrochemical facies.

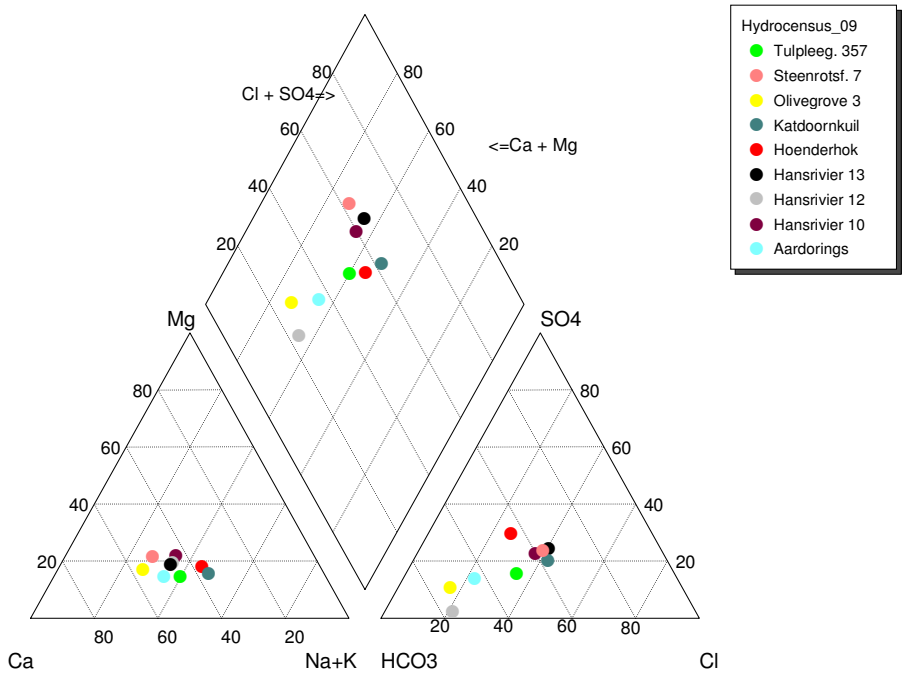

Figure 4.3 Piper diagram of boreholes sampled during (May 2009) hydrocensus.

4.1.2 Interpretation of the pH-electrical conductivity logs

In the study of flow and transport through fractured rocks, knowledge on the locations of fractures and their hydraulic properties are essential (Doughty and Tsang, 2005). For the delineation of water bearing fractures in fractured rock formations of the Karoo, ph-electrical conductivity (EC) logging with depth was carried out on most of the boreholes visited (Figure 4.4). Two of the boreholes, namely HR.10 and G29936HB were included and later used for both the aquifer and tracer test (Table 4.1).

Table 4.1 Borehole details.

Boreholes	Location		Depth (m)	Water Level(mbgs)	EC at water table	EC at bottom depth
	Longitude	Latitude				
HR.10	22.64031	32.39105	27.68	5.36	1572	1874
G29936HB	22.64070	32.39090	38.24	5.65	923	1344

EC in µS/cm at observed temperature and depth in meters below land surface

Before injection with non-iodated salt commenced, borehole G29936HB situated 41.8 meters from the pumping borehole (HR.10) was circulated using a small diameter pump to a depth of 12m. The circulation process lasted about 30min before a pulse injection using 500g of non-iodated salt dissolved in 5l of site water took place into borehole G29936HB. EC was measured for the duration of the test to pick up any breakthrough at HR.10. Figure 4.5 shows the EC-pH graphs for boreholes HR.10 and G29936HB, respectively.

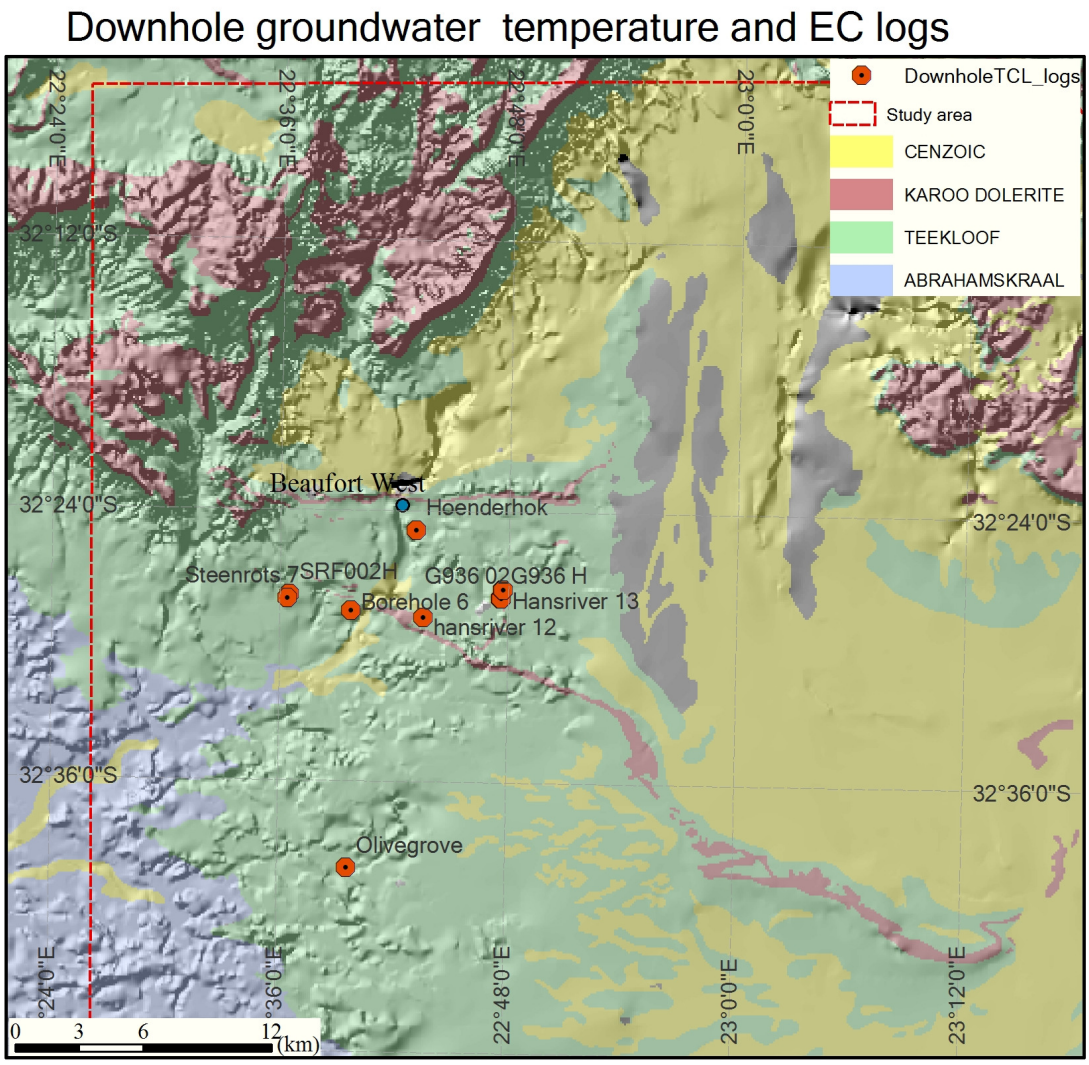

Figure 4.4 Map indicating boreholes logged during the May 2009 hydrocensus

To verify historical borehole logging data on fracture location at the observation borehole G29936HB, camera logging was also carried out before uranin was injected into borehole G29936HB. Based on the camera logging inspection, it could be seen that multiple fracture zones occur at depths of 14m and 17m, which agrees well with historical data from the National groundwater archives (NGA) of the Department of Water Affairs (DWA). These multiple fracture zones were also visible in one of the EC-pH logs of (Figure 4.5) for borehole HR.10. Borehole G29936HB displays an active flow system on top, indicating low mineralised recently recharged water with more evolved, highly mineralised/stagnant water occurring at the bottom of the borehole. The fracture zone has a higher pH than the host rock, probably due to the exsolution of CO_2 in the

fractures causing precipitation of carbonates and in the process changing the water composition of the fractures to become more alkaline. Vertical, sub-vertical and horizontal (bedding-plane) fractures were also shown on the camera logging inspection, with the latter contributing to the overall transmissivity as shown from the aquifer test data and therefore the strength of the borehole yield. Not all fractures appear to be transmissive, as the majority of fractures occurring at greater depths were closed due to secondary weathering processes.

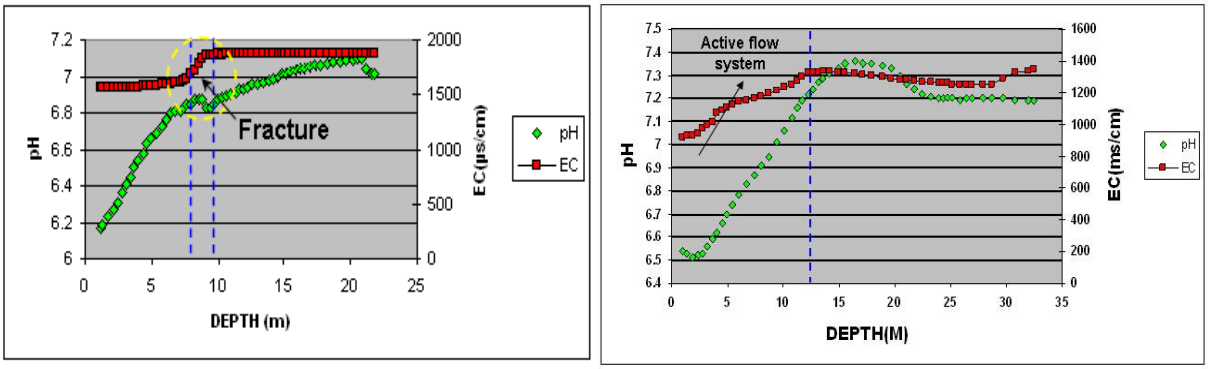

Figure 4.5 EC-pH profiles for the abstraction (HR.10) and injection (G29936HB) boreholes.

4.2 RADIOACTIVITY

Due to budgetary constraints only 15 samples were taken for radioactivity analysis according to the project proposal (Figure 4.6). The limited number of samples still provided a good estimate of whether there is radionuclide contamination in the study area and to what extent it exceeds the natural background levels (Table 4.2). The concentration values of the various uranium isotopes found in nature are 99.3% U^{238}, 0.7% U^{235} and 0.01% U^{234}. Based on the above concentration values it can be seen that U^{235} (0.7%) is more or less 5% that of U^{238} (99.3%), implying that they are fixed inside the rock lattice in a ratio of 10:1. Therefore, U^{238} and U^{235} should be essentially equal due to their respective percentages. Appendix.B contains all the technical information for the uranium and thorium decay series.

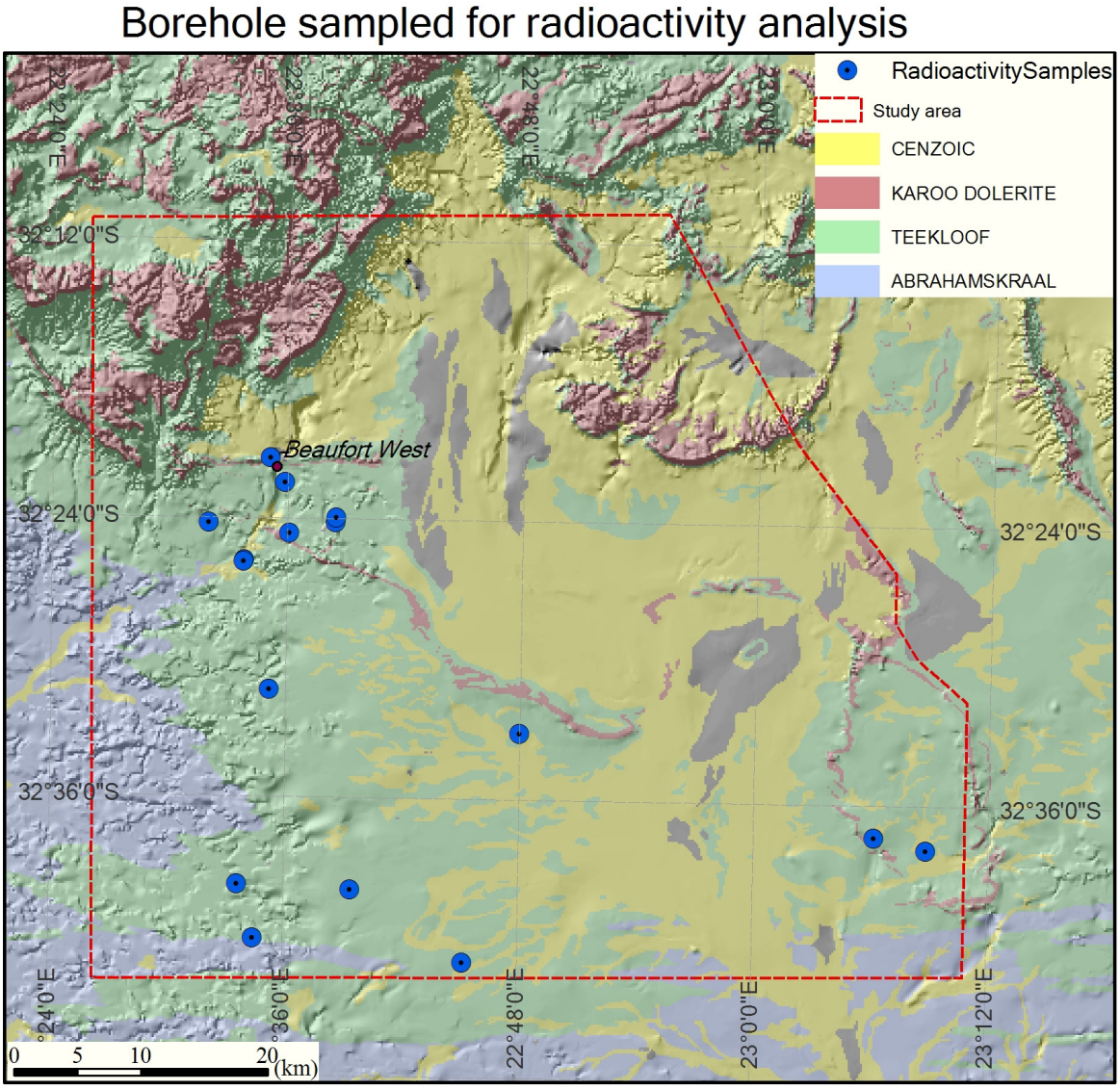

Figure 4.6 Boreholes sampled for radioactivity.

4.2.1 Uranium distribution in groundwater across the study area

The results in Table 4.2 shows that for all the boreholes sampled U^{234} is approximately between two and three times higher than that of U^{238}, indicating uranium - series disequilibria between these two isotopes. This is mainly due to water-host rock interaction; leading to preferential mobilisation of U^{234} caused by the alpha recoil of its parent U^{238} (Figure 4.7). This type of phenomena is normally associated with natural conditions not influenced by mining activities.

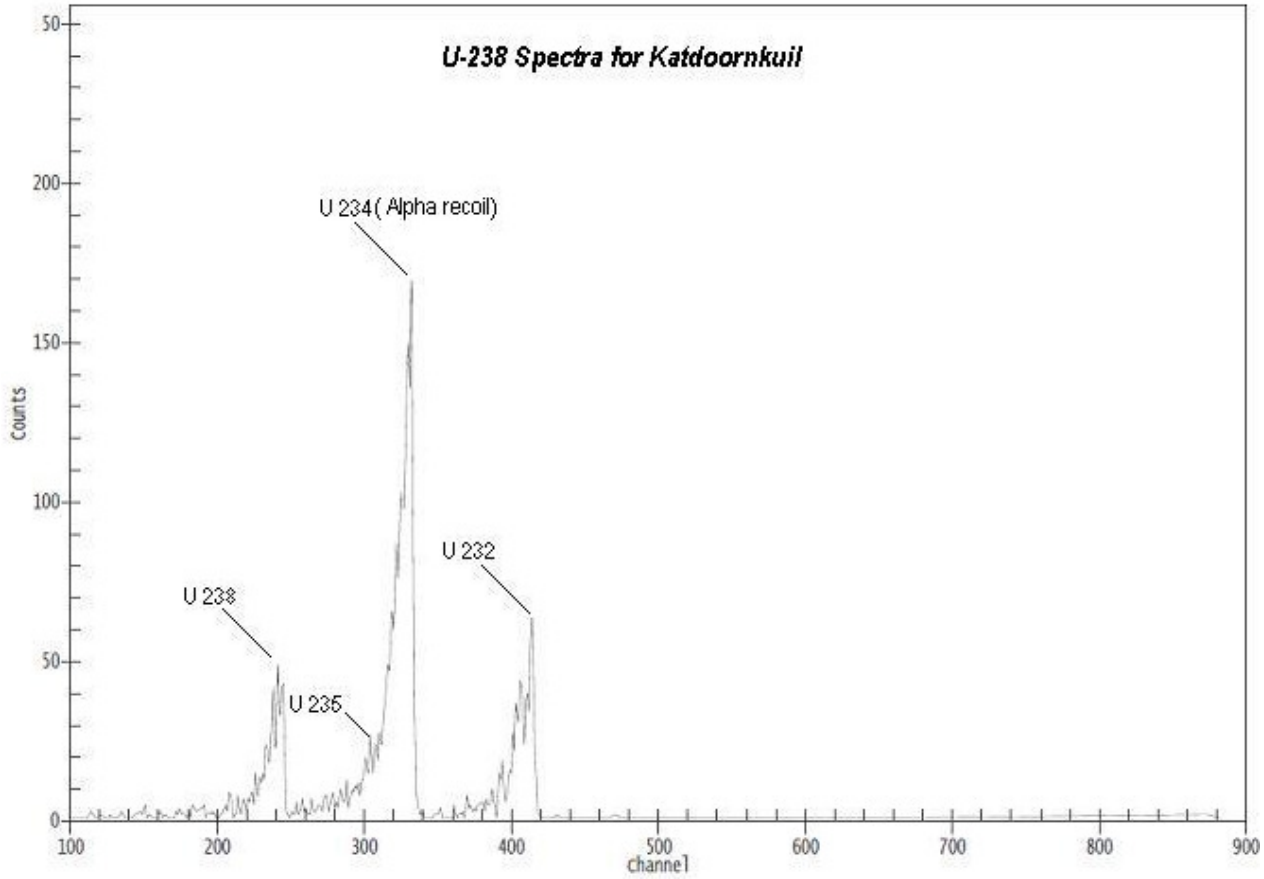

Figure 4.7 Spectrum indicating the effect of alpha recoil on the U^{234} isotope.

A brief survey using a variety of isotopes including uranium and other environmental tracers of groundwater at Beaufort West was conducted by Vogel et al., (1980). In their study it was found that U^{234} was also preferentially leached from the rock, with U^{234}/U^{238} activity ratios being greater than unity. Similarly significant disequilibrium between the U^{238} and U^{234} isotopes were found by Reyes and Marques, (2008) in groundwater from a fractured bedrock aquifer in Southern Brazil. It was shown that samples taken from the oxidised part of the aquifer had activity ratios that were inversely related to the uranium concentration. This was possibly due to mixing occurring with the high activity ratio and low uranium content groundwater, which may be pore water old enough to have allowed significant U^{234} recoil to occur.

Based on the activity ratios given in Table 4.3, it can be seen that all the activity ratios are above unity, which correlate well with the above findings. This is normally the case, whereby higher U^{234} isotopes are indicative of pre-mining conditions. If however, the U^{234} is much lower and the activity ratio in the groundwater sample approaches unity then the opposite is true as the host rock is being disturbed through both mining and milling processes, allowing the U^{238} and U^{234} to become equally mobile as the groundwater comes into contact with the mined ore body, ultimately resulting in the U^{238} and U^{234} activity ratio approaching unity. Theoretically the Th^{228} daughter isotope should be more leachable than its parent Th^{232}, due to it being very loose in the damaged crystal lattice and thus more likely to undergo alpha recoil. In Table 4.2 it can be seen that the Th^{228} values are less than that of its parent Th^{232}. A possible explanation could be that the Ra^{228} and Ac^{228} daughter isotopes are found in between the two thorium isotopes and might therefore influence the concentration of Th^{228} in the groundwater. Consideration was initially given to the use of gross alpha and beta measurements for estimating the dose contributions from the radionuclides that were not individually measured. In practice, however, the uncertainties inherent in the determination of gross alpha and beta activity, typically around 20% to 30%, lead to unacceptably large uncertainties in the final dose determinations and were thus not used.

Table 4.2 Radioactivity results of samples taken during 2008-2009 fieldwork.

mBq/L	Blydskap 01			Blydskap 02			Schr Fontein 2			Steenrotsfontein			Spring		
Nuclide	Value	Unc.	MDA	Value	Unc.	MDA	Value	Unc.	MDA	Value	Unc.	MDA	Value	Unc.	MDA
^{238}U	123	8	4.9	158	10	4.2	132	8	1.3	641	26	7.6	184	13	6.6
^{234}U	554	16	3.3	584	18	4.2	380	13	1.3	1380	40	9.5	465	21	2.4
^{230}Th	7.9	8.1	15	6.3	6.6	14	6.8	7	14	15.1	3.4	7.8	7.9	8.6	20
^{226}Ra	9.49	2.1	4.9	16.4	2.4	0.93	6.07	1.53	3	12.9	2.1	3.2	1.6	1	3.3
^{210}Pb	39.9	10.1	4.8	40.5	10.3	5.1	26.2	7	3.9	25	9.6	7.7	35.7	11.1	7.3
^{210}Po	-3.4	4.5	1.3	-3.2	4.5	0.85	-6.7	2.4	1.3	-4.1	5.2	1.1	-7.8	6	0.85
^{235}U	5.68	0.35	0.22	7.3	0.44	0.2	6.51	1.86	3.4	29.5	1.2	0.35	8.49	0.59	0.3
^{227}Th	2	1.3	4.1	2.4	1.2	2.7	2.5	1.1	2.8	6.79	2.26	4.3	7.3	3.2	8.4
^{223}Ra	-1	1.6	5.5	-1.5	1.4	1.2	0.47	1.3	3.8	10.9	2.9	5	4.85	1.77	4.6
^{232}Th	1.3	0.75	1.2	0.81	0.57	1.1	1.27	0.73	1.1	2.3	1	2.6	2.83	1.64	2.6
^{228}Th	1.8	1	2.8	2.2	1.1	3.3	0.42	0.42	1.1	13.9	2.3	0.99	3.9	2.6	8.4
^{224}Ra	3.18	1.42	1.7	1.5	1	2	0.68	1.2	5	6.94	2.38	4.9	1.6	1.1	2.2
	Tulplaagte 357			**Katdoornkuil**			**Aarddorings**			**Hansrivier 13**			**Olivegrove 3**		
Nuclide	Value	Unc.	MDA	Value	Unc.	MDA	Value	Unc.	MDA	Value	Unc.	MDA	Value	Unc.	MDA
^{238}U	244	11	3.4	325	12	4.4	95.4	6	2.7	175	8	1.1	164	9	3.3
^{234}U	738	19	3.4	1100	20	3.5	192	9	1	465	14	3.6	282	12	4.8
^{230}Th	12	3.1	17	16.3	3.7	16	12	2.9	16	8.2	8.4	14	22	4.8	16
^{235}U	11.2	0.5	0.16	15	0.6	0.2	4.54	1.51	3.5	8.05	0.38	0.049	7.55	0.4	0.15
^{227}Th	1.3	1.8	5.6	1.6	1.6	3.3	3.98	1.58	1.2	2.7	1.6	4.4	2.9	1.9	3.3
^{232}Th	8.8	2.12	3.4	15.7	2.7	1.2	5.34	1.54	1.2	9.3	1.94	1.1	5	1.51	1.2
^{228}Th	5	2.1	6	10.2	2.3	4.1	4.4	1.8	4.7	3.2	1.6	4.8	10.3	2.7	6.3
Gross alpha	472	147	460	490	160	500	-110	130	440	160	160	540	180	130	430
Gross beta	-150	340	1100	-22	340	1100	-440	330	1100	-120	340	1100	-110	330	1100
	Hoenderhok			**Saucyskuil**			**Steenrotsfontein 1**			**Hansrivier 10**			**Hansrivier 12**		
Nuclide	Value	Unc.	MDA	Value	Unc.	MDA	Value	Unc.	MDA	Value	Unc.	MDA	Value	Unc.	MDA
^{238}U	325	22	4	54.2	4.7	1.1	274	10	2.8	188	15	3.3	30.9	6.9	10
^{234}U	536	29	16	261	10	4.3	565	15	3.6	455	24	13	71.5	10.7	15
^{230}Th	6.7	6.9	15	19.1	4.3	18	37.5	7.3	21	17	3.9	17	19.6	4.1	15
^{235}U	15	1	0.19	2.5	0.22	0.051	12.6	0.5	0.13	8.66	0.7	0.15	1.42	0.32	0.48
^{227}Th	4.13	1.81	3.8	6.73	2.79	4.6	2.6	1.83	1.6	4.7	2	5.1	0.89	1.2	3
^{232}Th	33.1	3.7	3	2	1.2	3.7	4.71	1.67	1.6	7.13	1.84	1.3	1.2	0.92	3
^{228}Th	6.94	1.68	1.1	8.25	2.22	4.5	9.3	2.33	1.6	1.4	1.6	5.6	4.1	1.7	4.9
Gross alpha	84	160	540	87	130	420	637	179	560	130	150	500	-210	140	480
Gross beta	-51	340	1100	-10	330	1100	41	340	1100	-92	340	1100	-200	340	1100

Notes:
1. If a measured value (**Value** column) was recorded, it is reported regardless if the value is less than the minimum detectable activity concentration (**MDA** column) or even if the value is negative. In the case where a value could not be obtained, a less than MDA ("< MDA") will be indicated.

2. The reported uncertainty (**Unc.** column) is quoted at 1 sigma (or coverage factor k = 1). The uncertainty is calculated mainly from counting statistics and it is not the standard deviation obtained from replicate measurements. No uncertainty value is reported of a less than MDA ("< MDA") is indicated in the **Value** column.

3. The minimum detectable activity concentration (**MDA** column) is calculated with a 95% confidence level.

4. A value is reported with 3 significant digits if it is greater than the MDA value and the associated uncertainty will be reported the same precision. If a value is less than the MDA, the value and its associated uncertainty are reported with 2 significant digits regardless their respective magnitudes. A MDA value is always reported with 2 significant digits

Table 4.3 Activity ratios of uranium isotopes for all the boreholes sampled.

Water sample	Sampling date	pH	T (℃)	U^{238} (mBq/L)	U^{234} (mBq/L)	U^{234}/U^{238} ratio
Aarddorings	31/05/2009	7	19	95.4	192	2.01
Blydskap01	16/05/2008	7	19	123	554	4.50
Blydskap02	16/05/2008	7	20	158	584	3.69
Hansrivier 10	1/6/2009	7	22	188	455	2.42
Hansrivier 12	1/6/2009	7	23	30.9	71.5	2.31
Hansrivier 13	1/6/2009	7	22	175	465	2.65
Hoenderhok	1/6/2009	7	20	325	536	1.64
Katdoornkuil	31/05/2009	7	21	325	1100	3.38
Olivegrove 3	3/6/2009	7	21	164	282	1.72
Steenrotsfontein 1	15/05/2008	7	20	274	565	2.06
Steenrotsfontein 2	15/05/2008	7	23	641	1380	2.15
Saucyskuil	3/6/2009	8	12	54.2	261	4.82
Spring	12/5/2008	7	19	184	465	2.52
Schr Fontein 2	17/05/2008	7	25	132	380	2.87
Tulplaagte 357	31/05/2009	7	17	244	738	3.02

The South African water quality guidelines for domestic use are shown in Table 4.4. It can be seen that most of the samples fall in Class I (< 0.1mSv/a), indicating good water quality with the exception of 1 sample (Steenrotsfontein 2) falling in Class II (0.1 – 0.250 mSv/a) for the less than one year age group, with marginal water quality and therefore does not pose an immediate risk to people using borehole water for consumption. On average our radiation exposure due to all natural background sources amounts to approximately 2.4mSv/a (WHO, 2005). The recommended reference dose level (RDL) of 0.1mSv/a given by the WHO and adapted by the South African water quality guidelines, is only 5% of the dose from the total natural background, and can therefore be regarded as conservative.

Table 4.4 Radioactive dose results compared to the South African water quality guidelines.

Sample	< 1 a	1 - 2 a	2 -7 a	7 - 12 a	12 - 17 a	> 17 a	Average life-time
Activity	Total mSv/a						Exposure
Consumption(L/a)	200	260	300	350	600	730	mSv/a
Aardorings	0.039	0.012	0.009	0.009	0.015	0.013	0.016
Blydskap01	0.155	0.063	0.048	0.050	0.091	0.050	0.055
Blydskap02	0.169	0.067	0.051	0.054	0.100	0.055	0.060
Hansrivier 10	0.069	0.024	0.019	0.019	0.032	0.027	0.032
Hansrivier 12	0.028	0.006	0.005	0.005	0.007	0.007	0.010
Hansrivier 13	0.065	0.024	0.019	0.018	0.031	0.026	0.030
Hoenderhok	0.104	0.034	0.027	0.026	0.044	0.037	0.045
Katdoornkuil	0.140	0.052	0.041	0.040	0.068	0.056	0.066
Olivegrove 3	0.063	0.019	0.015	0.014	0.024	0.021	0.026
Steenrotsfontein 1	0.103	0.034	0.026	0.026	0.043	0.037	0.045
Steenrotsfontein 2	0.362	0.116	0.090	0.091	0.159	0.111	0.115
Saucyskuil	0.047	0.014	0.011	0.010	0.017	0.015	0.019
Spring	0.176	0.055	0.044	0.047	0.085	0.049	0.053
Schr Fontein 2	0.103	0.036	0.030	0.033	0.062	0.034	0.037
Tulplaagte 357	0.094	0.036	0.028	0.027	0.046	0.038	0.045

	Class 0 (Ideal water quality): Dose<=0.100mSv/a
	Class I (Good water quality): Dose 0.100 - 0.250 mSv/a
	Class II (Marginal water quality): Dose 0.250 - 1mSv/a
	Class III (Poor water quality): Dose 1 - 5mSv/a
	Class IV (Unacceptable water quality): Dose >5mSv/a

The fact that all the samples with the exception of one are within the acceptable range as specified above, could imply that the radioactivity in groundwater is controlled more by the hydrological and lithological settings. This would make sense as past mining activities focused on specific areas, especially to the East and Northwest of Beaufort West. Due to these areas currently undergoing prospecting rights for future mining, no access was allowed and hence no sampling data generated. Furthermore the exact extent and depth of the uranium ore body is also not known due to the mines treating all information relating to mining with confidentiality.

4.3 AQUIFER TESTS

4.3.1 Description of the aquifer test

The flow characteristic method (FC program), which was developed by Van Tonder et al., (2002) along with the software package AQTESOLVE Pro version 4.5, was used to interpret the pumping test data by using automatic curve fitting or manual fitting of late time data. One of the limitations identified in using the FC program was the insensitivity of the data analysis to changes in storativity *S*, leading to potentially large variations of *S* during the data fitting process with negligible changes in transmissivity *T* and as a result the value of *S* was set to 1E-03, with the FC program. AQTESOLVE Pro contains a large variety of methods for the modeling of pumping tests. In order to determine realistic aquifer parameters from pumping test data, the applied analytical solutions/conceptual model (e.g. confined, unconfined, leaky and fractured aquifers) must be representative of the aquifer system under investigation. The value of *S* was not fixed when using the software package AQTESOLVE Pro version 4.5.

4.3.2 Analysis and interpretation

Diagnostic or qualitative analysis of drawdown data was undertaken to identify component flow geometries during the pumping test. Derivative analysis, in which the derivative of drawdown is plotted against the log of time, was used to characterise the drawdown response and to identify the component flow regimes of the aquifer test. It has been shown that the use of the derivative technique for heterogeneous systems may yield valuable information relating to the characteristics of the aquifer (Raghavan, 2004).The derivative is sensitive to small variations in the rate of pressure change, which may be less obvious in the drawdown versus time plots (Bourdet et al., 1983). As will be shown the derivative method can be exploited to identify well-bore storage, boundaries, leakage, linear flow, unconfined flow and radial flow conditions.

A constant-discharge aquifer test was carried out on 08-02-2010 at the Hansrivier site in Beaufort West with the goal of obtaining drawdown data in the pumping and observation boreholes. Only three of the four available boreholes (HR.10, New BH, HR10.1 and G29936HB) were monitored in the aquifer test, as there was no available information on the new borehole drilled by the municipality. The details of the tested boreholes are given in Table 4.5.The pumping test was done over a period of 88 hrs by pumping HR.10 at a rate of 10 *l/s*, achieving a final drawdown of about 3.59 meters in the abstraction borehole HR.10 and a maximum drawdown of 2.9m and 3m in the observation boreholes HR.10.1 and G29936HB respectively. Water levels during pumping and after pumping stopped (recovery) were recorded in both the pumping borehole and observation boreholes.

Table 4.5 Selected technical data of the boreholes tested.

	HR 10	New BH	HR10.1	G29936HB
Coordinates	S32.39105°	S32.39105°	S32.39105°	S32.39090°
	E022.64031°	E022.64026°	E022.64043°	E022.64070°
Date of Constant discharge test	08/02/2010	08/02/2010	08/02/2010	08/02/2010
Diameter (mm)	170	170	170	170
Elevation (m)	852	825	848	845
Depth(mbgs)	27.68	71.3	10.68	38.24
Distance of observation boreholes (m)		1.6	9	41.8
Pump installation depth (m)	16			
Static water level (mbgs)	5.36	5.37	5.61	5.65
Final drawdown (m)	3.59		2.9	3
Geological setting	Fractured Teekloof formation intruded by a Dolerite Dyke			

A plot of displacement versus time for the abstraction and observation boreholes is shown in Figure 4.8. All boreholes exhibit the same behaviour, with the drawdown curves displaying the same shape and the water level recovering to within 85% of the original water level. To get an initial approximation of the transmissivity (T) and storativity (*S*) values for HR10, the late-time data was fitted with the Cooper-Jacob analytical solution. The T-value determined from the Cooper-Jacob method was 110m^2/day, with an S-value of 9.00E-03. Important to note is that two monitoring boreholes and the abstraction borehole were used to compute drawdown and therefore the estimated parameters have a higher confidence level, especially that of storativity.

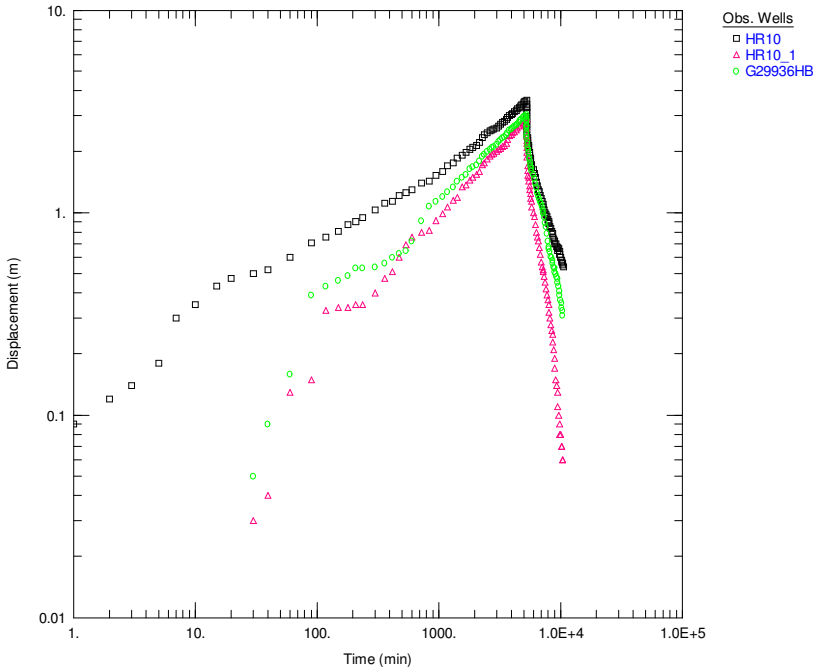

Figure 4.8 Log-log plot for pumping borehole (HR10) and observation boreholes.

As shown in Figure 4.8 drawdown in all the boreholes appear to be supported at intermediate times by flow from the rock matrix (double porosity concept) at the position of the fracture, with increasing drawdown towards later time. The water level remained at 7.26mbgs for about an hour of pumping and this could be explained by using the double porosity concept. Initially, most of the water pumped comes from the fractures and the head in the fractures drops rapidly. As pumping continuous, the matrix begins to supply water to the fractures, causing the head in the fractures to stabilise and the head in the matrix to drop. As the heads in the fractures and matrix equalises, both systems produce water to the borehole.

Based on the derivatives and diagnostic plots (Figure 4.9 and Figure 4.10, respectively) it can be seen that the aquifer behaves as a double porosity system, with a characteristic dip in the derivative after well bore storage. The position of the fracture is usually seen, whereby the first derivative (s') shows a decrease and after the fracture is dewatered the s' increases again and this occurred at 48 hrs of pumping.

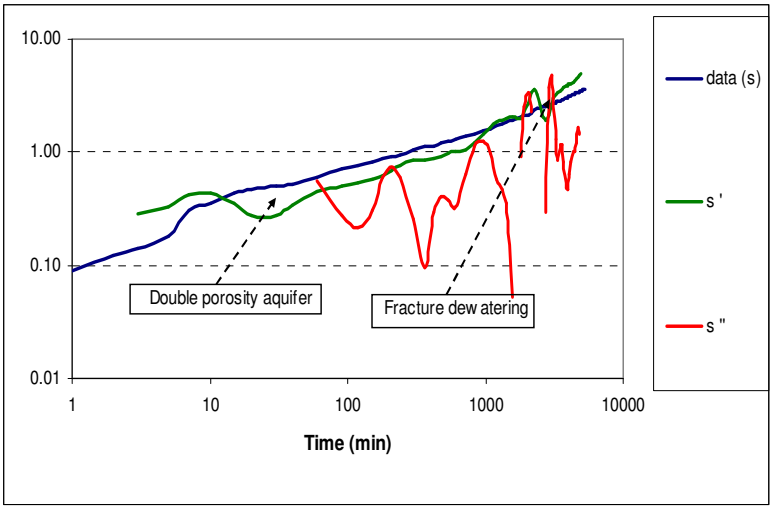

Figure 4.9 Log-derivative graphs for constant discharge test of HR10.

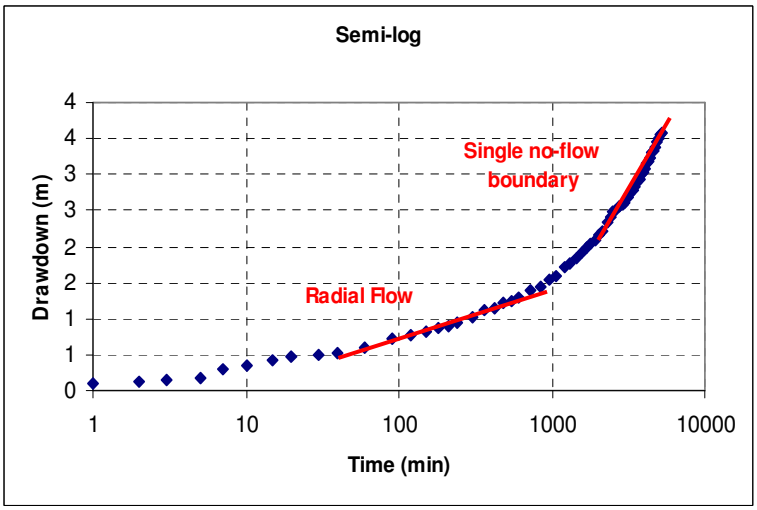

Figure 4.10 Semi-log plots for constant rate test of HR10.

The time-drawdown relationship indicates a linear flow for the first 10 minutes, changing to radial flow up to 1000 minutes at intermediate times, before the drawdown increases Figure 4.10. Such behaviour indicates that the test was influenced by a no-flow boundary at late times with a subsequent increase of the slope in a drawdown plot. To obtain more accurate estimates of the aquifer parameters, the time-drawdown data for HR.10, HR.10.1 and G29936HB was fitted with various applicable analytical solutions Figure 4.11 - 4.13.

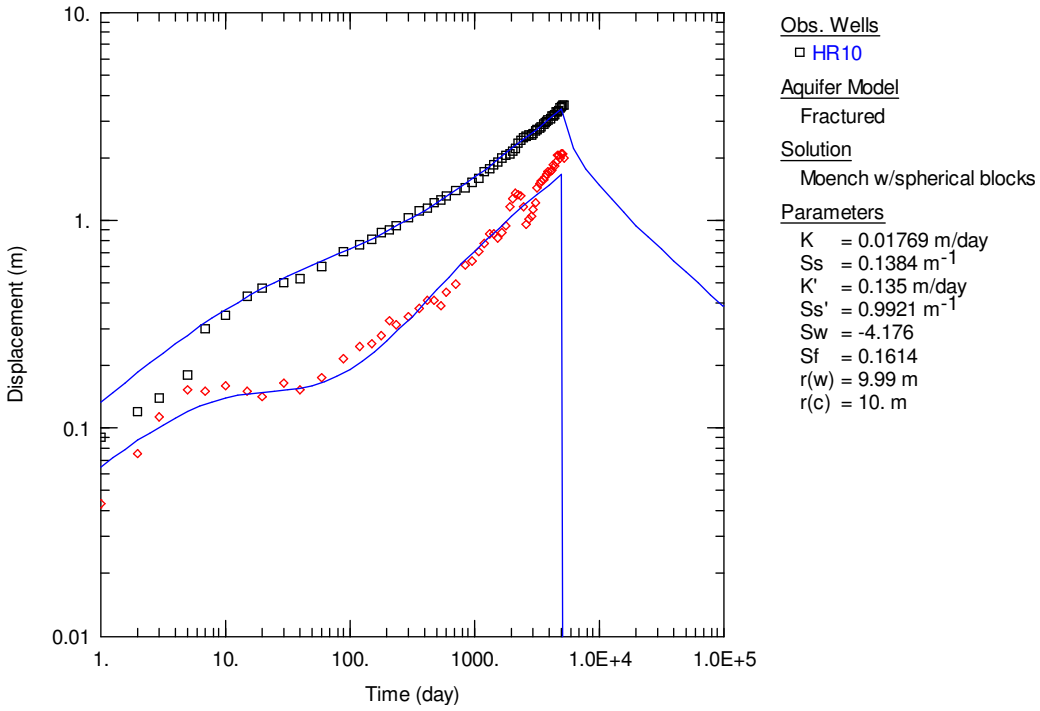

Figure 4.11 Log-log plot of drawdown vs. time including the derivative for HR.10 fitted with Moench solution (w/spherical blocks).

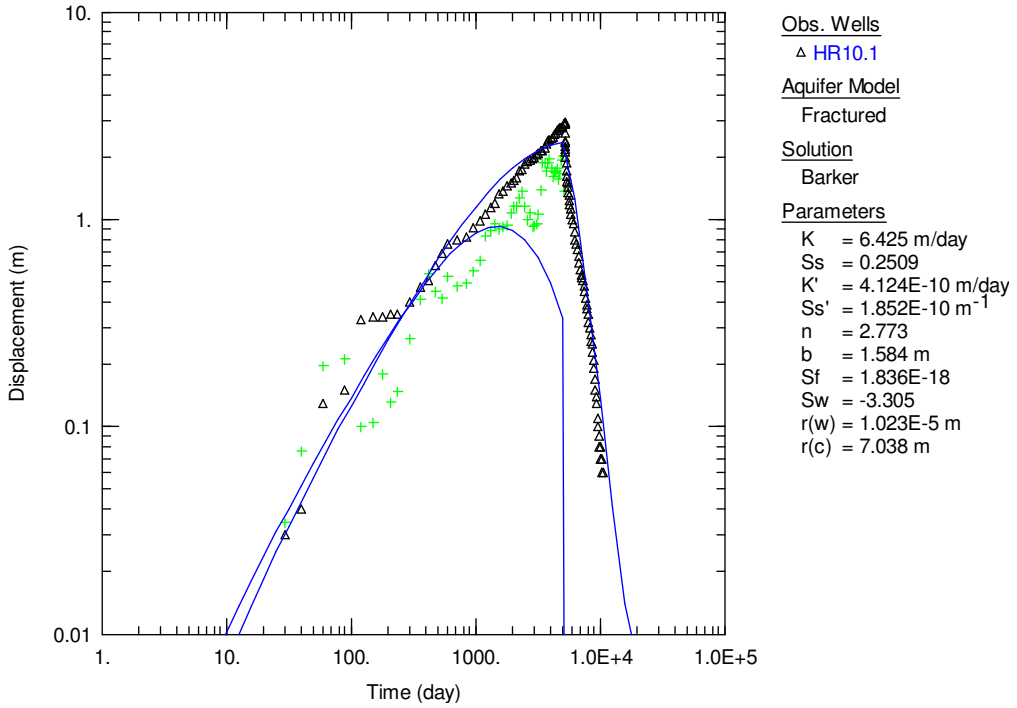

Figure 4.12 Log-log plot of drawdown vs. time including the derivative fitted with Barker's solution (Gringarten-Ramey).

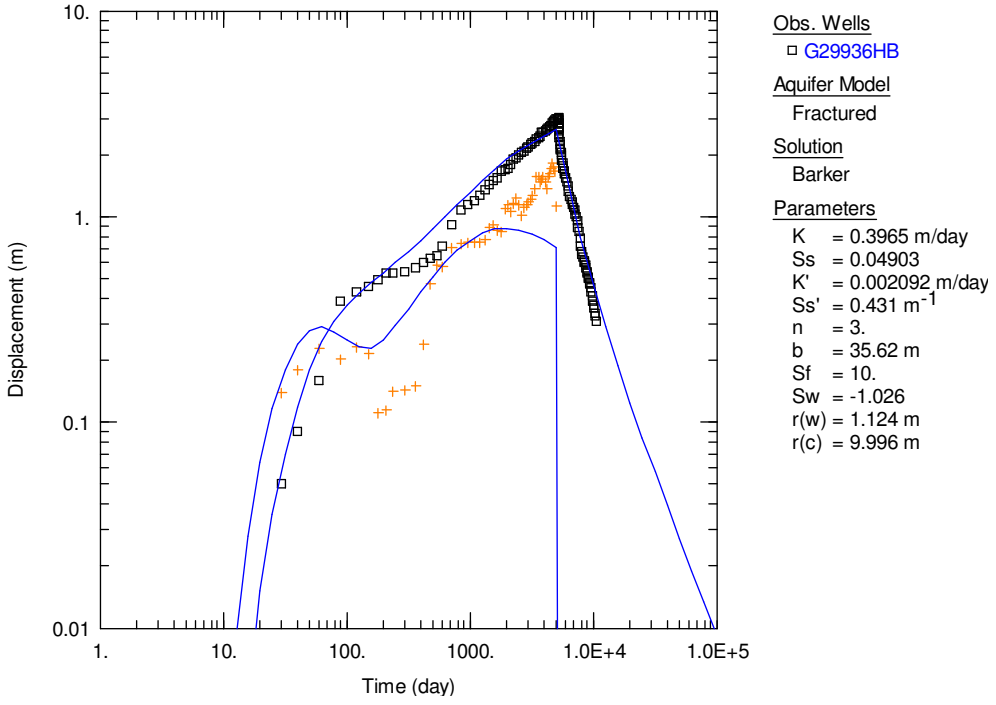

Figure 4.13 Log-log plot of drawdown vs. time including the derivative fitted with Barker's solution (w/spherical blocks)

The methods that gave the best fit after a no-flow boundary was fitted 9m from the abstraction borehole were the Moench (w/spherical blocks) and the Gringarten-Ramey (w/horizontal fracture) methods for fractured rock aquifers. The determined transmissivity and storativity values using the applicable analytical solutions are given in Table 4.6. The transmissivity and storativity vales given in the table compares favourably with that of Rose, (2008), who reported T-values greater than 100m^2/d for the Beaufort West region.

Table 4.6 T and S values determined for all boreholes (HR.10, HR.10.1 and G29936HB) using various analytical solutions.

Boreholes	HR10		HR10.1		G29936HB	
Solution	**T (m^2/d)**	***S*(-)**	**T (m^2/d)**	***S*(-)**	**T (m^2/d)**	***S*(-)**
Logan approximation	298	1.00E-03	363	1.00E-03	352	1.00E-03
Unconfined Aquifer						
Neuman	190	5.00-E-01	120	9.90E-03	149	1.67E-03
Confined Aquifer (initial estimate)						
Cooper-Jacob	110	9.00E-03				
Fractured Aquifer (Double- Porosity)						
Moench w/spherical blocks	167	5.00E-02	15	4.89E-03	22	6.33E-01
Fractured Aquifer (Single Fracture)						
Gringarten-Ramey-horizontal fracture	167	5.00E-02	268	2.20E-03	205	1.75E-03
Most probable value	**178**	**3.00E-02**	**184**	**3.96E-03**	**211**	**3.00E-03**

4.4 TRACER TESTS

4.4.1 Experimental setup and methodology

On the 10-02-2010 a tracer experiment under radially convergent flow conditions (pumping) were conducted to obtain more constrained aquifer parameters of the area surrounding the dolerite dyke on the farm Hansrivier, Beaufort West (Figure 4.14). The boreholes utilised for the tracer test was HR.10 (pumping) and G29936HB (injection). The experiment consisted of two components i.e. a tracer dilution in the injection borehole using non-iodated salt (Nacl) followed by the addition of the fluorescent dye uranin ($C_{20}H_{10}Na_2O_5$) and recovering it from HR.10. The salt injection process was carried out as a trial run before the actual tracer test with uranin in order to optimise the sampling schedule.

Approximately 20grams of uranin was dissolved in 500ml of site water and injected using a low flow pump into borehole G29936HB with 5l of chase fluid, once the drawdown stabilised (linear gradient).The injection process lasted less than 4 minutes, which can be assumed to be instantaneous with respect to the mean residence time of the tracer (~366minutes).After the tracer (Dirac pulse) was injected, the borehole column was mixed using a slug/bailer in order for the entire borehole section to be uniform with respect to the tracer solution, thus allowing the tracer to flow in fracture zones to the abstraction borehole (HR.10). The volume of both the tracer and chase fluid were reduced to the smallest possible amount in order to minimise the initial spreading of the tracer plume around the injection borehole. A spectroflourimeter was installed above the pump and was used to measure the uranin concentration at 2min intervals. Following the surprisingly fast arrival of the uranin (indicating good fracture connectivity between the boreholes), the sampling interval was reduced to 10s.

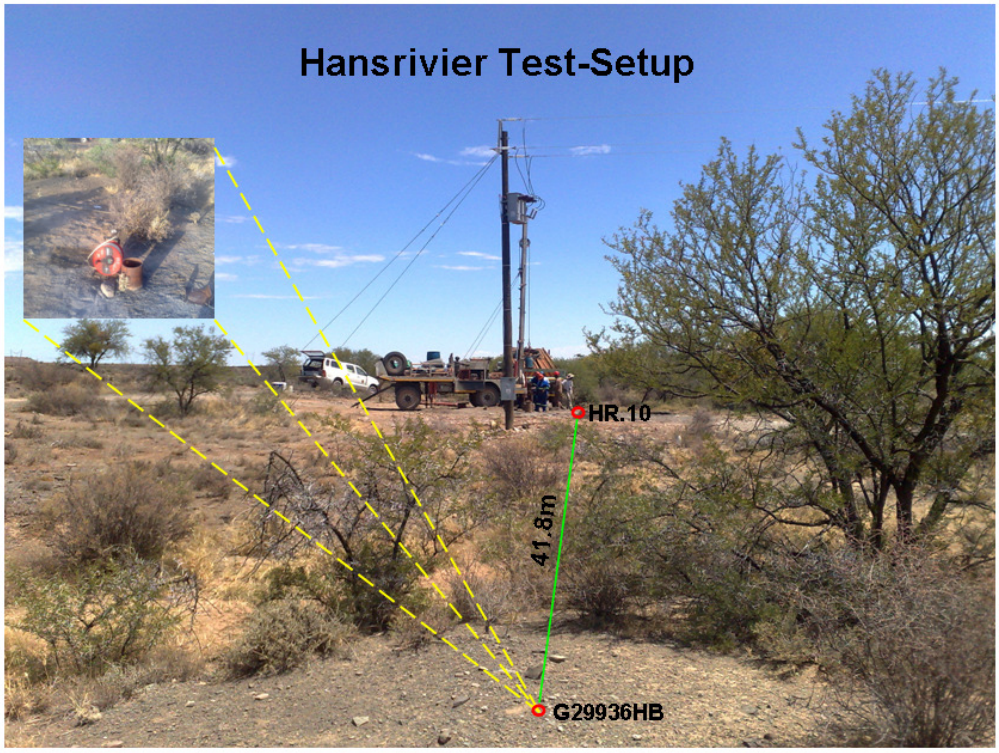

Figure 4.14 Principle sketch of tracer experimental setup.

4.4.2 Assessment of the Breakthrough Curve (BTC)

Linear groundwater flow velocities were calculated from the tracer test by dividing the distance between the injection point (G29936HB) and the sampling point (HR.10) by the travel time of the tracer. These linear flow velocities are lower than the real velocities along complex tortuous flow paths. The first appearance of the uranin at HR.10 was after approximately 140 seconds (t_{max}), which correspond to a maximal flow velocity (v_{max}) within the fractured dolerite dyke of 0.29m/s. The maximal flow velocity is normally defined the worst, because it is directly connected to the first appearance of the tracer at the sampling site and reduced with the analytical detection limit for the tracer (Käss, 1998). To obviate the above constraint, it is better to report the mean (v_{mean}) or dominant (v_{dom}) flow velocities, which in this instance equate to 0.0036m/s and 0.0112m/s respectively. The mean flow velocity is the ratio of the flow distance (injection – observation borehole) and corresponds to the time (t_{mean}) at which 50% of the recovered tracer mass passed the observation borehole. Whereas the dominant flow velocity,

corresponds to the time (t_{dom}) at which the maximal tracer concentration is observed (Käss, 1998).The breakthrough continued for at least 1.7 days, after which the sampling was stopped as the tracer concentration reached 0.36 ppb, close to the background value of 0.17ppb. A very good recovery of 70% the injected mass was observed for the dolerite dyke section. The tracer test results are given in Table 4.7 below.

Table 4.7 Summary of tracer experiment at the Hansrivier dyke area, Beaufort West.

Experiment	Hansrivier dyke
Date of injection	10-Feb-10
Amount of tracer (g)	20
linear distance (m)	42
Q (l/s)	10
Recovered mass (%)	70
t_{max} (s)	140
t_{mean} (s)	11755
t_{dom} (s)	3750
v_{max} (m/s)	0.29857
v_{mean} (m/s)	0.00356
v_{dom} (m/s)	0.01115

The tracer-breakthrough curve (BTC) generated by plotting measured tracer concentration at the Hansrivier dyke site versus time is presented in Figure 4.15. The BTC is characterised by a narrow peak and flat extended tailing, indicating dominant advective transport in the fracture(s) with diffuse coupling to the matrix (tailing). Most of the tracer mass was already recovered after 5.5hrs. As long as the migration of the tracer follows a discrete fracture set connecting both boreholes directly, the dispersion will be small. If the tracer migration however follows several discrete fracture sets intercepting each other, the dispersivities will increase due to interstitial mixing between different fracture sets (Maloszewski et al., 1999). The multiple peaks at intermediate times of the breakthrough curve points to the existence of secondary flow paths within the fracture network, allowing the uranin tracer to travel at different velocities. This can also be seen in the distinct rise of the relative recovery curve.

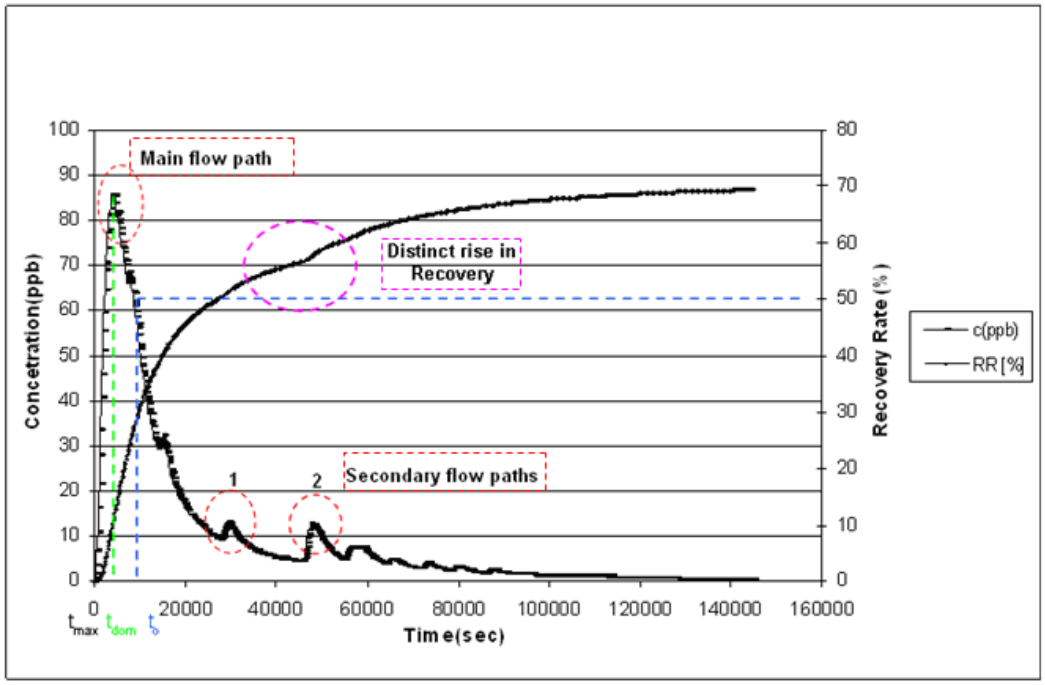

Figure 4.15 Tracer Breakthrough and recovery curves for the uranin test at HR.10.

4.4.3 Analytical Modeling

The Single Fissure Dispersion Model (SFDM) developed by Maloszewski and implemented in the software Traci95 was used to fit the observed BTC (Käss, 1998).The Traci95 software program was also used for modeling the tracer breakthrough curves and determining the hydraulic properties of the main and secondary flow paths shown in Figure 4.15. The theoretical tracer breakthrough curves were simulated using the best-fit method on the basis of measured concentrations. The parameters of the SFDM obtained by fitting Eq.15 to the tracer concentration measured at HR.10 are summarised in Table 4.8.

Table 4.8 Fitting Parameters of the SFDM (*Pe*, t_0, and *a*) and derived physical parameters (*2b*, α_l, D_{eff}, n_f, and v)

Uranin		Main flow path	Flowpath.1	Flowpath.2
Pe	[-]	0.88	6556	3152
t_o	[s]	22003	29027	47706
a	[s^-0.5]	0.00097	0.00046	0.00039
2b	[µm]	828	721	563
α_l	[m]	47.5	0.0064	0.0133
Deff	[m^2/s]	6.46E-12	1.10E-12	4.82E-13
nf	[%]	4.01	5.29	8.69
v	[m/s]	1.90E-03	1.44E-03	8.76E-04

The mean residence time (t_o) and longitudinal dispersivity (α_l) obtained from the BTC, indicating the main flow path Figure 4.16 was 6hrs and 47.5m, respectively. Appendix.C, gives the mean residence time and longitudinal dispersivity for the dataset using a statistical method as a first order estimate. The high longitudinal dispersivity (47.5m) is mainly due to the extensive tailing effect of the BTC. The fracture aperture and porosity shown in Table 4.8 were calculated using the following equations (Maloszewski et al., 1999):

$$2b = \sqrt{\ln\frac{X}{r_w}\cdot\frac{6\cdot v\cdot\tau_{f2}\cdot X^2}{g\cdot t_0\cdot\Delta H_t}} \qquad \text{Equation 36}$$

$$nf = \frac{Q\cdot t_0}{\pi\cdot m\cdot X^2} \qquad \text{Equation 37}$$

For the main and secondary flow paths the derived values for the fracture aperture (2b) and fracture porosity (nf) was in the range of (563 - 828µm) and (4.00 – 8.69%).

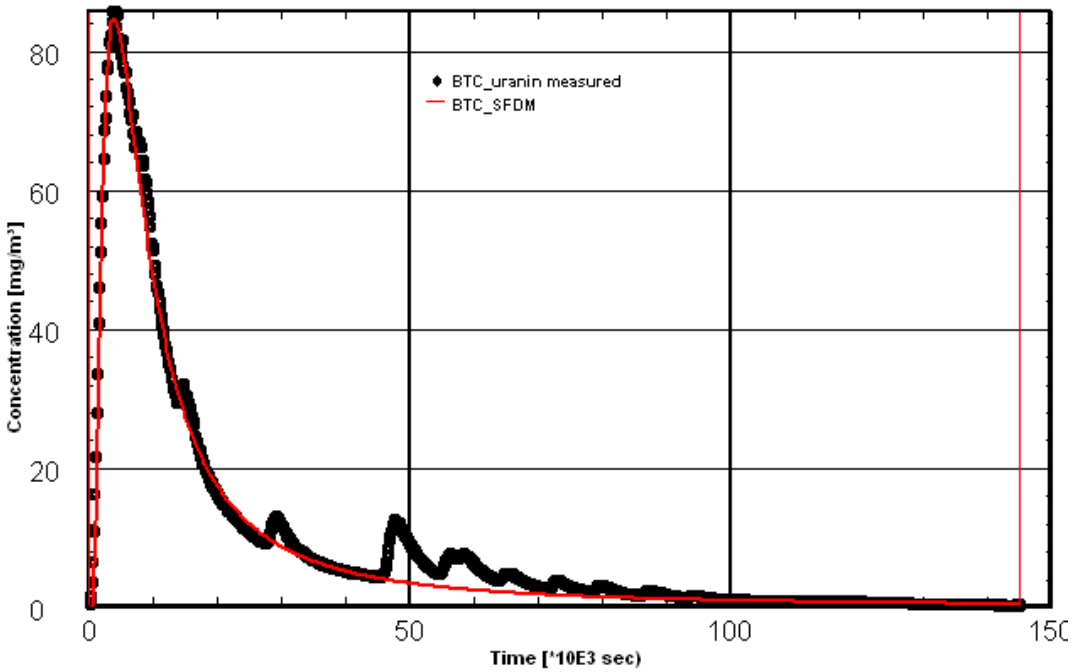

Figure 4.16 Best_SFDM fit of the observed uranin breakthrough curve (Main flow path).

While the overall fit of the BTC is good (Figure 4.16), there are obvious deviations from the fitted SFDM at intermediate to late times. This points to the existence of secondary flow paths as mentioned earlier. Interpretation of these deviations can be based on the assumption that the final BTC is a superposition of several BTC's in each flow path. This can be modeled by applying the multi-channel model (MCM) of the SFDM (Maloszewski et al., 1999). Figure 4.17 and Figure 4.18 are the BTC's to which the MCM of the SFDM was applied, with the relevant parameters given in Table 4.8 as flowpaths.1 and 2. In general, minor variations of the modeled parameters are observed, with the exception of the Pe and α_l values. The MCM gave Pe values, which ranged from 0.8 for the main flow path to 6556 for the secondary flow paths (flow path 1 and 2). This implies that the modeled peaks on the BTC travelled purely by advection, with very small longitudinal dispersivities in the order of (0.0064 – 0.0133) for the secondary flow paths.

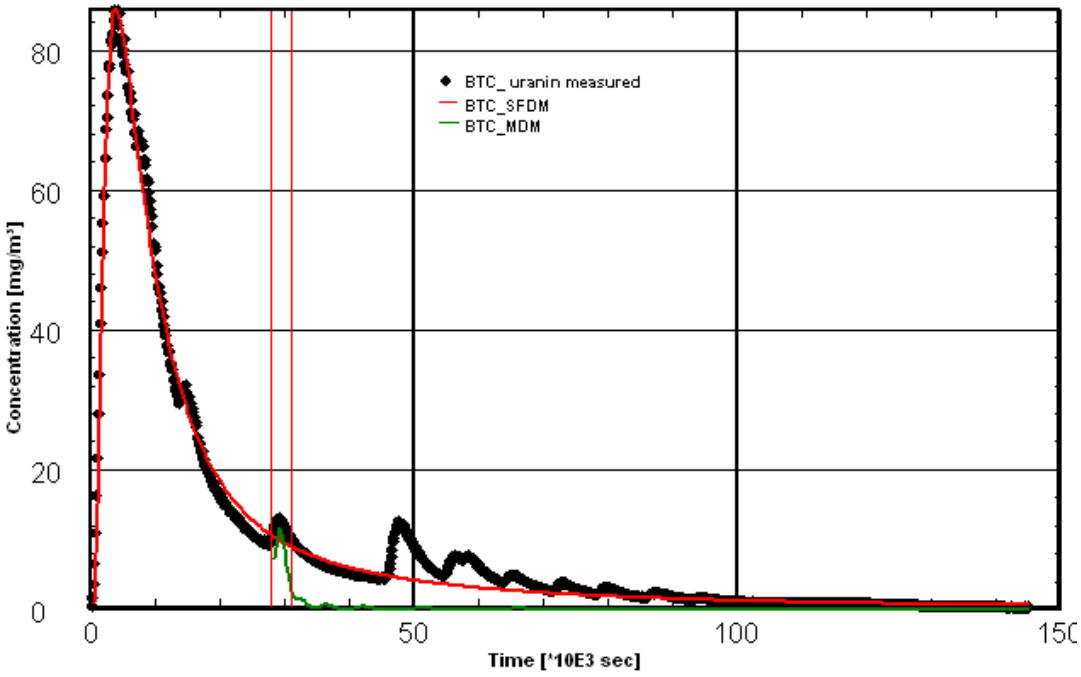

Figure 4.17 Best_SFDM fit of the observed BTC (Flowpath.1)

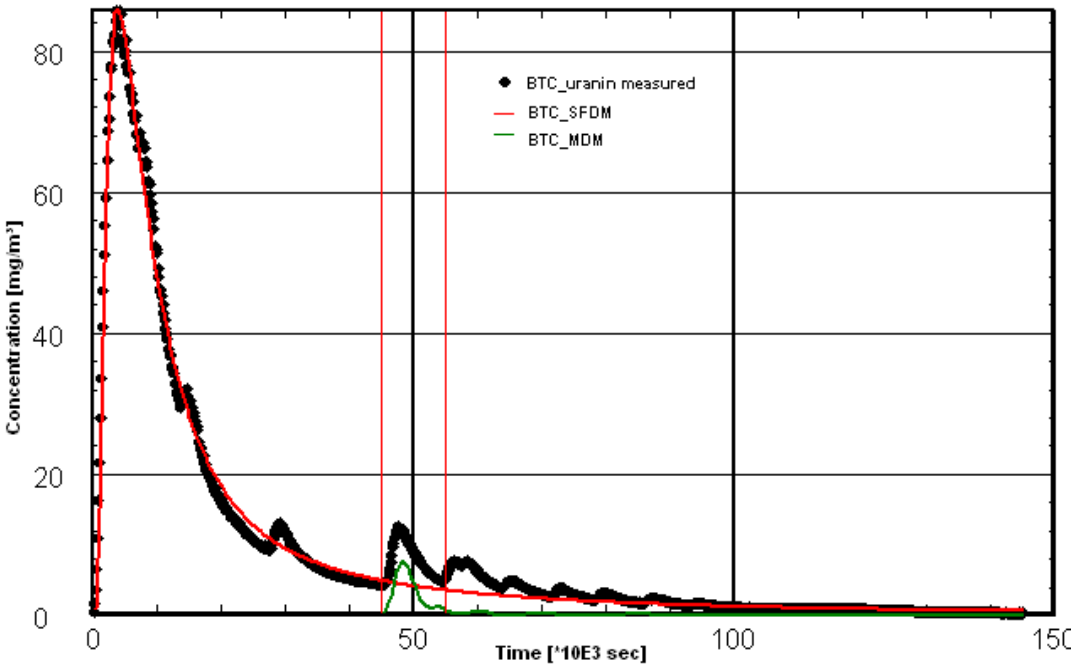

Figure 4.18 Best_SFDM fit of the observed BTC (Flowpath.2)

In order to effectively interpret the BTC's with respect to matrix diffusion, the tailing effects needed to be characterised. Becker and Shapiro, (2000) have shown that extensive tailing of BTC's conducted in fracture networks of crystalline rocks are not always an artifact of diffusion processes, but rather an advective-dominated process caused by spatial and temporal heterogeneous transport. A diffusion determined tailing can however, be identified by a decrease in the concentration of the tailing according to $t^{-1.5}$ (Tsang, 1992). From Figure, 4.19 it can be seen that matrix diffusion is indeed evident in the BTC as the data plot on a straight line fitted with $t^{-1.5}$ up to a time of 50 000 seconds. Thereafter the graph displays oscillating peaks that does not seem to fit the straight line section fitted with $t^{-1.5}$. It appears as if there is an underdamp hydraulic pressure response in the abstraction borehole (HR.10), which could be as a result of power fluctuations in the pumping rate, allowing for the retarded release of the tracer from the injection borehole.

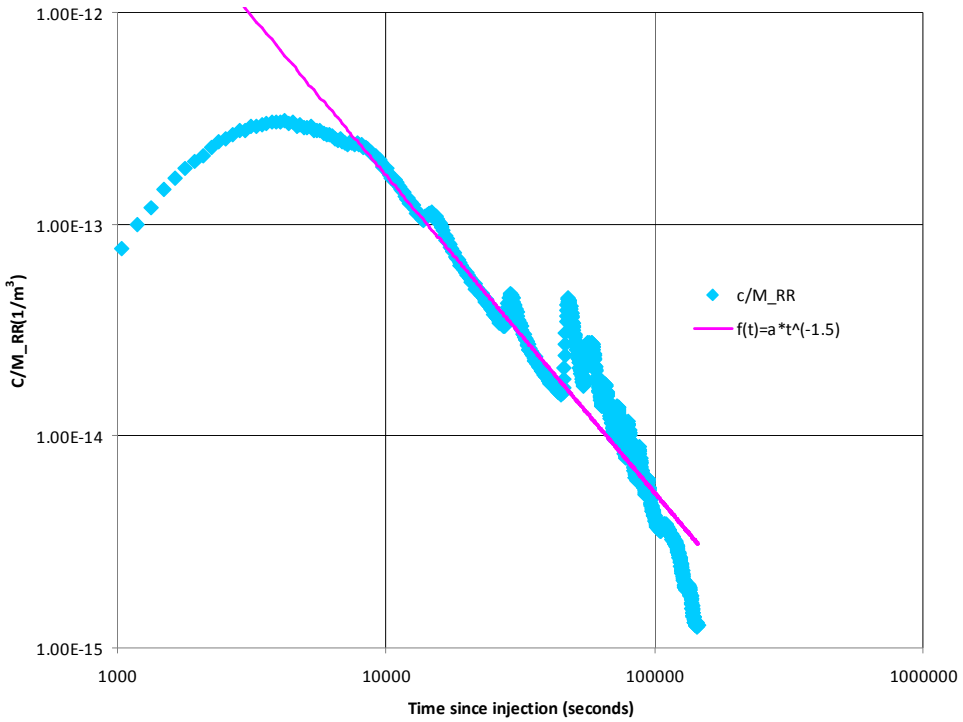

Figure 4.19 Log-log plot of the normalised uranin breakthrough curve

The derived effective diffusion coefficient (Deff) for the main flow path equaled 6.46E-12 m^2/s, which is in good agreement with laboratory determined values for sandstones (1.69E-11 to 7.10E-11) given by Boving and Grathwohl, (2001).

4.4.4 Conclusion

The tracer test results have confirmed the existence of a good hydraulic connectivity between boreholes HR.10 and G29936HB, situated 41.8m from each other. More importantly it was shown that transport occurred via multiple pathways with different hydraulic properties. The flow velocities of the fractures was in accordance with the cubic law (Equation.16), which states that flow will increase with the cube of the fracture aperture (Witherspoon et al., 1980).Furthermore, tracer diffusing into stagnant water zones within the fracture and the matrix was identified as an important retardation mechanism. Modeling of the experimental data with the multi-channel SFDM captured the overall response of the BTC's very well and gave satisfactory estimates of the transport parameters. In summary, interpretation of the tracer test in combination with geological information and aquifer tests have resulted in an improved understanding of the physical transport processes at the Hansrivier site.

4.5 FLOW CONCEPTUALISATION

The localised flow dynamics of the Hansrivier dyke and the contaminant transport processes of the groundwater system will form the basis of this discussion. According to McMahon et al., (2000) the conceptual model should be based on a sound understanding of the groundwater flow system in order to represent properly the advective component of contaminant transport and it should identify all source pathway receptor linkages. Based on the results as described in the above sections, a cross-section was developed to summarise the important aquifer parameters. Figure 4.20, shows the extent of the cross-section profile (X-Y) that was drawn perpendicular to the Hansrivier dolerite dyke.

Karoo fractured-rock aquifers associated with dolerite intrusions store water in the interconnected fractures that have developed in the surrounding sediments. Based on field and borehole information the importance of bedding-plane fractures is clearly demonstrated as the dominant permeability in the aquifer system. This can be seen from Figure 4.21 as the main conductive zone connecting boreholes HR.10, HR10.1 and G29936HB, with borehole yields in excess of 10l/s. The dolerite dyke can be regarded as a groundwater barrier, due to the groundwater quality differing on either side of the dyke (EC = >150mS/m East, <100mS/m West) Rose, (2008). The arrows (blue) on the eastern side of the dyke indicates flow within the 3m conductive zone (weathered), which was identified by camera and pH-EC logging. The fractured rock aquifer was further characterised by conducting a pumping and radially convergent tracer test. As mentioned previously the aquifer medium was found to be of dual porosity, with both fractures and matrix supplying the boreholes with groundwater at late times. The fracture aperture (828µm), porosity (4%) and velocity (1.90E-03m/s) is very high, which can mainly be attributed to intense weathering allowing flow to be channeled in flow paths of least resistance. The transmissivity and storativity values obtained from the pumping test were found to be more than adequate for municipal purposes Table 4.6.

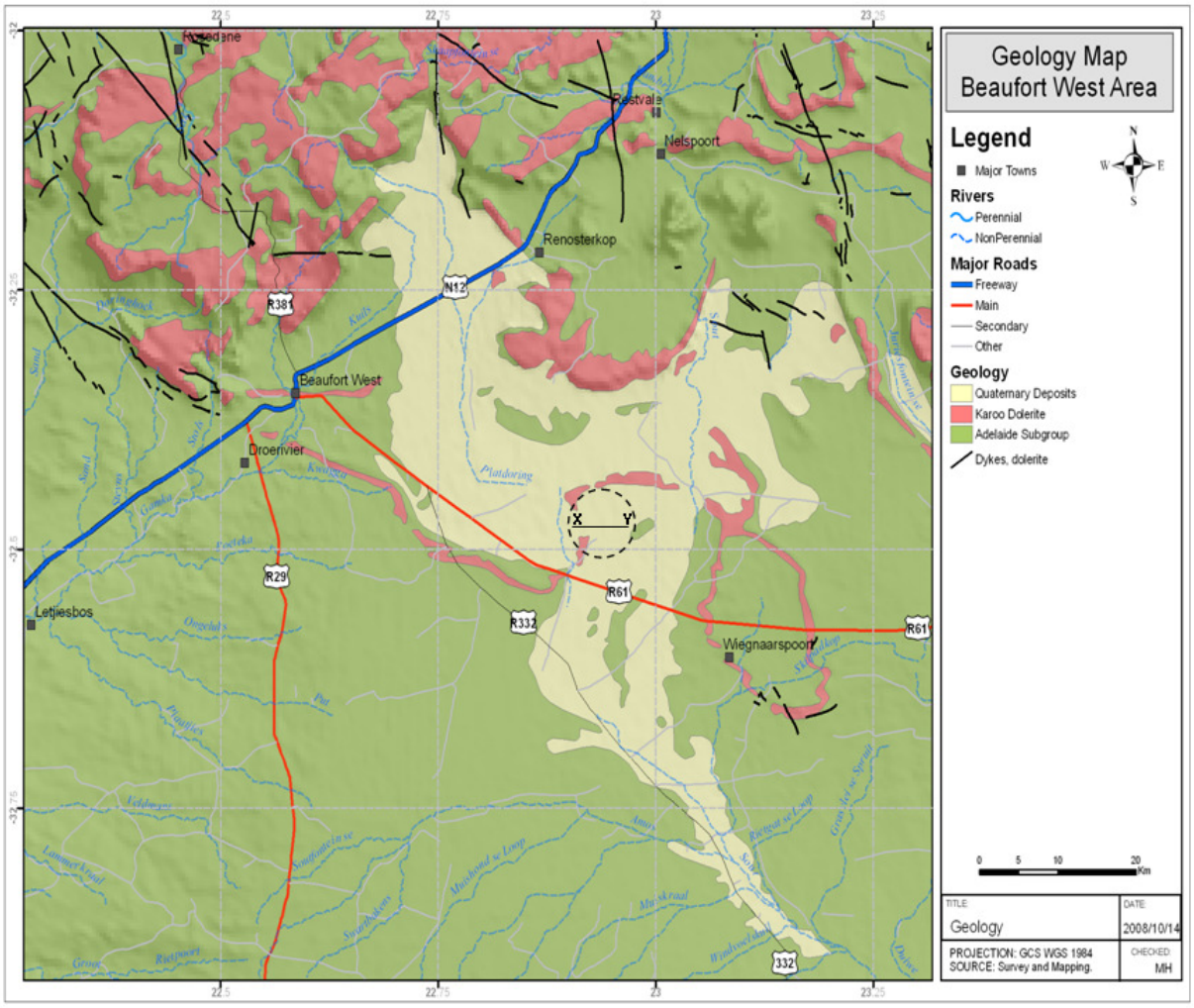

Figure 4.20 Geological map indicating location of cross-section (X-Y).

In terms of radioactivity uranium-series disequilibria exists in all three boreholes. The activity ratios are all above unity, implying that the groundwater has been in contact with the uranium host-rock (koffieklip), through water rock interaction. This allowed the U^{234} isotope to be preferentially leached from the crystal lattice by means of alpha recoil. As mentioned previously this is normally associated with natural radioactivity conditions.

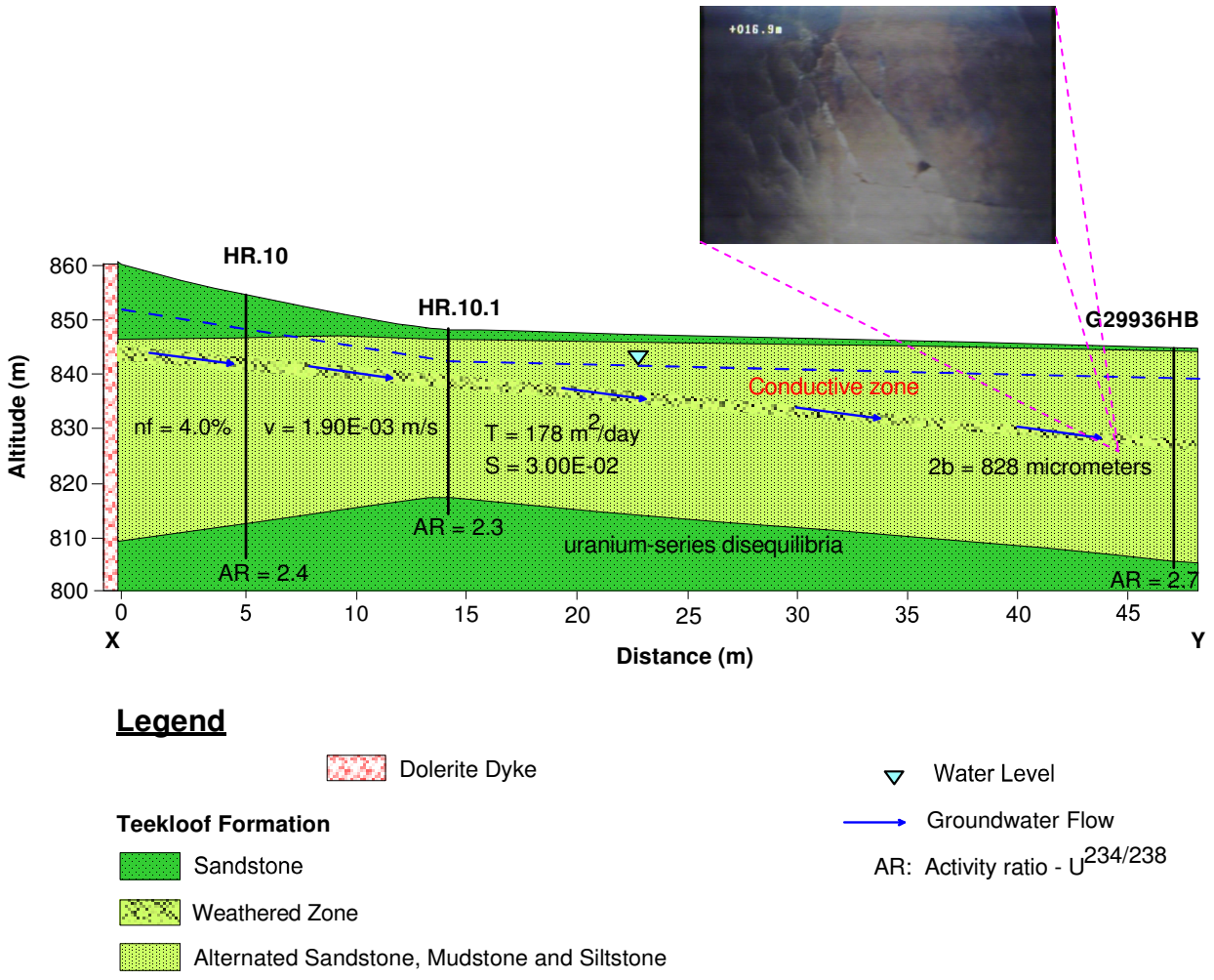

Figure 4.21 Cross-section of the Hansrivier Dyke as illustrated in Figure 4.18, indicating the major aquifer properties.

In conclusion horizontal bedding-plane fractures are persistent throughout lithological units as seen from the camera logging, and based on the aperture size allow flow to occur along them. Geological contacts and intrusive dykes form low flow boundaries effectively controlling the localised flow direction (West to East) along the strike, based on the water level measurements Figure 4.21.Conceptualising flow although at a very small scale has shown the dynamics of the flow system, and implications for further development of the resources. This information is critical as all these boreholes in conjunction with the municipal wellfield North of Beaufort West, are currently being used to supply the town with water. Therefore the sustainable utilisation of this resource is of fundamental importance for the future development of Beaufort West.

CHAPTER 5 – CONCLUSIONS AND RECOMMENDATIONS

5.1 SUMMARY

The main objective of this study, since its outset, was to asses the various transport mechanisms of radionuclides in fractured-rock aquifers. The review of literature showed the different approaches that are used both locally and in other parts of the world to address this issue. The focal point of the review was to integrate the various components of the study, to meet the objectives upon which this research is based.

The objectives have been achieved. The study identified the various transport mechanisms, namely advection, matrix diffusion, mechanical dispersion, sorption and decay. It provided detail descriptions of each process, and went further to evaluate the effects and controls they have on contaminant transport behavior particularly in fractured rock aquifers. The hydrogeological investigation characterised the heterogeneity of the fractured rock aquifer by sampling for water quality and by conducting various aquifer tests. The hydrochemical description of the groundwater was typical of shallow fresh groundwater, changing composition to a more sulphate hydrochemical facies along the flow path. In terms of radioactivity, although the uranium does not seem to be present in unsafe levels in groundwater throughout the study area, it still remains a concern especially when mining commences, which will ultimately alter the physico-chemical properties of the underlying geology. The considerable heterogeneity of rock types within the Karoo appears to play a role in the varying levels of uranium in the groundwater; however, it is more likely the differing solubility of uranium in the various lithologies (Moordernaars, Poortjie and Oukloof formations) that affects its concentration in the water. The fractured-medium of the aquifer system served as a conduit for groundwater flow as well as storage. The complexity of the aquifer system was further established during the pumping and tracer tests. It was shown that transport took place via multiple flow paths having different hydraulic properties and that the effects of matrix diffusion was evident. Furthermore, the high transmissivity and borehole yields obtained from the pumping test, confirmed the aquifers potential as a major source of water supply that needs to be managed

sustainably. The conceptualisation of flow at a local scale using all the information and data gathered was utilised to construct a cross-section depicting the main aquifer parameters of the system. Dyke intrusions were looked at as hydraulic boundaries contributing to compartmentalisation of the aquifer and creating unique, site specific flow conditions. Probably of greatest importance is the role of the joints, making up predominantly bedding-planes and sets of interconnected fractures. These have been shown to be persistent, at least on the scale of investigation, with their cumulative effect on flow being considerable.

5.2 RECOMMENDATIONS

The town of Beaufort West has grown dramatically over the past few years with major companies exploring for uranium, reminiscent of the 1970's when uranium exploration was at its peak in the Karoo. This has led to a huge influx of locals from neighboring towns in search of better jobs. This influx of people has placed a huge demand on the already over -utilised water resource of the town. It is against this backdrop and to large extent the current drought and competing usage for groundwater by farmers that the local municipality decided to drill an additional wellfield on the farm Hansrivier targeting the dolerite dykes to alleviate the pressure on the demand for water. It is quite clear that water in the Karoo is a scarce commodity that needs to be managed sustainably in order for the town of Beaufort West to continue developing its economic sector though mining.

Based on the present study a number of areas for future and further investigation are suggested.

- In the interest of further constraining both the extent of uranium contamination and the characteristics of the various rock types in the region, it is recommended that the DWA implement a monthly sampling campaign of the various boreholes to look at seasonal variations in water quality and groundwater levels.

- In order to test the validity of the two controlling factors identified by this study, namely the hydrological and lithological settings in the solubility of uranium. Bulk-rock geochemistry analysis using neutron activation along with optical analysis of thin sections should be carried out to quantify the concentration of uranium in the rock samples and whether or not it correlates with uranium levels in boreholes.

- The high flow velocities, concentrations and recovery rates of the tracer used demonstrated the high vulnerability of the groundwater to radionuclide contamination. Therefore the implementation of aquifer protection zones around water supply boreholes (HR10, HR10.1 and G29936HB) is critical, as it is currently being used to augment the current water supply to Beaufort West.

- Furthermore the determination of sustainable yields of all the boreholes in the wellfield using the FC-method must be given a high priority and should take into account the hydrological system, concerns and needs of the inhabitants, potential impacts to groundwater quality, and environmental side effects. This will undoubtedly assist the local municipality in effective water resource management and ultimately to make more informed decisions on how to best utilise this dwindling resource.

REFERENCES

Abelin, H., Birgersson L., Widen H., Argen T., Moreno L., and Neretnieks I. (1994). *Channeling experiments in crystalline fractured rocks*. Journal of contaminant hydrology, **1**, 129 – 158.

Acocks, J.P.H. (1988). *Veld Types of South Africa*. 3rd edition. Botanical Research Institute, South Africa.

Bain, J.G., Mayer, K.U., Blowes, D.W., Frind, E.O., Molson, J.W.H., Kahnt, R. and Jenk, U. (2001). Modelling the closure – related geochemical evolution of groundwater at a former uranium mine. *Journal of Contaminant Hydrology*, **52**, 109 – 135.

Barker, J. A. (1988). *A Generalized Radial-flow Model for Pumping Tests in Fractured Rock*. Water Resources. Res. **24**(10). pp. 1796 – 1804.

Bear J, Tsang C.F, de Marsily G. (1993). *Flow and contaminant transport in fractured rock* .San Diego: Academic Press, Inc. Chapters 1, 2 &5.

Becker, M.W. & Shapiro, A.M. (2000). *Tracer transport in fractured crystalline rock: Evidence of nondiffusive breakthrough tailing*. Water resource research, **36**, No.7: 1677 – 1686.

Becker, M.W. (2003). *Distinguishing Advection, Dispersion, and Diffusion in fractured bedrock*. Groundwater in fractured rocks Prague, Czech Republic: Krasny – Hrkal – Bruthans.

Berkowitz, B. and Nativ, R. and Adar, E. (1999). *Evaluation of conceptual and quantitative models of fluid flow and chemical transport in fractured media*. U.S. national committee for rock mechanics.

Berkowitz, B. (2002). *Characterizing flow and transport in fractured geological media: A review*. Water resource research, **25**: 861 – 884.

Black, J. H. (1994). *Hydrogeology of Fractured Rocks – A Question of Uncertainty about Geometry*. In: Voss, C. I. & Wilson, W. E. (eds.) (1994). Applied Hydrogeology. **2**(3). Verlag. Hanover. pp. 56 –70.

Bodin, J. and Delay, F. and de Marsily, G. (2003). *Solute transport in a single fracture with negligible matrix permeability: 1. Fundamental mechanisms.* Hydrogeology Journal, 11.

Bonotto, D. M. and Mello, C.B. (2006). A combined method for evaluating radon and progeny in waters and its use at Guarani aquifer, Sao Paulo State, Brazil. *Journal of Environmental Radioactivity*, **86**, 337 – 353.

Botha, J.F., Verwey, J.P., van der Voort, I., Vivier, J.J.P., Buys, J., Colliston, W.P, and Loock, J.C. (1998). *Karoo aquifers Their Geology, Geometry and Physical Properties*. WRC Report no: 478/1/98.

Bourdet, D., Whittle, T.M., Douglas, A.A. and Pirard, Y.M. (1983). A new set of type curves simplifies well test analysis, Word Oil: 95-106.

Brunke, E.G. (1977). *Hydrogeochemical orientation surveys at two uranium deposits in the Beaufort West area*. Geological Survey, Pretoria. Report no: 1978 – 0047.

Boving, T.B, and Grathwohl, P. (2001). *Tracer diffusion coefficients in sedimentary rocks: correlation to porosity and hydraulic conductivity*. Journal of Contaminant Hydrology, **53**: 85-100.

Carrera, J., Sanchez-Vila, X., Benet, I., Medina, A., Galarza, G. and Guimera, J. (1998), *On matrix diffusion: formulations, solution methods and qualitative effects*, Hydrogeology Journal, **6**,178-190.

Catuneanua, O., Hancox, and Rubidge. (1998). *Reciprocal flexural behaviour and contrasting stratigraphies: a new basin development model for the Karoo retroarc foreland system, South Africa*. Basin Research **10** (4), 1998: 417-439.

Cole, D.I., Labuschagne, L.S. and Sohnge, A.P.G. (1991). *Aeroradiometric survey for uranium and ground water follow up in the main Karoo Basin*. Memoir 76 of the Geological Survey. Department of Minerals and Energy Affairs, 145pp.

Cole, D.I. and Wipplinger, P.E., (2001). *Sedimentology and Molybdenum Potential of the Beaufort Group in the Main Karoo Basin, South Africa*. Memoir **80**. Council for Geoscience, Pretoria, South Africa.

Cook, P.G. (2003). *A guide to regional groundwater flow in fractured rock aquifers*. CSIRO Land and Water, Glen Osmond, SA, Australia, Chapters 1 – 6.

Cooper, H. H. & Jacob, C. E. (1946). *A Generalized Graphical Model for Evaluating Formation Constants and Summarizing Well Field History.* Am Geophys. Union Trans **27**. pp. 526-534.

Dickin, A.P. (2005). *Radiogenic Isotope Geology*. 2nd Edition. Cambridge University Press, New York. pp. 112-135.

Domenico, P.A. & Schwartz, F.W. (1998). *Physical and chemical hydrogeology*. 3rd edition. New York: John Wiley.

Doughty, C and Tsang, C.F. (2005). *Signatures in flowing fluid electric conductivity logs.* Journal of Hydrology, **310**: 157-180.

Drever, J.I. (1988). *The Geochemistry of Natural Waters*. 2nd Edition. Prentice -Hall publishers, New Jersey. pp. 367-381.

Fetter, C.W. (1999*). Contaminant hydrogeology*. 2nd edition. Prentice – Hall, Chapters 2 -3.

Department of Water Affairs and Forestry, (1996). *South African Water Quality Guidelines (second edition)*. Volume 1: Domestic Use.

Department of Water Affairs and Forestry, (2002). *Radioactivity dose calculation and water quality guideline for domestic water use*. Pretoria

Folger, P.F, Poeter, E, Wanty, R.B, Day, W, and Frichman, D. (1997). *Rn^{222} transport in a fractured crystalline rock aquifer: results from numerical simulations.* Journal of Hydrology, **195**: 45 – 77.

Giammar, D. (2001). *Geochemistry of uranium at mineral – water interfaces: rates of sorption – desorption and dissolution – precipitation reactions*. Pasedena, California: PhD thesis, California Institute of Technology

Grainger, L. (1985). *Uranium and thorium*. London, George Newnes Ltd

Hantush, M. S. and Jacob, C. E. (1955). *Nonsteady Radial Flow in an Infinite Leaky Aquifer*. Trans.Am. Geophys. Union. **36**. pp. 95 – 100.

Hem, J.D. (1985). *Study and interpretation of the chemical characteristics of natural water.* 3rd edition, Department of the Interior, U.S. Geological Survey.

Himmelsbach, T., Hötzl, H. and Maloszewski, P. (1995). *Long distance tracer tests in a highly permeable fault zone at the Lindau fractured rock test site*. In: Tracer Technologies for Hydrological Systems (ed. by Ch. Leibundgut) (Proc. IUGG Symp., Boulder, Colorado, July 1995, 133-140. IAHS Publ.no. 229.

Hiscock, K. (2005). *Hydrogeology: principles and practice.* Blackwell Science Ltd, UK – 208pp.

Hobday, DK, and WE Galloway. (1999). *Groundwater processes and sedimentary uranium deposits*.Hydrogeology Journal, **7**, 127-138.

Hoadley, M. (2007). *Proposed Ryst Kuil Uranium Project*. Environmental Impact Assessment. Public Information Document. pp. 3-17.

Hounslow, A.W. (1995). *Water Quality Data: Analysis and Interpretation*, CRC Lewis Publishers, Boca Raton, FL, pp. 86-87.

Ivanovich, M and Harmon, R.S. (1982). Uranium series disequilibrium, applications to environmental problems. Oxford: Clarendon Press: 120 – 128.

Johnson, M.R., Anhaeusser, C.R. and Thomas, R.J. (Eds.) (2006). The Geology of South Africa. Geological Society of South Africa, Johannesburg/Council for Geoscience, Pretoria, 691 pp.

Käss, W. (1998). *Tracing Technique in Geohydrology*. A.A Balkema Publishers, Netherlands. pp. 315-384.

Kotze, J.C., Pointer, C. and Rosewarne, P.N. (1997). *Assessment of the Hydrogeological potential of the Brandwacht aquifer Phase.2*. Beaufort West Municipality, Report no: 227331/1.

Kotz, J.C. and Treichel, P. (1999). *Chemistry & chemical reactivity*. 4th edition. Saunders College Publishing, United States of America. – 1089pp.

Kruseman, G.P. and De Ridder, N.A. (1991). *Analysis and Evaluation of Pumping Test Data.* (2nd ed.) International Institute for Land Reclamation and Improvement. Wageningen, Netherlands.

Kurttio, P., Auvinen, A., Salonen, L., Saha, H., Pekkanen, J., Mäkeläinen, I., Väisänen, S.B., Penttilä, I. M. and Komulainen, H. (2002). *Renal effects of uranium in drinking water. Environmental Health Perspectives*, **110** (4), 337 – 342.

Langmuir, D. (1997). *Aqueous environmental geochemistry.* Prentice – Hall, Upper Sadle River, New Jersey. – 486pp.

Maloszewski, P. & Zuber, A. (1990). *Mathematical Modeling of Tracer Behaviour in Short-Term Experiments in Fissured Rocks*. Water Resources Research **26** (7) 1517-1528.

Maloszewski, P., Herrmann, A. and Zuber, A. (1999). *Interpretation of tracer test performed in fractured rock of the Lange Bramke basin, Germany*. J Hydrol. 7. pp 209-218.

Maréchal, J. C., Dewandel, B. and Subrahmanyam, K. (2004). *Contribution of Hydraulic Tests at Different Scales to Characterize Fracture Network Properties in the Weathered-fissured Layer of a Hard-rock Aquifer*. Water Resources Research. **40**. W11508.

McMahon, G. A. Arunkumaren, H. J., and Bajracharya, K. (2000). Hydrogeological conceptualisation of the Burdekin River Delta. 2000. Hydro 2000 - proceedings of the 3rd International Hydrology and Water Resources Symposium of the Institution of Engineers.

Moreno, L and Neretnieks, I. (1993). *Flow and nuclide transport in fractured media: The importance of the flow- wetted surface for radionuclide migration.* Journal of contaminant hydrology**, 13**: 49 – 71.

Moreno, L., Gylling., B, Neretnieks, I. (1997). *Solute transport in fractures media – the important mechanisms for performance assessment.* Journal of contaminant hydrology, **25:** 283 – 298.

National Research Council. (1996*). Rock fractures and fluid flow – Contemporary understanding and applications*. Washington, D.C. (National Academy Press). Chapters 2 – 5.

Nhleko, L. and Dondo, C. (2008). *The Hydrogeology of Beaufort West.* Council for Geoscience. Project no: ST-2008-0974. Report no: 2008-0050.

Przylibski, T.A. (2000). *Estimating the radon emanation coefficient from crystalline rocks into groundwater*. Applied Radiation and Isotopes, **53**, 473 – 479.

Rama and Moore, W.S. (1984). *Mechanisms of transport of U-Th series radioisotopes from solids into groundwater.* Geochimica et Cosmochimica Acta, **48:** 395 – 399.

Raghavan, R. (2004). A review of applications to constrain pumping test responses to improve on geological description and uncertainty. Am. Geophys. Union Trans., v.**42**, p 1-29.

Raven, K.G and Gale, J.E (1985). *Water flow in a natural rock fracture as a function of stress and sample size.* Int. J. Rock Mech. Min. Sci. & Geochem. Abstr, **22** (4): 251 – 261

Rose, R and Conrad, J. (2007). *A regional reconnaissance to identify areas fro groundwater development in Beaufort West*. GEOSS Report no: G2007/05-03.

Rose, R. (2008). *Aquifer characterisation and groundwater flow regimes of Karoo aquifers in Beaufort West, Western Cape Province*. GEOSS Report no: G2008/07-01.

Reyes, E. and Marques, L.S. (2008). Uranium series disequilibria in ground waters from a fractured bedrock aquifer (Morungaba Granitoids – Southern Brazil): Implications to the hydrochemical behavior of dissolved U and Ra. Applied Radiation and Isotopes, **66**, 1531 – 1542.

Sami, K and Druzynski, Al. (2003). *Predicted spatial distribution of naturally occurring Arsenic, Selenium and Uranium in groundwater in South Africa-Reconnaissance survey.* WRC report: 1236/03.

Saxena, V.K., Mondal, N.C., Singh, V.S and Kumar, D. (2005). *Identification of water-bearing fractures in hard rock terrain by electrical conductivity logs, India*. Environ Geol, **48:** 1084-1095.

Shapiro, A. M., Hsieh P.A., Williams, C. Burton and Gregory, J. W. (2007). *Integrated Multi –Scale Characterization of Groundwater flow and chemical transport in fractured crystalline rock at the Mirror lake site, New Hampshire*. American Geophysical Union, Geophysical Monograph Series **171**: 201 – 223.

Theis, C. V. (1935). *The Relation between the Lowering of the Piezometric Surface and the Rate and Duration of Discharge of a Well using Ground-water Storage*. Am. Geophys. Union Trans., v.**14**, pt. 2, p. 519-524.

Tsang, Y.W and Tsang, C.F. (1989). Flow channeling in a single fracture as a two-dimensional strongly heterogeneous permeable medium. Water Resource Research, **25** (9): 2076 – 2080.

Tsang, C.F., Tsang, Y.W and Hale, F.V. (1991*). Tracer transport in fractures: Analysis of field data based on a variable –aperture channel model*. Water resource research, **27** (12): 3095 – 3106.

Tsang, Y.W. (1992). *Usage of "Equivalent Apertures" for rock fractures as derived from hydraulic and tracer tests.* Water resource research, **28** (5): 1451 – 1455.

U.S. EPA, (2006). E*ditions of the Drinking Water Standards and Health Advisories*. U.S. Environmental Protection Agency, Washington, DC. EPA 822-R-06-013.

Van der Merwe, A.J and De Beer, J.H. (2006). *Competent persons report on the uranium-molybdenum mineral properties of Western Uranium (PTY) LTD in the Karoo, South Africa*. SRK Consulting. Report no: 359566.

Van Tonder, G., Bardenhagen, I., Riemann, K. Van Bosch, J., Dzanga, P and Xu, Y. (2002). *Manual on pumping test anlysis in fractured rock aquifers*. Water Research Commision. Report No. 1116/1/02.

Vogel, JC., Talma., AS, and Heaton., T.H.E. (1980). *The isotopic, chemical and dissolved gas concentrations in groundwater near Beaufort West*. Natural Isotopes Division. CSIR research report 392.

Vogel, JC., Talma., AS, Heaton., THE, and Kronfeld, J. (1999). *Evaluating the rate of migration of an uranium deposition front within the Uitenhage Aquifer.* Journal of geochemical exploration, **66**: 269 – 276.

Walker, D. D. & Roberts, R. M. (2003). *Flow Dimensions Corresponding to Hydrogeologic Conditions*. Water Resour. Res. **39**(12). pp. 7.1 – 7.8.

WHO, (1993). *Guidelines for Drinking-Water Quality.* 2nd Edition. Geneva, Switzerland: World Health Organization.

WHO, (1998). *Guidelines for Drinking-Water Quality. A*ddendum to Volume 1. Recommendations. Geneva, Switzerland: World Health Organization.

WHO, (2005). *Guidelines for drinking – Water quality: First addendum to third edition*. Volume.1 recommendations, Geneva. World Health Organization.

Witthüser, K., Reichert, B. and Hotzl H. (2003). *Contaminant transport in fractured chalk: laboratory and field experiments*. Groundwater Journal, **41** (6).

Witthüser, K., Arnepalli., D and Singh, D. N. (2006). *Investigations on diffusion characteristics of granite and chalk rock mass*. Geotechnical and geological engineering, **24**: 325 – 334.

Witherspoon. P.A., Wang, J.S.Y., Iwai, K. and Gale, J.E. (1980). *Validity of cubic law for fluid flow in a deformable rock fracture*. Water resource research, **16** (6): 1061 – 1024.

Woodford, A.C, and Chevallier, L (2002). *Hydrogeology of the Main Karoo Basin: Current knowledge and future research needs.* Water Research Commission, Pretoria: WRC Report TT 179/02.

Wood, W.W., Thomas, F., Kraemer and Shapiro, A. (2004*). Radon (^{222}Rn) in groundwater of fractured rocks: A Diffusion/Ion Exchange model*. Groundwater, **42** (4): 552 – 567.

Appendix.A – Sampling Boreholes

Table 1 Sampling Boreholes

Borehole ID	X-Coord	Y-Coord	Elev	pH	EC (ms/m)	Date
Lemoenfontien Noord	22.64304	32.29179	889	6.67	120	12/5/2008
Lemoenfontien Wes	22.62961	32.29840	881	6.83	138	12/5/2008
Tweeling wellfield	22.71901	32.22036	966	6.45	120	12/5/2008
Brandwag no:8	22.79169	32.21398	965	7.08	117	12/5/2008
Brandwag no:9	22.83581	32.21239	971	6.92	211	12/5/2008
Nigrini's Farm no:1	22.85314	32.21669	985	7.14	161	12/5/2008
Nigrini's Farm no:2	22.80223	32.23645	958	6.92	290	12/5/2008
Basson family	22.58600	32.35472	937	6.88	109	12/5/2008
Townspring	22.58524	32.34573	851	6.92	62	12/5/2008
Steenrotsfontein no:1	22.56430	32.41827	808	7.13	250	15/5/2008
Steenrotsfontein no:2	22.56389	32.41899	806	7.13	351	15/5/2008
Blydskap no:1	23.13905	32.61653	842	7.07	104	16/5/2008
Blydskap no:2	23.09525	32.60788	831	7.11	87	16/5/2008
Meyerspoort	22.45094	32.68124	811	7.02	47	17/5/2008
Scheeurfontein no:1	22.55612	32.68570	837	6.99	72	17/5/2008
Scheeurfontein no:2	22.57533	32.68559	871	7.01	76	17/5/2008
Steenrotsfontein.7	22.53447	-32.39173	815	6.64	160	31/5/2009
Aardorings	22.56148	-32.64715	838	7.00	73	31/5/2009
Tulpleegte	22.65663	-32.65033	874	7.41	125	31/5/2009
Kardoornkuil	22.75134	-32.70107	866	7.06	169	31/5/2009
Hansrivier 10	22.64032	-32.39104	844	6.99	148	1/6/2009
Hansrivier 12	22.60189	-32.39853	833	7.01	110	1/6/2009
Hansrivier 13	22.64117	-32.38757	845	6.99	160	1/6/2009
Hoenderhok	22.59773	32.36280	841	7.00	184	1/6/2009
Saucyskuil	22.79733	-32.53846	847	7.96	73	3/6/2009
Olivegrove.3	22.58652	-32.50932	838	7.44	62	3/6/2009
Olivegrove.2	22.56522	-32.50490	822	7.25	113	2/6/2009
Olivegrove.1	22.56608	-32.39692	813	6.98	97	2/6/2009
BH 06	22.53529	-32.39022	813	6.78	102	29/5/2009
G936H	22.64042	-32.39102	843	7.57	146	1/6/2009
G936 02	22.64055	-32.39103	844	7.64	72	1/6/2009
Hansrivier 13.1	22.64155	-32.38734	845	6.98	85	1/6/2009

Appendix.B – Radioactivity Decay Series

Decay series of Uranium and its daughter products									
Symbol	**Element name**	**Radionuclide**	**Atomic weight**	**Half life**	**Radiation**	**Alpha Energy**	**Abundance (%)**	**Beta energy (MeV)**	**Abundance (%)**
^{238}U	Uranium	Uranium I	238	$4.468*10^{9}$ yrs	Alpha	4.195	77		
					Alpha	4.147	23		
					Alpha	4.038	0.23		
^{234}Th	Thorium	Uranium X_1	234	24.1 days	Beta			0.191	81
					Beta			~0.103	19
^{234}Pa	Protactinium	Uranium X_2	234	1.18 min	Beta			2.29	98
				6.66 hrs	Beta			0.53	66
^{234}U	Uranium	Uranium II	234	$2.48*10^{5}$ yrs	Alpha	4.768	72		
						4.717	28		
						4.6	0.3		
^{230}Th	Thorium	Ionium	230	$7.52*10^{4}$ yrs	Alpha	4.682	76		
					Alpha	4.615	24		
					Alpha	4.476	0.12		
					Alpha	4.437	0.03		
^{226}Ra	Radium	Radium	226	1602 yrs	Alpha	4.781	94.5		
						4.598	5.5		
						4.34	0.007		
						4.191	0.001		
^{222}Rn	Radon	Radon	222	3.825 days	Alpha	5.486	~100		
					Alpha	4.983	~0.08		

Appendix.B – Radioactivity Decay Series (Continuation)

Decay series of Uranium and its daughter products									
Symbol	**Element name**	**Radionuclide**	**Atomic weight**	**Half life**	**Radiation**	**Alpha Energy**	**Abundance (%)**	**Beta energy (MeV)**	**Abundance (%)**
^{218}Po	Polonium	Radium A	218	3.05 min	Alpha and Beta	6.11		0.33	100
^{214}Pb	Lead	Radium B	214	26.8 min	Beta			1.03	6
^{218}At	Astatine		218	2 sec	Alpha	6.7		0.67	94
^{214}Bi	Bismuth	Radium C	214	19.7 min	Alpha and Beta	5.61		3.26	100
^{214}Po	Polonium	Radium C'	214	$1.64*10^{-04}$	Alpha	7.83	100		
^{210}Tl	Thallium	Radium C"	210	1.32 min	Beta		100	2.3	
^{210}Pb	Lead	Radium D	210	~22 yrs	Alpha and Beta	3.7	$1.8*10^{-08}$	0.017	85
^{210}Bi	Bismuth	Radium E	210	5.02 days	Alpha and Beta	4.93	60	1.155	100
						4.89	34		
						4.59	5		
^{210}Po	Polonium	Radium F	210	138.3 days	Alpha	5.305	100		
^{206}Hg	Mercury		206	8.6 min	Beta			1.3	100
^{206} Tl	Thalliium		206	4.19 min	Beta			1.52	100
^{206}Pb	Lead	Radium G	206		Stable				

Appendix.B – Radioactivity Decay Series (Continuation)

Decay series of Thorium and its daughter products									
Symbol	**Element name**	**Radionuclide**	**Atomic weight**	**Half life**	**Radiation**	**Alpha Energy (MeV)**	**Abundance (%)**	**Beta energy (MeV)**	**Abundance (%)**
^{232}Th	Thorium	Thorium	232	$1.39*10^{10}$yrs	Alpha	4.007	76		
					Alpha	3.952	24		
					Alpha	3.882	0.2		
^{228}Ra	Radium	Mesothorium 1	228	5.75 yrs	Beta			0.055	100
^{228}Ac	Actinium	Mesothorium 2	228	6.13 hrs	Beta			2.11	100
^{228}Th	Thorium	Radiothorium	228	1.913 yrs	Alpha	5.421	71		
					Alpha	5.338	28		
					Alpha	5.208	0.4		
					Alpha	5.173	0.2		
					Alpha	5.137	0.03		
^{224}Ra	Radium	Thorium X	224	3.64 days	Alpha	5.684	94.5		
					Alpha	5.447	5.5		
^{220}Rn	Radon	Thoron	220	55.6 sec	Alpha	6.296	100		
					Alpha	5.761	0.3		
^{216}Po	Polonium	Thorium A	216	0.145 sec	Alpha	6.777	100		
^{212}Pb	Lead	Thorium B	212	10.64 hrs	Beta			0.58	complex
^{212}Bi	Bismuth	Thorium C	212	60.5 min	Beta and Alpha	6.09	30	2.25	100
					Beta and Alpha	6.05	70		
^{212}Po	Polonium	Thorium C'	212	$3.04 * 10^{-7}$ sec	Alpha	8.78	100		
^{208}Tl	Thallium	Thorium C"	208	3.1 min	Beta			1.8	100
^{208}Pb	Lead	Thorium D	208		stable				

Appendix.C – Mean residence time and dispersion length of the dataset using the method of moments

#	Time	time [sec]	dt	c [ppb]	M0 = c(t)*dt	M1 = c(t)*t*dt	M2 = c(t)*t^2*dt
1	10/02/10-18:20:34	0	10	0.17	1.7	0	0
2	10/02/10-18:20:44	10	10	0.19	1.9	19	190
3	10/02/10-18:20:54	20	10	0.2	2	40	800
4	10/02/10-18:21:04	30	10	0.23	2.3	69	2070
5	10/02/10-18:21:14	40	10	0.26	2.6	104	4160
6	10/02/10-18:21:24	50	10	0.28	2.8	140	7000
7	10/02/10-18:21:34	60	10	0.3	3	180	10800
8	10/02/10-18:21:44	70	10	0.33	3.3	231	16170
9	10/02/10-18:21:54	80	10	0.37	3.7	296	23680
10	10/02/10-18:22:04	90	10	0.4	4	360	32400
11	10/02/10-18:22:14	100	10	0.44	4.4	440	44000
12	10/02/10-18:22:24	110	10	0.47	4.7	517	56870
13	10/02/10-18:22:34	120	10	0.5	5	600	72000
14	10/02/10-18:22:44	130	10	0.55	5.5	715	92950
15	10/02/10-18:22:54	140	10	0.6	6	840	117600
16	10/02/10-18:23:04	150	10	0.63	6.3	945	141750
17	10/02/10-18:23:14	160	10	0.69	6.9	1104	176640
18	10/02/10-18:23:24	170	10	0.71	7.1	1207	205190
19	10/02/10-18:23:34	180	10	0.79	7.9	1422	255960
20	10/02/10-18:23:44	190	10	0.85	8.5	1615	306850
21	10/02/10-18:23:54	200	10	0.91	9.1	1820	364000
22	10/02/10-18:24:04	210	10	0.97	9.7	2037	427770
23	10/02/10-18:24:14	220	10	1.05	10.5	2310	508200
24	10/02/10-18:24:24	230	10	1.12	11.2	2576	592480
25	10/02/10-18:24:34	240	10	1.22	12.2	2928	702720
26	10/02/10-18:24:44	250	10	1.29	12.9	3225	806250
27	10/02/10-18:24:54	260	10	1.35	13.5	3510	912600
28	10/02/10-18:25:04	270	10	1.46	14.6	3942	1064340
29	10/02/10-18:25:14	280	10	1.59	15.9	4452	1246560
30	10/02/10-18:25:24	290	10	1.65	16.5	4785	1387650

Appendix.C – Mean residence time and dispersion length of the dataset using the method of moments (Continuation)

#	Time	time [sec]	dt	c [ppb]	**M0 = c(t)*dt**	**M1 = c(t)*t*dt**	**M2 = c(t)*t^2*dt**
31	10/02/10-18:25:34	300	10	1.77	17.7	5310	1593000
32	10/02/10-18:25:44	310	10	1.84	18.4	5704	1768240
33	10/02/10-18:25:54	320	10	1.94	19.4	6208	1986560
34	10/02/10-18:26:04	330	10	2.02	20.2	6666	2199780
35	10/02/10-18:26:14	340	10	2.12	21.2	7208	2450720
36	10/02/10-18:26:24	350	10	2.29	22.9	8015	2805250
37	10/02/10-18:26:34	360	10	2.39	23.9	8604	3097440
38	10/02/10-18:26:44	370	10	2.49	24.9	9213	3408810
39	10/02/10-18:26:54	380	10	2.67	26.7	10146	3855480
40	10/02/10-18:27:04	390	10	2.85	28.5	11115	4334850
41	10/02/10-18:27:14	400	10	2.94	29.4	11760	4704000
42	10/02/10-18:27:24	410	10	3.12	31.2	12792	5244720
43	10/02/10-18:27:34	420	10	3.28	32.8	13776	5785920
44	10/02/10-18:27:44	430	10	3.46	34.6	14878	6397540
45	10/02/10-18:27:54	440	10	3.63	36.3	15972	7027680
46	10/02/10-18:28:04	450	10	3.74	37.4	16830	7573500
47	10/02/10-18:28:14	460	10	3.95	39.5	18170	8358200
48	10/02/10-18:28:24	470	10	4.08	40.8	19176	9012720
49	10/02/10-18:28:34	480	10	4.26	42.6	20448	9815040